



Diese Dissertation haben begutachtet

Prof. Dr. Guido KICKELBICK

Prof. Dr. Helmuth HOFFMANN

Dissertation

Organophosphonates on Titanium Dioxide Photocatalysts: Isotropic and Anisotropic Modification and Photocatalytic Properties

ausgeführt zum Zwecke der Erlangung des akademischen Grades einer
Doktorin der technischen Wissenschaften

unter der Leitung von

Univ.Prof. Dipl.-Chem. Dr.rer.nat. Guido KICKELBICK

eingereicht an der Technischen Universität Wien
Fakultät für Technische Chemie

von

Dipl.-Ing. Angelika BACHINGER

Mat.Nr. 0102848

Braunhirschengasse 5/8

1150 Wien

Wien, 23.03.2011

Dipl.Ing. Angelika Bachinger

Mut steht am Anfang des Handelns,

Glück am Ende

Demokrit

Für meine Eltern

Danksagung

Ich danke meinem Betreuer Prof. Guido Kickelbick für die Möglichkeit, an einem interessanten und fordernden Projekt mitzuarbeiten. Die Freiheit eigene Ideen umzusetzen ermöglichte es mir, meine wissenschaftlichen Fähigkeiten zu beweisen und weiterzuentwickeln. Insbesondere bedanke ich mich für sein Verständnis für die Gründe, die mich in Wien hielten.

Außerdem danke ich Prof. Schubert für seine Unterstützung und vor allem für sein Engagement, meine Finanzierung auch nach Guidos Wechsel nach Saarbrücken zu gewährleisten.

Diese Arbeit wäre nicht möglich gewesen ohne die Kooperation mit anderen Arbeitsgruppen und Forschungseinrichtungen. In diesem Zusammenhang möchte ich Dr. O. Lorret und Dr. G. Waldner (ARC Seibersdorf) für photokatalytische Untersuchungen, Dr. J. Bernardi und Dr. M. Stöger-Pollach (USTEM TU Wien) für ihre Unterstützung bei TEM Messungen und Dr. R. Haberkorn (Universität des Saarlandes) für Rietveld Analysen danken.

DANKE an meine ehemaligen und aktuellen Kollegen Bernhard (für viele kurzweilige Unterhaltungen über Gott und die Welt, besonders in SB), Christian Mau. (für die Erkenntnis, dass manche Dinge es nicht wert sind, sich darüber aufzuregen), Christian Mar., Christine, Christoph L. (den besten Laborkollegen, den man sich vorstellen kann), Christoph R., Claudia, Denisa, Denise, Hongzhi, Jakob, Jasmin, Maia, Majka, Marco (für gute Ratschläge und geduldiges Zuhören), Marina, Matthias, Michael, Mirka, Mohsin, Philipp, Ralf, Robert L., Robert P., Rupali, Rupert (fürs Zusammenschweißen der Reaktoren und diverse Reparaturen), Sarah, Simas, Sorin (für seine Fürsorge), Stefan, Stephan, Sven und VanAn dafür, dass man mit ihnen auch mal was anderes als über Chemie reden kann.

Ich danke Christian Mau., Christoph L., Jakob und Marco für das Korrekturlesen dieser Arbeit.

Besonderer Dank gilt meiner Familie und Max für den starken Rückhalt und die Unterstützung, die sie mir bieten.

Kurzfassung

Selbstreinigende Oberflächen sind eine der wichtigsten Entwicklungen in der Glastechnologie der letzten Jahre. Es handelt sich dabei um photokatalytisch aktive Beschichtungen, die unter Einstrahlung von Licht organische Verunreinigungen abbauen können. Solche Systeme sind für organische Oberflächen nicht einsetzbar, da durch den photokatalytischen Prozess nahezu alle organischen Verbindungen angegriffen werden, das Substrat eingeschlossen. Darüberhinaus wird für organische Substrate, um eine stabile Anbindung zu gewährleisten, ein Kupplungsreagenz benötigt. In dieser Arbeit sollte daher ein System entwickelt werden, das eine stabile Anbindung des photokatalytisch aktiven Films an organische Substrate ermöglicht.

Zunächst wurde die Synthese von photokatalytisch aktiven TiO₂ Nanopartikeln durch Sol-Gel Chemie und der Einfluss unterschiedlicher Parameter auf Größe und Morphologie der Partikel untersucht. Die photokatalytische Aktivität der Partikel wurde studiert und mit kommerziell erhältlichen Systemen verglichen. Um eine Anbindung an organische Substrate zu ermöglichen, wurden die photokatalytisch aktiven Nanopartikel mit organischen Phosphonaten und Phosphaten modifiziert, die eine stabile kovalente Bindung zu TiO₂ bilden. Die Stabilität dieser Systeme wurde unter photokatalytischen Bedingungen untersucht. Die Ergebnisse zeigten, dass eine Phosphonat-Brücke die organischen Gruppen nicht vor dem Abbau schützen kann. Mechanistische Untersuchungen ergaben, dass der Abbau sowohl durch Hydroxylradikale als auch durch Löcher im Valenzband des Halbleiters initiiert werden kann. Durch Festkörper-NMR Spektroskopie konnten diverse Zwischenprodukte identifiziert werden, was auf einen sequentiellen Abbau der organischen Gruppen hinweist. Es konnte außerdem gezeigt werden, dass die nach dem Abbau der Organik zurückbleibenden Phosphatgruppen die photokatalytische Aktivität der Partikel drastisch erhöhen.

Eine kovalente Anbindung unter Erhalt der photokatalytischen Aktivität kann durch anisotrope Modifizierung der TiO₂ Nanopartikel erreicht werden. Eine Hemisphäre der sogenannten „Janus“ Partikel kann an das Substrat angebunden werden, während die andere „nackt“ – also photokatalytisch aktiv – bleibt. Solche anisotrop modifizierten Partikel wurden durch Modifizierung in einer Partikel-stabilisierten Emulsion erhalten. Die amphiphile Natur der Partikel konnte durch eine drastisch erhöhte Stabilität der Emulsion beobachtet werden. Weitere Untersuchungen zielten auf einen optischen Nachweis der Anisotropie ab.

Abstract

Titanium dioxide nanoparticles are photocatalytically active and the light-induced redox process can lead to the degradation of organic compounds. This effect can be used for dirt-degrading films on inorganic substrates such as glass or ceramics. The application of such coatings for organic surfaces is, however, a challenging task. Two major problems arise: (i) The organic substrate can be degraded upon direct contact with the photocatalytic film and (ii) for a stable connection between the substrate and the photocatalytic film, coupling agents are required. Aim of this work was the development of a system that allows a stable connection of the photocatalytic coating to the organic substrate.

In this work, the synthesis of photocatalytically active TiO₂ nanoparticles by the sol-gel process and the influence of different parameters on the size and morphology of the particles were investigated. In order to achieve covalent interaction with the substrate, the particles were modified with organic phosphonates and phosphates, which are known to form a stable covalent bonding to TiO₂ surfaces. Investigations on the stability of these systems under photocatalytic conditions revealed that a phosphonate bridge cannot protect the organic moieties from degradation. Mechanistic studies showed that the degradation can be initiated by at least two different species: hydroxyl radicals and surface trapped holes. Various degradation intermediates identified by solid state ¹³C NMR studies lead to the conclusion that the organic species are degraded sequentially. Moreover, it was shown that after complete degradation of the organic moieties, a phosphate species is left on the particles' surface. A drastically increased photocatalytic activity of the particles after illumination could be assigned to the presence of these phosphate species.

An additional requirement for the coating is a bare photocatalytic surface. Thus, in this work photocatalytic titanium dioxide nanoparticles exhibiting anisotropic surface modification were prepared. One side of the nanoparticles' surface should remain blank and photocatalytically active, while the functionalized section protects the substrate from degradation and can in addition interact with the substrate. These so called "Janus" particles were obtained by modification in a differentiating environment, which is provided by particle-stabilized emulsions. The amphiphilic nature of particles modified in emulsion could be observed by a drastically increased stability of the emulsion. Nevertheless, further investigations were conducted, aiming an optical proof for the anisotropic nature of these particles.

Parts of this work have been published

“Pickering Emulsions Stabilized by Anatase Nanoparticles”; Angelika Bachinger,
Guido Kickelbick: Monatshefte für Chemie (2010), 141 (6), 685-690

Index of Abbreviations

General Abbreviations and Symbols

2θ	diffraction angle
A	Absorption
A_0	initial Absorption
BLB	black light black
C	concentration
C_0	initial concentration
DLVO	Derjaguin, Landau, Verwey and Overbeek
e^-	electron
eV	electron Volt
h^+	hole
k	reaction rate constant
λ	wavelength
o/w-emulsion	oil-in-water emulsion
pzc	point of zero charge
rpm	rounds per minute
S_N	nucleophilic substitution
UV	ultraviolet
UVA	near ultraviolet
VOC	volatile organic compound
w/o-emulsion	water-in-oil emulsion
Θ_{ow}	angle at the oil-water-solid interface

Abbreviations of Chemicals and Substances

AIBN	2,2'-azobis(2-methylpropionitrile)
------	------------------------------------

AuNP	gold nanoparticles
DDA	dodecanoic acid
DDA@TiO ₂	TiO ₂ nanoparticles modified with DDA
DDAmine	dodecyl amine
DDAmine@TiO ₂	TiO ₂ nanoparticles modified with DDAmine
DMMP	dimethyl methylphosphonate
DMSO	dimethyl sulfoxide
DPA	dodecyl phosphonic acid
DPA@TiO ₂	TiO ₂ nanoparticles modified with DPA
DPA-Et	diethyl dodecyl phosphonate
Et	ethyl
EtOH	ethanol
MB	methylene blue
MPA	11-mercapto undecanyl phosphonic acid
MPA@TiO ₂	TiO ₂ nanoparticles modified with MPA
PA	phosphoric acid
PA@TiO ₂	TiO ₂ nanoparticles modified with PA
PEG	poly(ethylene glycol)
PEG-PA	poly(ethylene glycol) phosphoric acid
PEG-PA@TiO ₂	TiO ₂ nanoparticles modified with PEG-PA
P-123	BASF Pluronic P-123 surfactant
P25	Evonik AEROXIDE [®] TiO ₂ P25
ⁱ Pr	isopropanol
PPA	phenyl phosphonic acid
PPoA	phenyl phosphoric acid
SDS	sodium dodecylsulfate
SDS@TiO ₂	TiO ₂ nanoparticles modified with SDS
Ti(O ⁱ Pr) ₄	titanium (IV) isopropoxide

s	singlet
d	doublet
t	triplet
q	quartet
m	multiplet
ppm	parts per million

Table of Contents

<i>1</i>	<i>Introduction</i>	<i>1</i>
1.1	Motivation.....	1
1.2	Photocatalysis	1
1.2.1	General Remarks	1
1.2.2	Principles of Photocatalysis.....	2
1.2.3	Photocatalytic Activity	5
1.2.4	Self-Cleaning Surfaces	7
1.3	Titanium Dioxide.....	8
1.3.1	Properties of Titanium Dioxide	8
1.3.2	Titanium Dioxide Nanoparticles.....	10
1.3.3	Synthesis of Titanium Dioxide Nanoparticles.....	11
1.4	Phosphonates and Phosphates on TiO ₂ Surfaces	13
1.4.1	Synthesis of Organic Phosphonates and Phosphates	13
1.4.1.1	Synthesis of Organic Phosphonates.....	14
1.4.1.2	Synthesis of Organic Phosphates.....	15
1.4.2	Modification of Titanium Dioxide with Organic Phosphonates.....	15
1.4.3	Stability of Organophosphonates under Photocatalytic Conditions	17
1.5	Janus Particles.....	18
1.5.1	Synthesis of Janus Particles	18
1.5.2	Pickering Emulsions	20
1.5.3	Anisotropic Modification in Pickering Emulsion.....	22
1.5.4	Proving Anisotropy by Imaging Techniques.....	22
1.6	Gold Nanoparticles	23
1.6.1	Properties of Gold Nanoparticles.....	23
1.6.2	Synthetic Strategies for the Formation of Gold Nanoparticles.....	23
<i>2</i>	<i>Scope of the Work</i>	<i>25</i>
2.1	Photocatalytic TiO ₂ Nanoparticles.....	25
2.2	Stability of Coupling Agents under Photocatalytic Conditions.....	25

2.3	Anisotropic Surface Modification	26
3	<i>Results and Discussion</i>	27
3.1	Photocatalytic TiO ₂ Nanoparticles	27
3.1.1	Sol-Gel Synthesis of TiO ₂ Nanoparticles	27
3.1.2	Photocatalytic Activity of Sol-Gel TiO ₂ Nanoparticles	30
3.1.2.1	Photocatalytic Activity in Suspension.....	30
3.1.2.2	Photocatalytic Activity of Films on Glass.....	34
3.1.3	Conclusions	38
3.2	Stability of Organophosphonates under Photocatalytic Conditions	39
3.2.1	Degradation of Phenylphosphonic acid.....	40
3.2.2	Kinetics and Mechanism	46
3.2.2.1	Phosphonate versus Phosphate.....	47
3.2.2.2	Arylphosphonate versus Alkylphosphonate.....	50
3.2.2.3	Solvent.....	55
3.2.2.4	Surface Coverage	58
3.2.2.5	Particle Concentration	59
3.2.2.6	Degradation of the Solvent.....	60
3.2.3	Characterization of Illumination Products	61
3.2.4	Conclusions	69
3.3	Anisotropic Modification of TiO ₂ Nanoparticles	70
3.3.1	Pickering Emulsions Stabilized by TiO ₂ Nanoparticles.....	71
3.3.2	Modification in Pickering Emulsion	76
3.4	Proof of the Anisotropy	80
3.4.1	Synthesis of Gold Nanoparticles	81
3.4.1.1	Synthesis of Gold Nanoparticles by the Turkevich Method	82
3.4.1.2	Reduction of Auric Acid in the Presence of an Organic Thiol	82
3.4.1.3	Synthesis of Gold Nanoparticles by the Brust Method	84
3.4.1.4	Stabilization of Gold Nanoparticles obtained by the Brust Method with an Organic Thiol	85
3.4.1.5	Synthesis of Gold Nanoparticles by the Martin Method.....	85

3.4.2	Synthesis of Janus TiO ₂ Nanoparticles.....	86
3.4.2.1	Poly(ethylene glycol) Janus Nanoparticles.....	86
3.4.2.2	Thiol-functionalized Janus Nanoparticles	89
4	<i>Summary</i>	102
4.1	Photocatalytic TiO ₂ Nanoparticles.....	102
4.2	Stability of Organophosphonates under Photocatalytic Conditions	102
4.3	Anisotropic Modification with Organophosphonates.....	105
5	<i>Experimental</i>	106
5.1	Materials	106
5.2	Analytical Techniques	106
5.3	Experiments	109
5.3.1	Synthesis of TiO ₂ Nanoparticles.....	109
5.3.1.1	Synthesis of TiO ₂ Nanoparticles with 4-10 nm Diameter	109
5.3.1.2	Synthesis of TiO ₂ Nanoparticles with 60 nm Diameter	110
5.3.2	Synthesis of Dodecylphosphonic Acid (DPA)	111
5.3.2.1	Synthesis of Diethyl Dodecylphosphonate (DPA-Et)	111
5.3.2.2	Synthesis of Dodecylphosphonic Acid (DPA)	111
5.3.3	Synthesis of Poly(ethylene glykol)phosphonic Acid (PEG-PA)	112
5.3.3.1	Synthesis of Poly(ethylene glykol) Monovinyl Ether	112
5.3.3.2	Synthesis of Diethyl Poly(ethylene glycol)phosphonate.....	112
5.3.3.3	Synthesis of Poly(ethylene glycol)phosphonic Acid (PEG-PA) ...	113
5.3.4	Synthesis of 11-Mercapto Undecanylphosphonic Acid	113
5.3.4.1	Synthesis of Diethyl 11-Bromo Undecanylphosphonate.....	113
5.3.4.2	Synthesis of 11-Bromo Undecanylphosphonic Acid.....	113
5.3.4.3	Synthesis of 11-Mercapto Undecanylphosphonic Acid (MPA)	114
5.3.5	Modification of TiO ₂ Nanoparticles in Suspension.....	114
5.3.6	Preparation of Pickering Emulsions	116
5.3.7	Modification of TiO ₂ in Pickering Emulsion.....	117
5.3.7.1	Modification of one Hemisphere.....	117

5.3.7.2	Modification of two Hemispheres with Different Coupling Agents.....	118
5.3.8	Synthesis of Gold Nanoparticles	118
5.3.8.1	Synthesis of Gold Nanoparticles according to Turkevich ²⁴⁶	118
5.3.8.2	Synthesis of Gold Nanoparticles according to Brust ²⁴⁸	119
5.3.8.3	Synthesis of Gold Nanoparticles according to Martin ²⁵¹	119
5.3.8.4	Reduction of Auric Acid in the Presence of MPA.....	120
5.3.8.5	Exchange Reaction on TOAB Stabilized Gold Nanoparticles.....	120
5.3.9	Experiments for Proving the Anisotropy	120
5.3.9.1	Decoration of Janus-DPA/PEG@TiO ₂ with Gold Nanoparticles (AuNP) (PEG1-3).....	120
5.3.9.2	Decoration of Janus-MPA@TiO ₂ with Citrate Stabilized AuNP (MPA1).....	121
5.3.9.3	Reduction of Auric Acid in the Presence of Janus-MPA@TiO ₂ (MPA2).....	121
5.3.9.4	Decoration of Janus-MPA@TiO ₂ with TOAB Stabilized AuNP (MPA3+4)	121
5.3.9.5	Decoration of Janus-DPA@TiO ₂ with TOAB stabilized AuNP (DPA1)	122
5.3.9.6	Decoration of Janus-DPA@TiO ₂ with bare AuNP (DPA2)	123
5.3.9.7	Staining of Janus-DPA@TiO ₂ with Auric Acid (DPA3).....	123
5.3.9.8	Decoration of Janus-DPA/MPA@TiO ₂ with TOAB stabilized AuNP (MPA5).....	124
5.3.9.9	Staining of Janus-DPA/MPA@TiO ₂ with Auric Acid (MPA6) ...	124
5.3.10	Illumination Experiments	124
6	<i>References</i>	126

1 Introduction

1.1 Motivation

Self-cleaning surfaces are state of the art and commercially available coatings allow the photocatalytic degradation of organic species on inorganic surfaces such as glass, ceramics or stone.¹⁻⁸ However, all kinds of organic molecules can be decomposed by the photocatalytic process, which renders these films unsuitable for organic substrates like polymers. Goal of this work was the development of a system that allows the formation of self-cleaning photocatalytic films on organic substrates. It is obvious that such systems need to involve an intermediate layer that protects the substrate from degradation and at the same time provides a linkage between the organic surface and the photocatalytic film. Such protective linkage could be provided by the formation of an inorganic barrier layer either on the substrate or on the particles. A more straightforward approach is provided by coupling molecules that exhibit a photocatalytically stable linkage to the photocatalyst and prevent the degradation of the substrate concurrently. Moreover, anisotropic modification of photocatalytic nanoparticles was aimed in order to make a connection to the substrate possible and render the particles photocatalytically active concurrently.

1.2 Photocatalysis

1.2.1 General Remarks

Semiconductor photocatalysis represents a versatile tool for the removal of pollutants from water and air and has thus gained considerable interest in Green Chemistry in the last decades.⁹⁻¹³ The generation of charge carriers by exposure to light has first been noticed by Wilderman and Meyer in 1908.¹⁴ They observed a “current

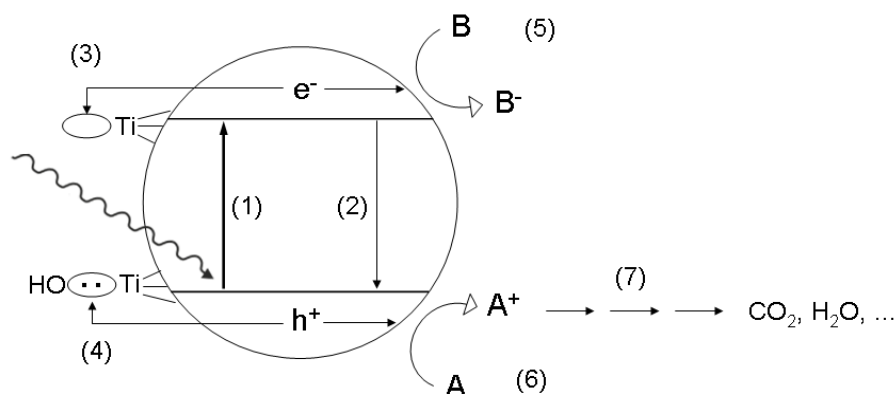
produced by the action of light” when one electrode in a galvanic cell was irradiated. In 1972, Fujishima and Honda reported the successful splitting of water to hydrogen and oxygen by photoelectrocatalysis.¹⁵ They constructed an electrochemical cell with a TiO₂ anode and a platinum black cathode in water. When the TiO₂ electrode was irradiated with light, they observed current flowing from the platinum electrode to the TiO₂ electrode. They concluded that water was oxidized at the TiO₂ electrode and reduced at the platinum electrode. This finding attracted much attention in terms of converting solar energy to chemical energy (H₂) for combustion engines or fuel cells.^{16, 17} Environmental interest in photocatalysis has arisen since Frank and Bard reported the decomposition of cyanide in water in 1977.^{15, 18} In 1983, Ollis and coworkers implemented semiconductor-initiated reactions for the oxidation of organic pollutants.^{19, 20} They studied the mineralization of halogenated organic compounds in the presence of a titanium dioxide photocatalyst. Numerous investigations on photo-induced processes followed up, leading to a wide variety of applications, especially for self-cleaning and anti-fogging surfaces,^{1-3, 21} wastewater treatment^{11, 13, 22} and photovoltaics.²⁴⁻²⁶

1.2.2 Principles of Photocatalysis

Semiconductor materials are able to create photo-electrons and photo-holes upon illumination with photons of energy higher than or equal to their band gap (Equation 1). Excited electrons and holes can recombine and dissipate their energy as heat or be trapped in metastable states (Equations 2-4). In titanium dioxide photocatalysts, reactions of electrons and holes with $>Ti^{IV}OH$ result in reactive surface trapped charge carriers (Equations 2+3), while trapping of electrons upon reaction with Ti^{IV} leads to the irreversible formation of Ti^{III} (Equation 4). The recombination of surface trapped electrons and holes leads to the formation of hydroxyl groups on the photocatalysts' surface (Equations 5+6). In fluid systems like water or air, reactants can adsorb on the surface of semiconductor materials and react with the photogenerated electrons or holes. In the presence of water, holes can form the highly oxidizing hydroxyl radicals (Equation 7), while electrons are consumed upon creation of O_2^- radicals in the presence of oxygen which can form hydrogen peroxide and subsequently hydroxyl radicals (Equations 8-11). Degradation of organic compounds can take place by hydroxyl radical addition or by reaction with surface trapped holes.²⁷⁻³² Although the two processes are vastly different, they lead to similar products which makes the distinction between them difficult. It has been generally accepted that in aqueous environments the degradation of organic compounds proceeds mainly via hydroxyl radicals.^{33, 34} However, in 2000

Hashimoto and coworkers found experimentally that the quantum yields of hydroxyl radicals (7×10^{-5}) are much lower compared to photocatalytic reactions (10^{-2}).³⁵ They concluded that the oxidation via valence band holes and surface trapped holes plays a major role. Furthermore, studies by Pelizzetti and coworkers on the degradation of phenol on fluorinated titanium dioxide indicated that holes can react directly with adsorbed organic molecules before they are trapped.³⁶ These results are in concordance with earlier reports by Carraway et al.³⁷ who observed oxidation of tightly bound electron donors by valence band holes.

In Scheme 1-1 the processes involved in a photocatalytic process are presented.



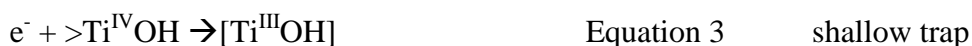
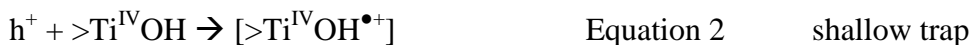
Scheme 1-1: Mechanism of photocatalysis, primary steps: (1) generation of charge carriers by a photon; (2) recombination of charge carriers; (3) trapping of an excited electron to yield Ti^{III} ; (4) trapping of a hole to yield reactive $[\text{>Ti}^{\text{IV}}\text{OH}^{\bullet+}]$; (5) initiation of a reduction process by a conduction band electron; (6) initiation of an oxidation process by a valence band hole; (7) further photocatalytic reactions that lead to mineralization of organic compounds.

Based on laser-flash photolysis measurements, the following processes have been proposed to be involved in photocatalytic reactions by Hoffmann and coworkers:^{38, 39}

Excitation:

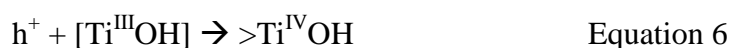


Trapping:





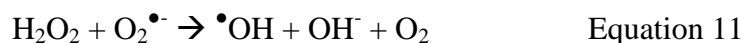
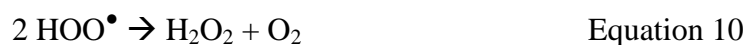
Recombination:



Charge transfer of positive charge:



Charge transfer of negative charge:



The surface-trapped holes, hydroxyl radicals, hydroperoxyl radicals and superoxide ions formed upon illumination of a photocatalyst are highly oxidative species that can degrade a large number of organic pollutants, including bioaerosols and volatile organic compounds (VOCs).^{40, 41} Complete mineralization of organic compounds can be achieved resulting in CO₂ and water and – depending on the functionalities involved – NO₃⁻, SO₄²⁻, PO₄³⁻ or halide ions.

The overall efficiency of a photochemical process is determined by two critical processes: (i) the competition between recombination and trapping and (ii) the competition between recombination of trapped charge carriers and interfacial charge transfer (i.e. the oxidation and reduction of donor and acceptor species respectively).

Photocatalytic materials need to fulfill a series of requirements: (i) for the excitation of electrons to the conduction band, a band gap that is in the energy range of UV or visible light is needed, which is provided by semiconductor materials. (ii) The chemical potentials of the photo-generated charge carriers need to be high enough for the oxidation and reduction of the donor and acceptor species respectively.^{33, 42} (iii) The photocatalyst needs to be stable upon UV irradiation which rules out for example CdS or GaP, which are degraded during repeated catalytic cycles upon formation of toxic products. (iv) As sunlight is the most economic source for photons, photocatalysts that are active upon illumination with sunlight are generally aimed.

Among many semiconductor materials that fulfill these requirements, titanium dioxide has been demonstrated by several groups to be the most active and stable photocatalyst.^{43,44}

1.2.3 Photocatalytic Activity

No normed testing method for the photocatalytic activity is existent, as the efficiency of a photocatalyst in degrading an organic compound depends on a variety of parameters:

- **Light intensity**

The kinetics of a photocatalytic degradation reaction depend on the amount of absorbed photons as confirmed by several investigations.⁴⁵⁻⁴⁸

- **Substrate**

As photocatalysis proceeds in the adsorbed state, the interaction of the organic compound with the photocatalysts' surface plays an important role.⁴⁹⁻⁵¹ It has been found for example that nitrophenol is degraded faster on titanium dioxide photocatalyst compared to phenol, owing to stronger adsorption.⁵¹ Moreover, at high substrate concentration, the photocatalysts' surface becomes saturated leading to deactivation of the catalyst.⁵²

- **Photocatalyst nature**

For heterogeneous reactions, the surface properties and surface area are crucial. Hence, the nature, surface, size and morphology of the photocatalyst have a significant impact on the photocatalytic reaction rate as discussed in a variety of publications.⁵³⁻⁵⁵

- **Concentration of photocatalyst**

Heterogeneous photocatalysis is strongly affected by the concentration of photocatalyst. Generally, the rate of photocatalytic reactions increases with increasing catalyst loading. However, with an excess of photocatalyst, unfavourable light scattering and reduction

of light penetration into the dispersion has been observed.^{56, 57} Thus, an optimal concentration of photocatalyst is required when the photocatalytic activity is tested.

- **pH**

The pH controls surface charge properties and the size of agglomerates and is thus an important parameter in reactions taking place on a surface. The effect of pH on the photocatalytic reactions and adsorption of organic compounds on titanium dioxide has been studied intensely.^{58, 59} Reaction rates revealed a maximum at moderately low pH, where the TiO₂ surface exhibits positive charge (pzc ~ 6). However, an excess of H⁺ on the photocatalysts' surface at very low pH can decrease reaction rates.⁶⁰

- **Reaction temperature**

Various investigations reveal the dependence of the photocatalytic degradation on the temperature. An optimum temperature range for efficient photocatalysis has been observed by several authors.^{13, 57, 61} At relatively low temperatures (< 20°C), the desorption of the products is the rate determining factor, whereas at elevated temperatures (> 80°C) the recombination of charge carriers and the desorption of reactants have been found to be enhanced, decreasing the reaction rate.

Hence, the photocatalytic activity cannot be studied by a normed procedure, but is rather investigated with regard to the aimed application. Photocatalysts are generally tested monitoring the degradation of a compound similar to the one that should be degraded in final application. For applications, where various different kinds of organic molecules should be degraded, model compounds are chosen. Most versatile testing procedures involve the degradation of phenol in liquid phase or 2-propanol in gas phase.³³ Moreover organic dyes with a characteristic UV-vis absorption spectrum are often used,^{62, 63} as a fast and reproducible characterization method is favorable.

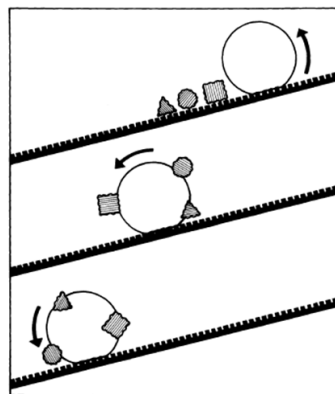
As no normed testing procedure is existent, the investigations on the photocatalytic activity of a new photocatalyst include the comparison with a standard commercial photocatalyst (typically Evonik AEROXIDE[®] TiO₂ P25) tested under similar conditions.^{32, 64, 65} If photocatalytic films are investigated, the standard commercial self-cleaning glass Pilkington Active[™] is used for comparison.⁶⁶

1.2.4 Self-Cleaning Surfaces

Self-cleaning surfaces present the most important advance in surface technology in recent years.⁸ Two oppositional approaches exist in this field of research: (i) Numerous investigations focus on superhydrophobic surfaces that are not wetted by water. (ii) Photocatalytic surfaces are able to degrade organic pollutants and at the same time photo-induced hydrophilicity leads to a perfect spread of water across the surface.

- **Superhydrophobic surfaces**

Superhydrophobic surfaces are based on the so-called lotus effect occurring in nature. A non-wetting surface is formed by a microstructured hydrophobic film imitating the leaves of the lotus plant. Correlations between the roughness of a surface and its wettability have already been studied in 1944 by Cassie and Baxter.⁶⁷ Later it was found by Barthlott and Neinhuis⁶⁸ that the water-repellant effect of microstructured surfaces leads to self-cleaning of the surface: contaminants adhere to the surface of the water droplets and are removed as the water rolls off as presented in Scheme 1-2.⁶⁹

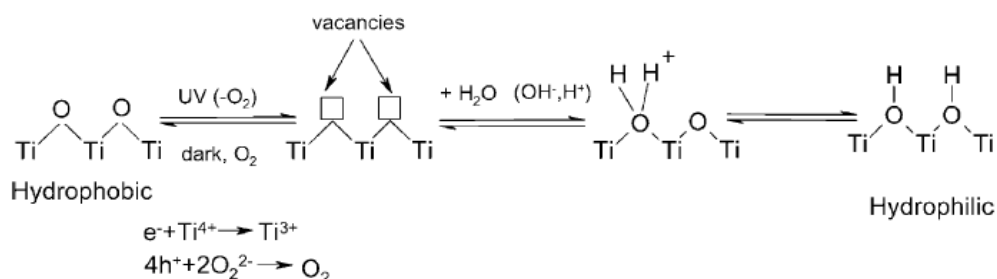


Scheme 1-2: Schematic representation of a rolling water droplet on a rough hydrophobic surface, adsorbing dirt particles on its surface. Scheme taken from Barthlott and Neinhuis⁶⁸.

- **Photocatalytic coatings**

Photocatalytic surfaces do not only take advantage of the photocatalytic decomposition of organic compounds, but also of the photoinduced hydrophilicity effect.^{1, 2, 33} Thus, upon illumination with UV light the surface of a photocatalyst changes due to reactions of photo-electrons and holes with surface species. For titanium

dioxide photocatalysts, oxygen vacancies are created when Ti^{IV} is reduced to Ti^{III} upon ejection of O_2^- anions. Water molecules occupy these vacancies upon formation of Ti-OH groups which make the surface hydrophilic as shown in Scheme 1-3.



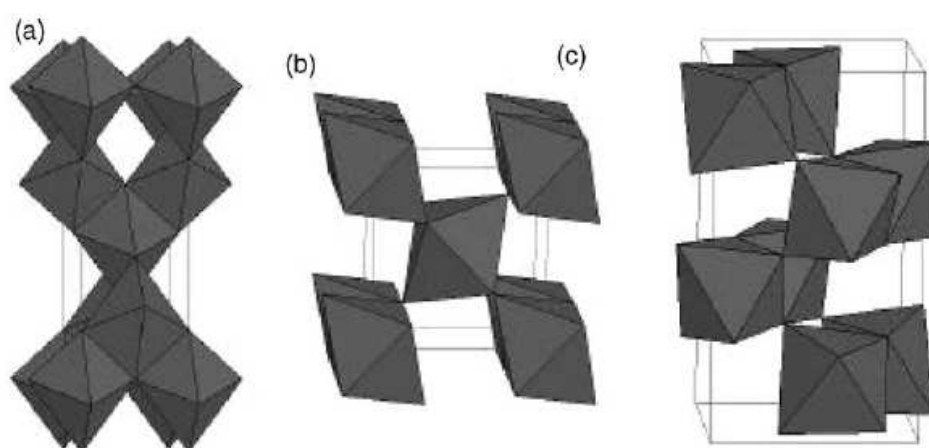
Scheme 1-3: Photoinduced superhydrophilicity. Scheme taken from Carp et al.⁴².

It has been proven that the water contact angle is decreasing with illumination time approaching zero after 30 minutes even with UV light sources of moderate intensity.¹ Hence, the surface is perfectly wetted by water which allows the removal of pollutants by water films.²

1.3 Titanium Dioxide

1.3.1 Properties of Titanium Dioxide

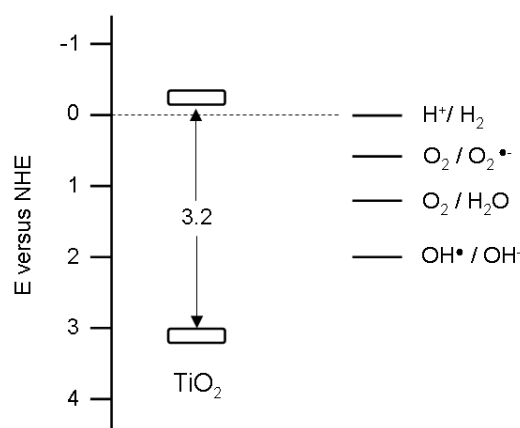
Titanium dioxide is a semiconductor material with a variety of interesting properties and is thus one of the most widely used oxidic materials nowadays. In nature titanium(IV)oxide exists in three modifications: anatase, rutile and brookite. All of these polymorphs can be described as more or less distorted TiO_6 octahedra connected in different ways via edges and vertices.^{42, 70-72} While anatase and rutile crystallize in tetragonal arrangements, brookite exhibits an orthorhombic structure. In anatase and rutile two of the Ti-O bonds are slightly longer than the other four and for anatase the distortion is slightly higher compared to rutile. The octahedra share four edges in anatase and two in rutile as presented in Scheme 1-4. Brookite on the other hand exhibits a more complicated structure with 6 different Ti-O bond lengths.⁷³



Scheme 1-4: Crystal structures of (a) anatase; (b) rutile and (c) brookite. Scheme taken from Carp et al.⁴².

Anatase can easily be obtained by low-temperature synthesis methods and rutile becomes predominant upon annealing at elevated temperatures.^{42, 72} Brookite is hard to obtain and has thus hardly been investigated. In contrast, anatase and rutile have been studied intensely and are widely used in commercial and industrial products due to their high stability, non-toxicity and easy availability.⁴² Rutile is used as a white pigment in paints⁷⁴, papers⁷⁴, plastics⁷⁵ and even in food⁷⁶ and as a UV absorber in sunscreens.⁷⁷ Applications of the anatase modification use the energy of photogenerated charge carriers either (i) electrically (photovoltaics²⁴), (ii) chemically (photocatalysis³³) or (iii) for changing the surface of the semiconductor (photoinduced superhydrophilicity¹).

TiO₂ is an n-type semiconductor owing to a low amount of oxygen vacancies compensated by the presence of Ti³⁺. The valence band of titanium dioxide is formed by overlapping oxygen 2p orbitals, while the conduction band consists mainly of empty 3d orbitals of Ti⁴⁺. The band gaps of 3.2 eV for anatase and 3.0 eV for rutile are in the region of the energy of light in the near ultraviolet range, which makes both modifications suitable for solar light photocatalysis.^{13, 32, 33, 42, 70} At the same time the redox potentials of the photo-electrons and holes allows the reduction of protons and the oxidation of water, the key processes for water splitting (Scheme 1-5).^{32, 42, 70, 72} Moreover, the formation of hydroxyl radicals and the reduction of oxygen to superoxide ions are possible, which makes titanium dioxide a versatile material for photocatalysis.^{78, 79}



Scheme 1-5: Band gaps and redox potentials (reference: normal hydrogen electrode - NHE) for titanium dioxide (anatase). Standard potentials of redox couples important for photocatalytic processes are indicated on the right side. Data according to Linsebigler et al.⁷⁰ Henglein⁷⁹, Rao and Hayon⁷⁸ and Kudo and Miseki⁸⁰.

Anatase is generally considered to exhibit highest photoactivity among the different TiO₂ polymorphs.^{33, 42, 70} This fact has been attributed to its higher Fermi level, lower capacity for the adsorption of oxygen and higher number of hydroxy groups on its surface.⁸¹ However, several investigations revealed the enhancing effect of both, rutile and brookite.⁸²⁻⁸⁴ This finding has been attributed to an improved efficiency of charge separation owing to the formation of n-p junctions at the contact area of the different phases.^{82, 83}

If the photo-generated charge carriers attack the semiconductor material, corrosion of photocatalysts can occur. However, for anatase the oxidation of water is thermodynamically favoured. Thus, titanium dioxide is the most versatile photocatalyst material for environmental applications, which generally include the presence of water.^{13, 32, 33, 42, 70}

1.3.2 Titanium Dioxide Nanoparticles

Semiconductor nanoparticles have been shown to exhibit significantly increased photocatalytic activity compared to bulk materials,⁸⁵⁻⁸⁷ especially when a particle size below 20 nm is reached.^{88, 89} Such small structures lead to better charge transport and higher surface area, which is crucial for heterogeneous reactions.⁸⁶ Additionally, the

photocatalytic activity is strongly influenced by surface defects (especially oxygen vacancies), which are uprated for nanoparticles.⁸⁵

Properties of bulk materials are independent of their size, while for objects in the nanometer regime chemical and electronic behaviour depend on their expansion. The small amount of atoms present in nanosized objects leads to changes in the electronic structure of materials, which is specifically true for semiconductors and metals. The continuous bands created by overlap of many discrete states, are objected to 'quantum confinement'.⁹⁰ When the amount of atoms that participate in such a material is decreasing, the energy levels become discrete.⁹¹ The band gap of a semiconductor is thus widened and consequently the redox potentials of the charge carriers are enhanced. However, such changes in band gap are small and the photoactivity changes are rather assigned to the above mentioned effects.⁸⁵ In metals the quantum effect leads to confinement of electrons which induces changes in optical and electronic properties compared to bulk materials. Gold nanoparticles for example exhibit different colour depending on their size.⁹²⁻⁹⁴

Furthermore, owing to a drastically increased surface to volume ratio, surface atoms have higher influence on the overall properties of the material. Surface atoms exhibit higher energy compared to bulk atoms due to under-coordination. The high surface area of such nanostructures leads to high surface energy which results in agglomeration of the particles.⁹⁵ Thus, anticipating agglomeration is one major challenge in nanotechnology nowadays.

1.3.3 Synthesis of Titanium Dioxide Nanoparticles

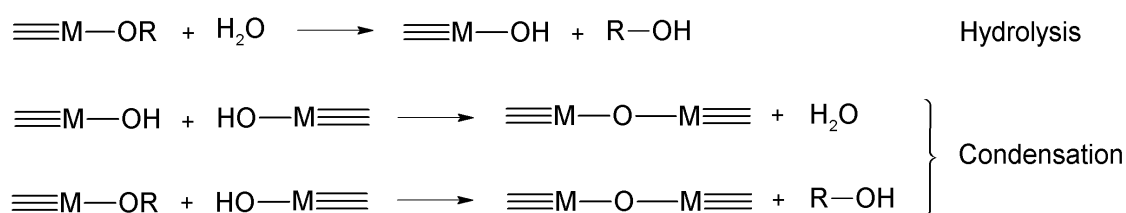
As discussed above, anatase is generally accepted to exhibit the highest photocatalytic activity and photostability among the modifications of titanium dioxide.^{44, 96} The initial crystalline phase formed upon synthesis of titanium dioxide nanoparticles is generally anatase,^{97, 98} which can be assigned to a less constrained molecular construction or to its lower surface free energy compared to rutile.⁹⁹ Approaches for the preparation of anatase nanoparticles include flame pyrolysis,^{100, 101} hydro- and solvothermal methods,^{97, 102-104} chemical and physical vapour deposition^{105, 106} and sol-gel process.^{107, 108} The size, shape and modification of TiO₂ nanomaterials can generally be tailored by any of these approaches. However, limitations for particle size tailoring, dispersibility and surface activity exist for most of these methods. The sol-gel process is a versatile synthesis method for highly dispersible titanium dioxide

nanoparticles with small particle sizes and high surface activity (high amount of Ti-OH groups) by mild reaction conditions.

Sol-Gel Process

The sol-gel process is a straightforward low-cost route for the synthesis of oxidic nanostructures under mild conditions. It was first developed as a low-temperature preparation method for silicon dioxide and later expanded on metal oxides.^{109, 110} Owing to its solvent based chemistry and mild reaction conditions the sol-gel process opens many possibilities for the structural design of oxidic materials.¹¹¹ Moreover, the incorporation of organic moieties has been widely applied for the preparation of inorganic-organic hybrid materials, due to the hydrolytic stability of Si-C bonds.¹¹²

Starting materials for a sol-gel process are silicon- or metal alkoxides or salts. Controlled hydrolysis and condensation of these precursors lead to the formation of colloidal sols as described in Scheme 1-6. Such sols are nanoparticle dispersions which can – depending on the conditions – either be stable or condense further to form a so-called gel, a continuous network enclosing a liquid phase.¹¹¹



Scheme 1-6: Reaction sequence of a sol-gel process.

The reactivity of (semi)metal alkoxides depends on the electronegativity of the metal atom and its ability to increase the coordination number. Silicon exhibits low reactivity in hydrolysis and condensation reactions owing to its low electrophilicity and its fully saturated fourfold substitution. Thus, acid or base catalysts are generally required for silicon sol-gel chemistry. Metal alkoxides in contrast are highly reactive against hydrolysis due to their more electropositive character and the larger number of coordination sites which facilitate nucleophilic attack.¹¹³ Thus, for the preparation of metal alkoxide nanoparticles the hydrolysis and condensation reactions need to be controlled in order to prevent the formation of bulk oxidic materials. Such control can be provided by introduction of complexing ligands¹¹² or addition of acids, which

anticipate extensive growth of the particles by electrostatic repulsion forces.¹⁰⁸ Another possibility is the reaction in microemulsion, where the particle size is limited to the size of the emulsion droplet.¹¹⁴ However, M-C bonds are in contrast to Si-C bonds broken upon hydrolysis. Hence, for the introduction of organic moieties strong complexing ligands, such as β -diketones or carboxylates, are required.¹¹² Such ligands provide thus control over the hydrolysis and condensation reactions and at the same time allow the introduction of organic groups.

1.4 Phosphonates and Phosphates on TiO₂ Surfaces

Most versatile coupling molecules for metal oxide surfaces are traditionally organoalkoxy- or chlorosilanes.^{115, 116} Due to the hydrolytic stability of Si-C bonds, they can be used in sol-gel processing resulting in M-O-Si-C bonds. However, silane coupling agents exhibit homocondensation and the conditions need to be adjusted carefully if monolayers of coupling molecules are aimed on metal or transition metal oxides.¹¹⁵⁻¹¹⁸ Thus, organophosphonates have been investigated thoroughly in recent years, regarding their applicability as coupling agents for metal oxide surfaces.¹¹⁹⁻¹²¹ Organophosphonates are compounds of the general formula R-PO(OR)₂. Bonding to metal oxide surfaces takes place via stable M-O-P bonds formed upon condensation of P-OR groups and M-OH surface groups. The bonding of organophosphates – of the general formula R-O-PO(OR)₂ – proceeds in a similar way and exhibits thus equal stability.^{122, 123}

1.4.1 Synthesis of Organic Phosphonates and Phosphates

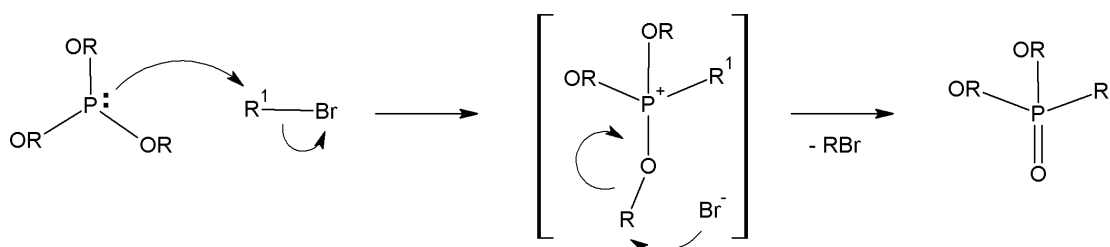
Synthetic approaches for the preparation of phosphonate and phosphate coupling agents are discussed beneath. The conversion of phosphonate or phosphate esters to the respective acids is normally carried out by hydrolysis under harsh conditions.¹²⁴ However, if milder conditions are required, a transesterification reaction with trimethyl silyl bromide can be carried out before hydrolysis.¹²⁵

1.4.1.1 Synthesis of Organic Phosphonates

Various synthetic approaches for the preparation of organophosphonate esters have been developed, starting either from alkyl halides or from unsaturated compounds:

Michaelis-Arbusov Reaction

Michaelis-Arbusov reaction¹²⁶ is a straightforward approach for the formation of organophosphonates by reaction of alkyl halides with triethyl phosphite. The reaction does not require any solvent and results in high yields of phosphonate upon heating to reflux.¹²⁴ The reaction is initiated by the nucleophilic attack of phosphorus on the α -carbon of the alkyl halide upon formation of a transition state (S_N2 -reaction). In a subsequent reaction step the formed trialkylphosphonium salt is dealkylated upon release of alkyl bromide (Scheme 1-7).



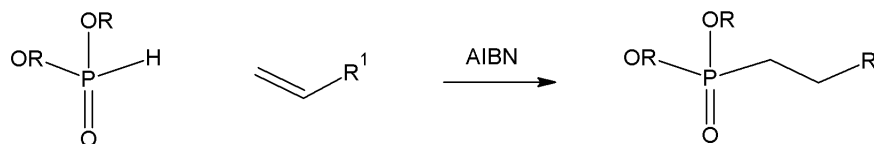
Scheme 1-7: Mechanism of the Michaelis-Arbusov reaction.

A versatile approach if lower reaction temperatures are required is the Michaelis-Becker reaction.¹²⁷ However, the reaction requires two steps and leads to lower yields of phosphonate. In a first step, a metal phosphite is prepared by reaction of dialkyl phosphite with a strong base. Subsequent S_N2 reaction with alkyl bromide analogue to the Michaelis-Arbusov reaction yields alkylphosphonates.¹²⁸

Pudovik-Abramov Reaction

The Pudovik-Abramov reaction¹²⁹ allows the preparation of organic phosphonates by reaction of P-H bonds (e.g. dialkyl phosphite) with unsaturated bonds.^{130, 131} It is widely applicable to a many unsaturated functionalities yielding a variety of different phosphonates. The reaction can proceed via radical or ionic mechanism, being initiated either by radical starter or base.¹³¹ The most versatile Pudovik-Abramov reaction is the

conversion of dialkyl phosphite with a terminal double bond initiated by decomposition of AIBN (Scheme 1-8).^{132, 133}



Scheme 1-8: Pudovik-Abramov reaction of alkenes.

1.4.1.2 Synthesis of Organic Phosphates

The preparation of phosphate coupling agents is simple compared their phosphonate analogues. Phosphates are generally obtained by the conversion of the respective alcohol with phosphoryl chloride.¹³⁴

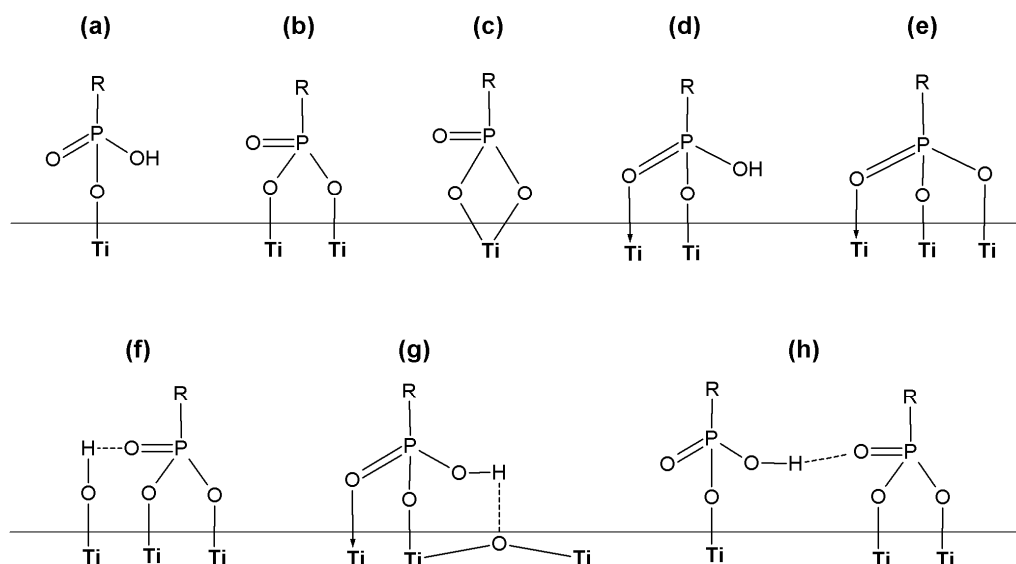
1.4.2 Modification of Titanium Dioxide with Organic Phosphonates

Organophosphonates exhibit high affinity to metal and transition metal oxides.^{119, 120, 135, 136} Their bonding to such surfaces involves the formation of M-O-P bonds whose stability is proven by many examples of metal phosphates and phosphonates reported in literature.^{122, 137, 138} Moreover, P-C and P-O-C bonds are stable towards hydrolysis and a variety of functional organic groups is available.^{132, 135, 139-143}

Highly stable Ti-O-P bonds are formed upon heterocondensation of P-OR groups with Ti-OH groups located at the surface of the particles.¹²³ In addition to that Ti-O-P bonds can also result from the coordination of the phosphoryl oxygen to titanium. As stated by Vioux and coworkers, the bond formation is likely to be initiated by such coordination of phosphoryl oxygen, which leads to an increased electrophilicity of the P atom and thus facilitates heterocondensation.¹³⁵ The bond formation of phosphonate esters with titanium dioxide surfaces, despite the relatively high hydrolytic stability of P-O-C bonds, is explained by this mechanism.¹³⁵

The formation of P-O-Ti bonds has been proven by FT-IR, ³¹P MAS NMR and elemental analysis.¹²³ Owing to the coordination of the phosphoryl oxygen to titanium and the heterocondensation of P-OH groups with Ti-OH groups, the connection can be

mono-, bi- or trivalent bridging or chelating.^{144, 145} Moreover, several investigations suggest that also hydrogen bonds are involved.¹⁴⁵ Thus, various different bonding modes are possible (Scheme 1-9).



Scheme 1-9: Schematic representation of different possible bonding modes for phosphonates on titanium dioxide surfaces: (a) monodentate, (b,c,d) bridging/chelating bidentate, (e) tridentate and (f,g,h) various possible modes involving hydrogen bonds.

However, investigations on the bonding modes of such species are difficult. Due to the formation of hydrogen bonds, the disappearance of P-OH and P=O vibrational signals do not prove trivalent bonding.¹⁴⁶ Furthermore, due to a variety of factors that influence the phosphorus shift, only limited conclusions about the bonding mode can be drawn from ³¹P NMR. Mutin and coworkers conducted ¹⁷O MAS experiments in order to determine the bonding mode of organophosphonates to titanium dioxide surfaces.¹⁴⁶ They observed chemical shifts consistent with bridging P-O-Ti bonds. Moreover, they concluded from the presence of residual P=O and P-OH bonds that several different binding modes are co-existent.

Furthermore, as stated by Guerrero et al.¹³⁵ phosphonic acids can break Ti-O-Ti bonds on the particles' surface under harsh conditions. Thus, the formation of bulk titanium phosphate species is possible when titanium dioxide is treated with phosphoric acid or upon heating during modification with organophosphonates.

1.4.3 Stability of Organophosphonates under Photocatalytic Conditions

The stable P-O-Ti bond is not broken upon thermal treatment of TiO₂ modified with organic phosphonates or phosphates as shown in numerous publications.^{10, 147-150} First investigations on the stability under photocatalytic conditions by Vioux and coworkers revealed a high stability of the P-O-Ti bond under photocatalytic conditions and indicated the formation of phosphate during UV illumination.¹³⁵ However, they did not confirm this assumption by extended characterization of the illuminated particles.

Furthermore, several investigations on the photocatalytic degradation of organic phosphonates in a fluid phase (gas or water) have been conducted.¹⁵¹⁻¹⁵⁸ However, the decomposition of pesticides and chemical warfare agents and the preclusion of the formation of toxic intermediates was of interest in all of these investigations. Hence, the organic compounds present in the fluid phase were studied while the anchoring of these compounds to the photocatalysts' surface was not considered. Only few publications exist where the degradation of organic phosphonates adsorbed to titanium dioxide surfaces is studied. Österlund and coworkers for example studied the photocatalytic degradation of diisopropyl fluorophosphates (DFP) and dimethyl methylphosphonate (DMMP) preadsorbed on wet and dry titanium dioxide surfaces.¹⁵⁹ They identified reaction intermediates and monitored the change of characteristic vibrational signals by DRIFT spectroscopy. Moreover, similar rates of decomposition for wet and dry surfaces were observed, but no conclusions on the mechanism of degradation were drawn. Hoffmann and coworkers performed similar investigations on DMMP including DRIFT and GC-MS analysis of the released degradation products.¹⁶⁰ They revealed the degradation of DMMP to PO₄³⁻ via a stepwise release of CH₃OH, which is further degraded to CO₂.

Moreover, enhanced photocatalytic activity has been detected by several groups in the presence of phosphate.^{136, 148, 149} Several investigations involved temperature treatment when organic phosphonates were applied,¹⁴⁹ which does not only generate phosphate on the surface of the particles, but also induces a migration inside the particles. Körösi et al. observed that the band gap energy is decreasing with increasing calcination temperature.¹⁴⁷ They assigned the decrease in band gap energy to the doping of phosphorus into the titanium dioxide framework. However, Zhao et al.¹⁴⁸ reported an enhanced photoactivity due to the formation of phosphate on the titanium dioxide surface by immersing the photocatalyst in H₃PO₄ even without calcination. They assigned the activity enhancement to the facilitated formation of hydroxyl radicals on

the photocatalysts surface due to hydrogen bond formation between the phosphate anions and water. Additionally, studies by Zhao and coworkers indicated an obstruction of the oxidation by surface trapped holes.¹⁴⁸ They assign this observation to a hindrance of interaction between the substrate and the TiO₂ surface.

1.5 Janus Particles

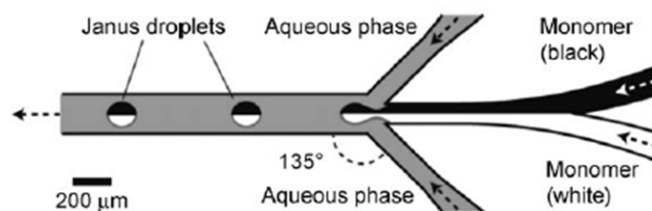
The term ‘Janus’ particles was first introduced by deGennes in 1992¹⁶¹ referring to the roman god Janus who had two faces looking into opposite directions. DeGennes described particles exhibiting different properties on their two hemispheres. His intention was the self-assembly of amphiphilic particles at the air-water interface resulting in a ‘breathing skin’ which would still allow small molecules to diffuse across the particle layer. Nowadays a huge potential of applications has been brought up, including switchable devices¹⁶², particular surfactants¹⁶³, optical devices^{164, 165} and many more.¹⁶⁶⁻¹⁷¹ For example particles with anisotropic superparamagnetic properties can be used to form superstructures for tissue engineering, photonic crystals and sensing.¹¹

1.5.1 Synthesis of Janus Particles

Generally, Janus particles are divided in particles exhibiting either (i) two compartments of different materials or (ii) anisotropic surfaces. A variety of synthetic approaches for the generation of particles exhibiting anisotropic properties has been developed.

Janus particles consisting of two different compartments can be prepared by microfluidic systems like electrohydrodynamic co-jetting of two different materials (Scheme 1-10). Such approaches have been extensively used in numerous variations¹⁷² for the preparation of Janus particles consisting of different polymers.^{162, 173-175} Two-component polymers have been prepared by this method in different shapes.^{162, 175-179} Moreover, Lahann and coworkers prepared nanoparticles exhibiting anisotropic magnetic properties for magnetically switchable surfaces by electrohydrodynamic co-jetting.¹⁸⁰ Additionally, photocuring or photolithography within such microfluidic

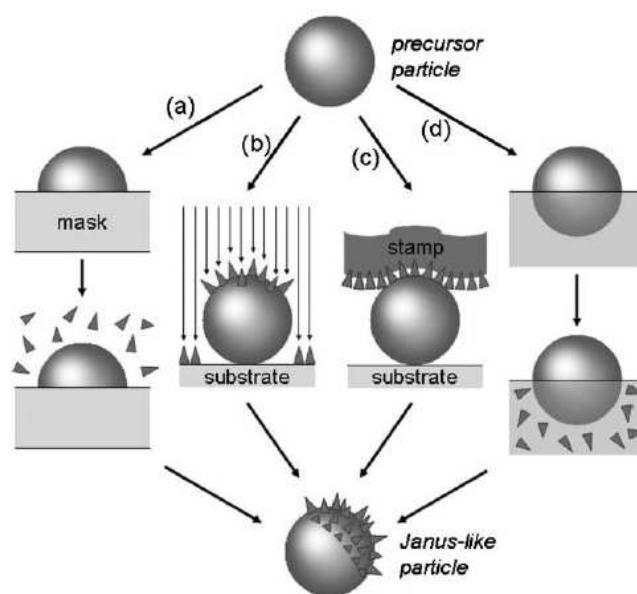
devices has been used for the preparation of polymer particles with anisotropic properties.¹⁸¹



Scheme 1-10: Schematic representation of a microfluidic device. Scheme taken from Wurm and Kilbinger¹⁸².

Snowman like structures of two different materials have been prepared by sonochemical routes taking advantage of nucleation-induced phase separation.¹⁸³

Most versatile approaches for the preparation of particles exhibiting anisotropic properties involve anisotropic surface modification. Various methods have been developed for the anisotropic surface functionalization of small particles – mostly based on the differentiating environment at interfaces.¹⁸⁴⁻¹⁸⁷ The oldest method is the masking of one hemisphere allowing the selective modification of the other. This approach has already been reported by Veysie and coworkers in 1988 for the preparation of amphiphilic glass microspheres.¹⁸⁸ Other approaches involve the deposition of particles at solid-gas, solid-liquid or liquid-liquid interfaces and subsequent functionalization from one side. In such monolayers, particles can be modified by sputtering,¹⁸⁹ microcontact printing^{185, 186} or Langmuir Blodgett deposition.¹⁸⁷ However, these approaches yield only a small amount of modified particles, as they all rely on the modification of a monolayer of particles. A versatile method for the anisotropic modification of a large amount of particles was recently developed by Granick and coworkers.¹⁹⁰ They used the differentiating environment at oil-water interfaces in particle stabilized emulsions, the so-called Pickering emulsions.¹⁹¹ This approach increases the yield of modified particles drastically as the water-oil interface area is maximized by the formation of an emulsion. The different strategies for the anisotropic surface modification of particles are presented in Scheme 1-11.



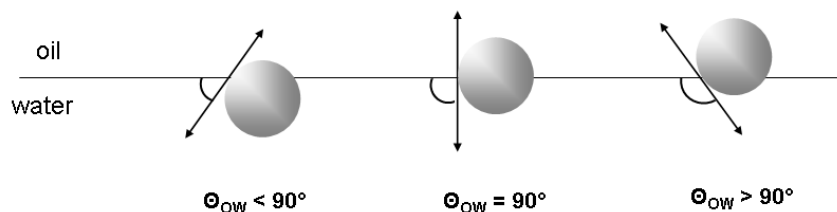
Scheme 1-11: Schematic representation of the strategies for anisotropic surface modification: (a) masking; (b) strategies using directional fluxes (sputtering); (c) microcontact printing and (d) strategies based on the differentiating environment at interfaces. Scheme taken from Perro et al.¹⁹²

1.5.2 Pickering Emulsions

Since Pickering discovered the ability of small particles to stabilize emulsions in 1907,¹⁹¹ colloidal particles represent an important class of emulsifying agents. Generally Pickering emulsions are oil-in-water (o/w) or water-in-oil (w/o) emulsions which are stabilized by solid particles. When an oil is mixed with the water phase containing colloidal particles, the colloids move to the interface between the two immiscible phases.

The efficiency of such colloids in stabilizing an emulsion depends on various parameters. Finkle et al. found that the stability and the type of emulsion depend on the wetting ability of aqueous and oil phase for the particles.¹⁹³ They stated that a powder must be wetted by both liquids to be able to form an interfacial film, and that the better wetting liquid will form the continuous phase. Schulman and Leja investigated the effect of different angles at the oil-water-solid line of contact on the type of emulsions.¹⁹⁴ They found that for contact angles slightly below 90° , oil-in-water emulsions were stabilized. However, if the contact angle is slightly greater than 90° , water-in-oil emulsions are stabilized. It was also shown that the contact angle needs to be near 90° to obtain stable emulsions (Scheme 1-12). Particles that are completely

wetted by either water or oil cannot be held at the interface but rather become dispersed in one phase.



Scheme 1-12: Schematic representation of the possible contact angles in Pickering emulsions.

Briggs observed that colloidal silica stabilized o/w emulsions, while carbon black stabilized w/o emulsions.¹⁹⁵ But when appropriate quantities of both compounds were mixed, the resulting mixture did not stabilize any emulsion. He concluded that for the stabilization of emulsions, the particles need to form a stable interfacial film. For this reason, the particles need to be in a state of incipient flocculation. No emulsion can be formed if the particles are either completely flocculated or completely dispersed.¹⁹⁶ The state of flocculation depends on the interparticle interactions and thus on the surface charge of the particles. As reported by Binks et al.,¹⁹⁷ the stability of emulsions can be controlled by the pH or by addition of electrolytes.

Numerous investigations have been conducted on emulsions stabilized by silica particles^{170, 197-201} including even mixtures of hydrophilic and hydrophobic silica particles.²⁰² Also different other metal oxides,²⁰³⁻²⁰⁵ clay mineral particles,²⁰⁶⁻²⁰⁸ noble metal particles,²⁰⁹ polymer particles,²¹⁰⁻²¹² and even cellulose fibrils^{213, 214} have been widely used for the stabilization of emulsions. Moreover, colloidal particles are used to stabilize emulsions in food or cosmetic products. For example, lipoprotein particles and fatty acid crystals have been used for stabilizing the emulsion state in mayonnaise or margarine.²¹⁵

Using TiO₂ particles as emulsifying agents can lead to various applications taking advantage either of their photocatalytic activity, UV absorption, non-toxicity, the good mechanical properties or the positively charged surface at pH below 6 (contrary to the negatively charged silica surface above pH 2).²¹⁶⁻²²² The most important application for titania particle stabilized emulsions are emulsifier-free cosmetics,^{221, 222} but also porous polymer foams have been prepared utilizing these emulsions.²¹⁶ Song et al. used titania nanoparticles not only for the stabilization of styrene-in-water emulsions, but

also for the first time for the initiation of the styrene polymerization by illuminating the emulsions with UV light.²¹⁷

1.5.3 Anisotropic Modification in Pickering Emulsion

The interface of water and oil provides the ideal medium for the synthesis of amphiphilic Janus particles because the reaction environment of the titania particles is differentiated between a hydrophobic and a hydrophilic phase.

In Pickering emulsions, the particles remain more or less mobile at the interface of two immiscible liquids. However, introducing oil-soluble coupling molecules that react very fast with the particles' surface, makes the particles less mobile and thus increases the stability of the emulsions.¹⁶³ It is still unclear to what extent the rotation of the particles at the interface effects the modification reaction. However, amphiphilic particles are more strongly adsorbed at the oil/water interface as shown by Binks and Fletcher.¹⁶³ Thus it is generally accepted that once the colloids have been grafted with hydrophilic and/or hydrophobic coupling molecules, rotation is hindered and the particles are immobilized at the interface. Especially for systems with fast reaction kinetics an amphiphilic surface is formed immediately.²²³ Nevertheless, frozen wax-in-water emulsions are often applied, where the rotation is prohibited.^{170, 190}

1.5.4 Proving Anisotropy by Imaging Techniques

The applicability of Pickering emulsions for the anisotropic surface modification of small particles has been proven extensively by electron microscopy. Most investigations in this field focus on the selective labelling of one hemisphere with metal nanoparticles.^{170, 223-225} Several investigations reported the selective decoration of a hemisphere containing amine groups with gold,^{170, 225} while Yang and coworkers utilized the interaction of poly(acryl amide) with colloidal gold.²²³ Moreover, confocal microscopy can be applied for the visualization of fluorescent hemispheres.¹⁸⁰ Chen and coworkers proved the anisotropic nature by adhesion force studies applying atomic force microscopy.²²⁶

1.6 Gold Nanoparticles

1.6.1 Properties of Gold Nanoparticles

Despite the inertness of bulk gold, its nanoparticles have been proven to be highly active catalysts for several reactions, including low-temperature CO oxidation,^{227, 228} oxidation of alcohols to acids and aldehydes,^{229, 230} the water-gas shift reaction^{231, 232} and the reduction of nitrogen oxides.^{233, 234} Moreover, possible applications for gold colloids in medicine are currently studied, focussing mainly on tumor detection^{235, 236} and drug carriers.²³⁷

Owing to the emerging use of gold nanoparticles in catalytic and medical processes, extensive research on the preparation of gold nanostructures is currently in progress.²³⁸⁻²⁴³

1.6.2 Synthetic Strategies for the Formation of Gold Nanoparticles

Colloidal gold has been known since ancient times and was originally used as a method for staining glass. The first pure sample of colloidal gold was prepared by Michael Faraday in 1857 by reduction of gold chloride with phosphorus.^{244, 245} Faraday described the obtained colloid as “finely divided metallic state” and ascribed the red colour to the small size of gold crystals.

Gold nanoparticles are generally prepared by the reduction of Au(III) (auric acid) to elemental gold in solution. The main challenge in the synthesis of gold nanostructures is the stabilization of small particles with narrow size distributions and minimum coarsening.

Turkevich Method

The traditional method for the preparation of colloidal gold was developed by Turkevich and refined by Frens.^{246, 247} In this approach, sodium citrate is applied for both, the reduction of auric acid and the stabilization of gold nanoparticles. The size of the formed particles can easily be tailored by the amount of citrate.

Brust Method

A synthetic approach for the preparation of hydrophobic gold nanoparticles was developed by Brust and Schiffrin.²⁴⁸ They reported the reduction of auric acid in toluene, enabled by the addition of tetraoctylammonium bromide (TOAB), which acts as a phase transfer agent. The gold nanoparticles exhibit limited stability owing to the weak interaction of TOAB with the gold surface. Hence, for long-term stabilization organic thiols are added, which bind to the gold covalently.²⁴⁹

Perrault Method

In 2009, Perrault reported the controlled growth of gold on gold nanoparticle seeds.²⁵⁰ In conjunction with hydroquinone gold nanoseeds can reduce auric acid on their surface. By this method particles of up to 250 nm can be obtained.

Martin Method

By this approach reported by Eah and coworkers, 'naked' gold nanoparticles can be obtained by the reduction of auric acid with sodium borohydride.²⁵¹ The addition of hydrochloric acid and sodium hydroxide allows the stabilization of small gold nanoparticles by electrostatic repulsion. Functionalization of these particles is performed bringing the aqueous suspension in contact with an organic solvent containing hydrophobic coupling molecules (i.e. organic thiols). The functionalized particles are then dispersed in the organic solvent, while the impurities remain in the aqueous phase. Moreover, Eah and coworkers report the preparation of 2D self-assembled films on air-toluene interfaces. Such monolayers of gold nanoparticles are formed when highly apolar coupling agents are applied for the functionalization. The modified particles are dispersible in n-hexane, but upon addition of toluene and slow evaporation of n-hexane, self-assembled monolayers at the air-toluene interface have been observed.

2 Scope of the Work

Aim of this work was the development of self-cleaning coatings for organic substrates. In order to protect the substrate from being degraded, a barrier layer between the substrate and the photocatalytic film was required. Owing to the high stability of P-O-M bonds and an inhibited hole oxidation,¹⁴⁸ organic phosphonates were assumed to suit the requirements. Moreover, upon formation of a dense film, the organic substrate as well as the organic moiety of the coupling agent might be protected from oxidation by hydroxyl radicals. However, the photocatalytic material could only be modified from one side in order to render the other side photocatalytically active. This work covers (i) investigations on the stability of photocatalytic particles modified with organic phosphonates under photocatalytic conditions and (ii) the anisotropic modification of photocatalytic nanoparticles.

2.1 Photocatalytic TiO₂ Nanoparticles

First investigations in this work focused on the development of a photocatalyst system exhibiting high photocatalytic activity and good film formation properties. A straightforward sol-gel synthesis method developed by Choi et al.¹⁰⁸ was investigated regarding the influence of different parameters on the size and morphology of the particles. The photocatalytic activity of films prepared from suspensions of these particles was investigated and compared with commercially available and literature known products.

2.2 Stability of Coupling Agents under Photocatalytic Conditions

The stability of the linkage between the substrate and the photocatalytic films is crucial in order to provide long term stability of the coating. Hence, different coupling

agents were investigated regarding their stability under photocatalytic conditions. The kinetic of the degradation reaction was investigated under various conditions in order to gain information on the mechanism of degradation and on the initiating species.

2.3 Anisotropic Surface Modification

A differentiated surface of TiO₂ nanoparticles was required in order provide interaction with the organic substrate on the one hand and render the other side accessible for photocatalysis on the other hand. For this reason, anisotropic surface modification represented another main issue of this work. Modification in Pickering emulsion is a straightforward technique for the preparation of large amounts of particles exhibiting anisotropic properties. One main scope of this work was thus the investigation of Pickering emulsions stabilized by titanium dioxide nanoparticles. Anisotropic modification of these particles was performed upon addition of hydrophobic or hydrophilic coupling molecules to the Pickering emulsion. An additional challenge that should be covered in this work was proving the anisotropic modification by imaging techniques.

3 Results and Discussion

3.1 Photocatalytic TiO₂ Nanoparticles

For photocatalytic coatings, nanoparticle suspensions are required exhibiting significant photocatalytic activity and good film formation properties. Subsequent modification with organic coupling agents demands a high amount of surface hydroxyl groups and for modification in Pickering emulsion a spherical shape is favorable. Hence, a synthetic approach for the preparation of TiO₂ nanoparticles exhibiting the described properties was aimed.

3.1.1 Sol-Gel Synthesis of TiO₂ Nanoparticles

Various preparation methods for photocatalytic titanium dioxide nanoparticles have been described in literature using titanium salts or alkoxides as precursors, such as thermolysis, hydrothermal treatment or the sol-gel process.¹⁰¹⁻¹⁰⁴ For further modification with phosphonates, a sol-gel synthesis method – which leaves many free surface hydroxyl groups for subsequent modification reactions on the particles' surface – was chosen. A simple sol-gel synthesis for anatase nanoparticles with diameters of about 5 nm was developed by Choi et al.¹⁰⁸ and refined by Ivanovici.²⁵² In this procedure Ti(OⁱPr)₄ in ethanol is hydrolyzed by addition to distilled water acidified with nitric acid. Anatase nanoparticles obtained after evaporation of the solvent still contain nitrate as found by Choi et al.¹⁰⁸ and confirmed by Ivanovici.²⁵² This straightforward method does not require harsh conditions and yields phase pure spherical anatase nanoparticles that are redispersible in water. The only drawback is the high solvent volume necessary for the synthesis of a rather low amount of particles. Thus, the first aim of this work was a scale-up of the synthesis method reducing the solvent volume by increasing the precursor concentration. Thus, titanium dioxide nanoparticles were prepared according to the procedure by Ivanovici²⁵² varying the precursor concentration

in ethanol between 0.17 M and 3.6 M. After three days of stirring at room temperature, samples were taken for DLS measurement and the solvent was removed under reduced pressure. In order to prove the reproducibility, three samples for every precursor concentration were prepared and the particle size of the original suspension as well as the particle size of the isolated particles were measured after redispersion. Before DLS measurement, the optical density of the DLS samples was adjusted to 0.02 in order to prevent multiple scattering. Particle size measured from the original suspension was found to be more reproducible compared to dried and redispersed particles due to a lower degree of agglomeration.

As observed from Figure 3-1, the particle size increased linearly from 4.2 ± 0.4 nm to 9.8 ± 0.4 nm diameter with increasing precursor concentration (Figure 3-1). However, the standard deviation did not increase with increasing particle size. Thus, the particle size can be tailored by varying the precursor concentration and narrow size distributions are obtained for all particle sizes.

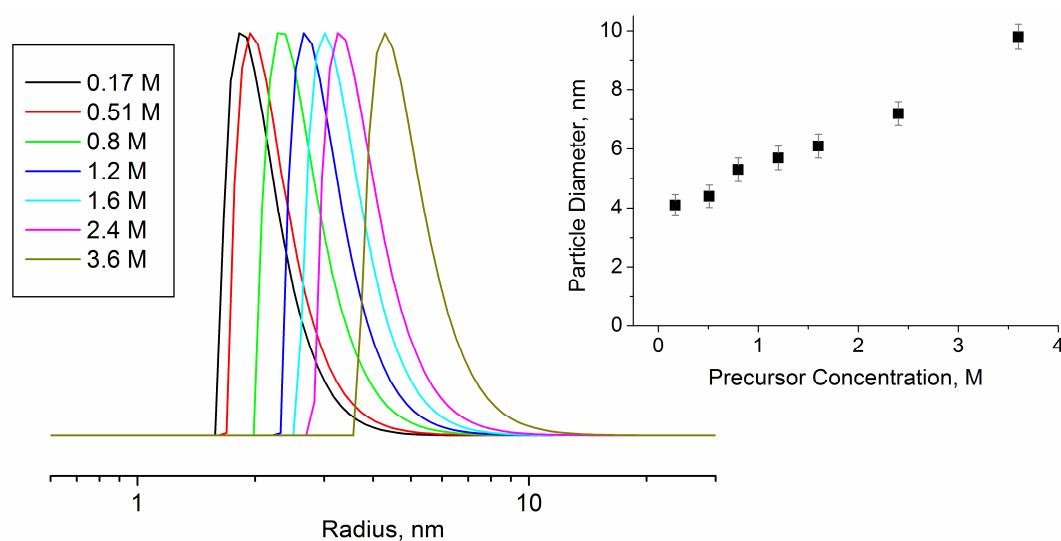


Figure 3-1: DLS plot of titanium dioxide nanoparticles prepared from different precursor concentrations. Insert: graph particle size versus precursor concentration, grey bars: standard deviation.

The sizes of the smallest particles as well as the largest particles were proven by HR-TEM. The smaller particles were found to exhibit a diameter of about 4 nm, whereas the larger particles obtained with higher precursor concentration were about 10 nm in diameter (Figure 3-2). These observations confirmed the results obtained by light

scattering. Furthermore, spherical particles were obtained for all precursor concentrations as seen from the electron microscope images.

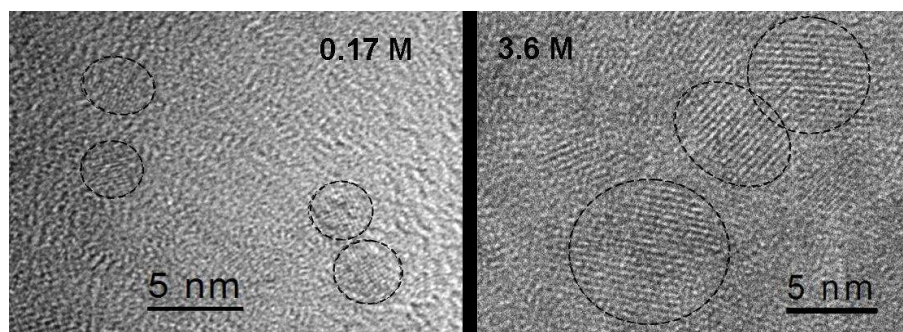


Figure 3-2: HR-TEM images of titanium dioxide nanoparticles prepared with 0.17 M $\text{Ti}(\text{O}^i\text{Pr})_4$ (left) and 3.6 M $\text{Ti}(\text{O}^i\text{Pr})_4$ (right).

XRD analyses presented in Figure 3-3 revealed pure anatase phase (JCPDS-21-1272) for samples prepared from low precursor concentrations (0.17 M – 1.2 M). At higher precursor concentration Rietveld analysis revealed increasing contribution of brookite with increasing precursor concentration.

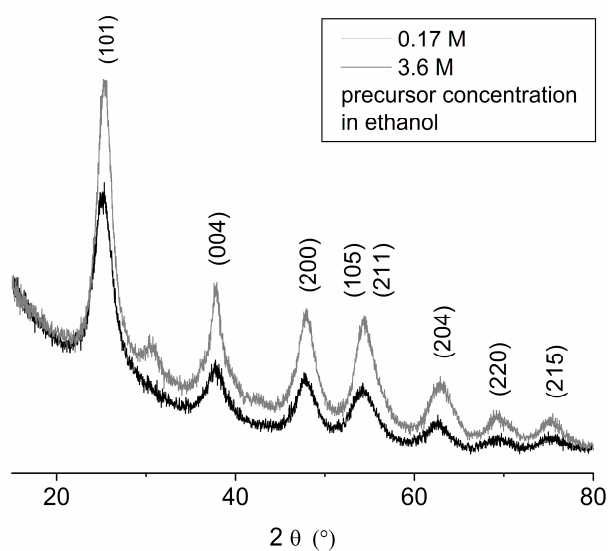


Figure 3-3: XRD plot of titanium dioxide nanoparticles prepared with 0.17 M and 3.6 M precursor concentrations.

For 3.6 M a composition of ~60% brookite, ~40% anatase and a small amount of rutile (~3%) was observed. However, an enhancing effect on the photocatalytic activity of both, brookite and rutile has been reported before.^{84, 253} Moreover particle size was found to be 3.6 nm for the anatase phase for both samples and 1.9 nm for the brookite particles at high precursor concentrations.

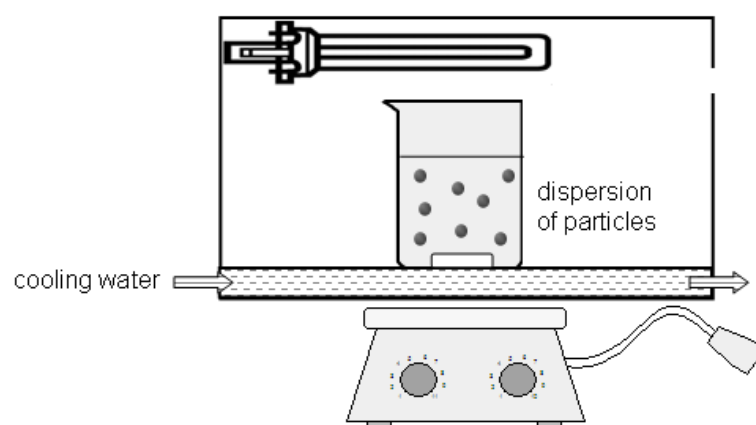
Thus, it has been shown that the particle size can be tuned between 4 and 10 nm without increasing the standard deviation by adjusting the precursor concentration. Particle size of TiO₂ nanoparticles is typically controlled by varying the pH,^{254, 255} temperature treatment²⁵⁶ or by addition of surfactants.²⁵⁷ However, also the precursor concentration has been reported previously to control the particle size.²⁵⁸ As all other factors were kept constant, the larger particle size can definitely be assigned to the higher precursor amount present in the reaction mixture. Additionally, the morphology of the particles can be tuned from pure anatase at low precursor concentration to 40% anatase and 60% brookite at high precursor concentrations. Sol-gel synthesis of TiO₂ usually yields amorphous titanium dioxide, which is converted to anatase at moderate temperature treatment. Brookite, however, is hard to obtain and only few low temperature synthesis methods have been reported to yield this modification. Generally basic conditions,²⁵⁹ heat treatment²⁶⁰ or phase selective additives²⁶¹ are required for the selective formation of brookite. Phase pure brookite has been prepared by hydrothermal treatment of Ti(SO₄)₂ under basic conditions.²⁶² Vioux and coworkers were able to control the morphology by etherolysis and alcoholysis of TiCl₄ with different alcohols.²⁶³ However, anatase-brookite mixed phase nanoparticles have been obtained by hydrolysis of Ti(OⁱPr)₄ in nitric acid and an increasing brookite content has been reported when the Ti/H₂O ratio was increased, which is in concordance with the presented results.²⁶⁴ Moreover, the yield per volume solvent could be increased 20-fold by increasing the precursor concentration compared to the highest yield obtained by Ivanovici.

3.1.2 Photocatalytic Activity of Sol-Gel TiO₂ Nanoparticles

3.1.2.1 Photocatalytic Activity in Suspension

The photocatalytic activity of the prepared TiO₂ nanoparticles was investigated by monitoring the degradation of methylene blue in an aqueous solution containing the dispersed particles according to a procedure by Nogueira and Jardim.⁶² As a fast and

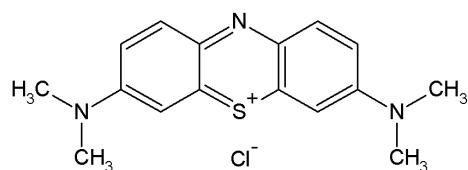
highly reproducible method for monitoring the degradation of an organic substance was required, methylene blue was chosen as a substrate, whose extent of degradation can easily be studied by UV-Vis measurements. Illumination experiments were conducted in a water-cooled chamber equipped with magnetic stirring and two 9 W UVA black light lamps (Sylvania Lynx-S 9W BLB) (Scheme 3-1). Furthermore, in order to ensure the presence of oxygen, the chambers exhibited a hole with 1 cm diameter. The presence of oxygen is essential for photocatalysis in order to prevent charge accumulation upon the consumption of holes (either for the formation of hydroxyl radicals or for direct oxidation). Electrons can be transferred to adsorbed oxygen to produce O_2^- radicals, which react with H_2O to produce hydroxyl radicals as discussed in the introduction.



Scheme 3-1: Experimental setup for the illumination of particle dispersions.

0.25 g/L suspensions of the corresponding particles (10 nm diameter) in 20 μ M methylene blue (MB, Scheme 3-2) solution were prepared and stirred for 1 hour in the dark prior to UV illumination. The degradation of methylene blue was monitored by UV-Vis measurements of centrifuged samples taken after stirring in the dark and various illumination intervals. Moreover a reference sample without particles was investigated, in order to account for eventual auto-degradation of methylene blue under UV illumination. The absorption maximum of the methylene blue dye at 664 nm was taken as a measure for the concentration of the dye (C). The initial absorbance at 664 nm of the suspensions stirred in the dark was taken as a measure for the initial dye concentration (C_0). The adsorption amount is the difference between the absorption of the methylene blue solution and the sample stirred in the dark for 1 hour. Figure 3-4

shows an example of a sequence of UV-Vis spectra taken after various illumination times.



Scheme 3-2: Methylene Blue (MB).

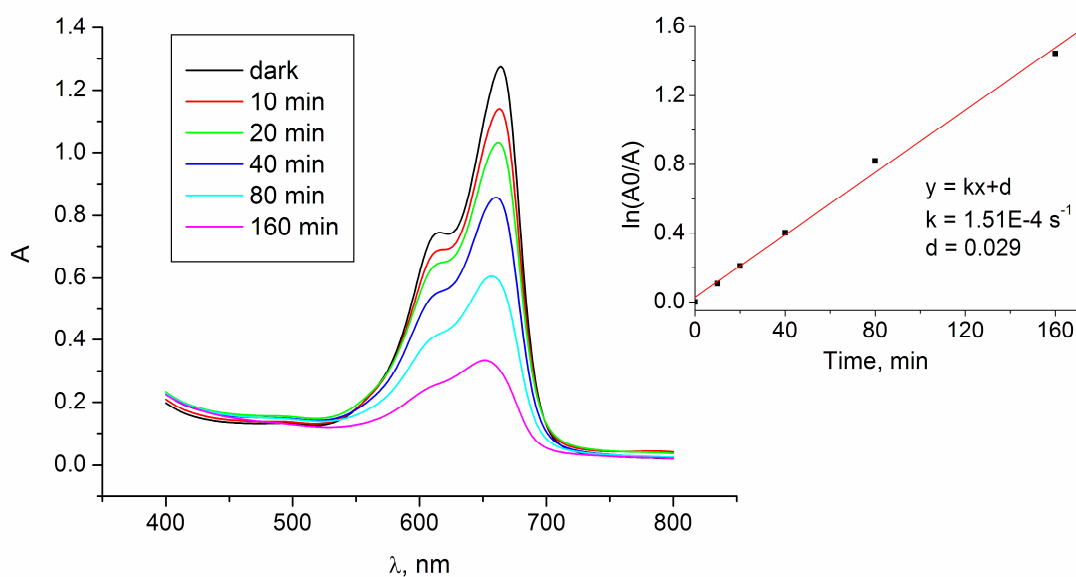


Figure 3-4: UV-Vis spectra of Methylene Blue illuminated in the presence of TiO₂. Insert: Plot for determining the reaction constant k.

According to literature reports, the degradation of methylene blue follows Langmuir-Hinshelwood reaction kinetics.^{31, 61, 266} The rate law is presented in Equation 12 and after integration Equation 13 is obtained.

$$k[A] = -\frac{d[A]}{dt} \quad \text{Equation 12}$$

$$kt = \ln\left(\frac{A_0}{A}\right) \quad \text{Equation 13}$$

Plotting $\ln(A_0/A)$ versus time the rate constant k can be determined from the slope in the graph. Thus, $\ln(A_0/A)$ is plotted versus time to determine k (Figure 3-4-insert), which is a measure for the photocatalytic activity.

As explained in the introduction, no normed testing procedure for the photocatalytic activity is existent. Hence, the efficiency of the prepared TiO₂ nanoparticles in degrading methylene blue can only be estimated in comparison with the commercially available standard catalyst Evonik AEROXIDE[®] TiO₂ P25 (P25, TiO₂ nanoparticles of 21 nm diameter consisting of 80% anatase and 20% rutile). In Figure 3-5 the adsorption and k values obtained for sol-gel synthesized particles are compared with the standard photocatalyst P25.

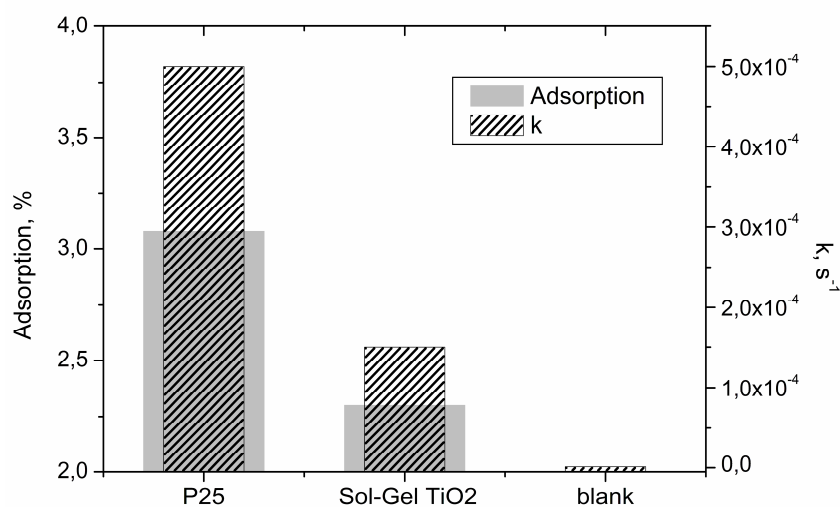


Figure 3-5: K-values for P25 and sol-gel synthesized titanium dioxide nanoparticles.

As seen from Figure 3-5, the photocatalytic activity of the TiO₂ nanoparticles was found to be low compared to commercially available Evonik P25. However, comparing with the blank experiment, the sol-gel particles exhibit significant photocatalytic activity. A possible explanation for the lower activity compared to P25 might be worse adsorption of dye on the sol-gel particles (Figure 3-5) owing to a high amount of ionic species (mainly nitrate) covering the surface. Moreover, an enhancing effect can be assigned to a synergism between anatase and rutile present in P25 as found by Ohno et al.²⁵³ Indeed, an enhancing effect has also been ascribed to brookite,⁸³ present in the sol-gel synthesized TiO₂ nanoparticles. However, the enhancing effect on the photocatalytic activity for anatase-brookite nanoparticles has been found to be highest at 25% brookite,^{83, 261} while the studied particles exhibited a brookite content of 60% (prepared from 1.6 M Ti(OⁱPr)₄). The found degradation rate for MB is comparable to literature reports on anatase-brookite nanoparticles with 50% brookite,²⁶¹ which is in the range of the brookite content of the investigated particles.

However, for film formation P25 is not suitable due to its bad dispersibility. Scattering of light on large agglomerates leads to opaque films, which makes this material unsuitable for films on transparent surfaces like glass or plexiglass.^{267, 268} Moreover, owing to their pyrolytic preparation route, P25 particles exhibit a lower amount of surface hydroxyl groups available for condensation reactions compared to sol-gel TiO₂ nanoparticles.²⁶⁹ Hence, the connection of P25 to glass surfaces is instable^{65, 268, 270} and only low interaction with coupling molecules required for films on organic surfaces can be achieved. Thus, the sol-gel prepared TiO₂ nanoparticles are used for further investigations, even if higher photocatalytic activity can be achieved with commercially available P25.

As the main aim of this work was the preparation of photocatalytically active coatings, films of the prepared TiO₂ nanoparticles on glass substrates were prepared and their photocatalytic activity was tested.

3.1.2.2 Photocatalytic Activity of Films on Glass

Films of sol-gel titanium dioxide nanoparticles on glass substrates were prepared in order to measure their photocatalytic activity. Different formulations of suspensions with 4 g/L particle concentration were tested regarding the homogeneity of the films after dip-coating. Glass substrates were cleaned and immersed in 3 M HF for 30 seconds to activate the surface. Subsequently the substrates were washed with acetone, dried and dip-coated in different suspension formulations with 0.4 cm/s withdrawing velocity.

It was found that suspensions in pure water or with high water/ethanol ratios resulted in very inhomogeneous films (Figure 3-6).

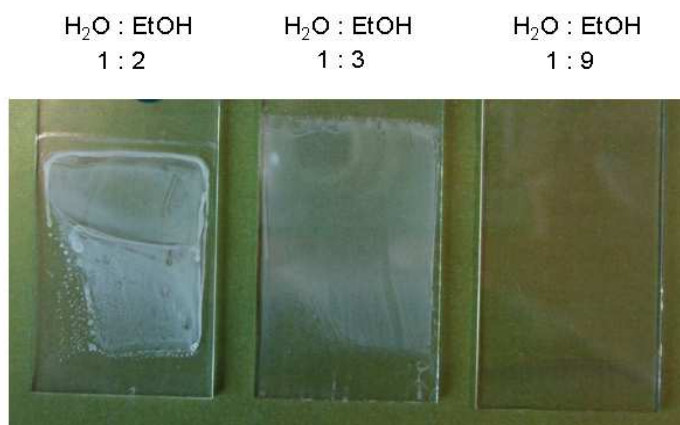


Figure 3-6: Films of titanium dioxide nanoparticles dip-coated from different suspensions.

Owing to its high surface tension and low fugacity, the homogeneity of the films increased with decreasing amount of water in the suspension. However, the TiO_2 particles are not dispersible in pure ethanol. For this reason, the optimal balance between particle dispersibility and film formation was investigated. A water/ethanol ratio of 1:9 was found to result in homogeneous films. However, from the DLS plot (Figure 3-7) a high amount of agglomerates was observed between 20 and 300 nm.

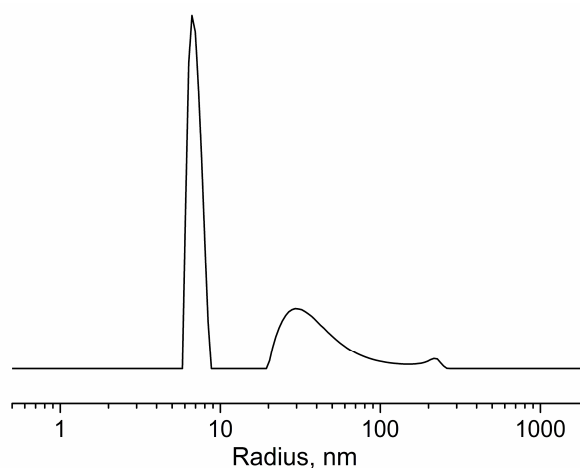
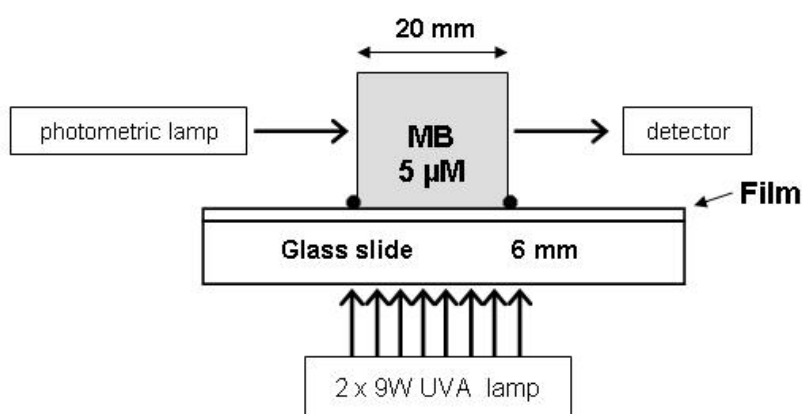


Figure 3-7: DLS plot of titanium dioxide nanoparticles dispersed in water/ethanol 1:9.

The dispersibility can be improved either (i) by addition of a surfactant or (ii) by dilution of the system. For this reason, the commercially available surfactant P123 was added to the suspensions.

Dip coating was performed from these suspensions according to the procedure described above. The films were dried at 100°C for 30 minutes before depositing the subsequent layer. The coating process was repeated several times, therefore several layers of TiO₂ nanoparticles were deposited on the substrates (5 or 8). After deposition of the last layer, the films were calcined at 500°C and the film thickness was measured by ellipsometry. The photocatalytic activity was measured by tracking the degradation of methylene blue in an experimental setup shown in Scheme 3-3. 1.6 mL of 5 μM methylene blue solution were brought in contact with the film and illuminated with UVA light. The degradation of methylene blue was investigated by in-situ UV-Vis measurements. Data analysis was then performed similar as explained in section 3.1.2.1 for suspensions of particles. As illumination with UV light was performed through the glass slide, the slides exhibited similar thickness and composition. The use of quartz glass was not necessary because the intensity of UV radiation penetrating through the substrate was constant for slides with similar thickness.



Scheme 3-3: Experimental setup for the measurement of the photocatalytic activity of films.
Scheme taken from Lorret.¹⁶⁰

As seen from Figure 3-8, thin films of about 15 nm thickness were obtained (due to dilute suspensions). These films exhibit significant photocatalytic activity compared to a blank glass slide (Figure 3-8). However, the photocatalytic activity of the films was significantly lower compared to commercially available Pilkington glass with similar film thickness.

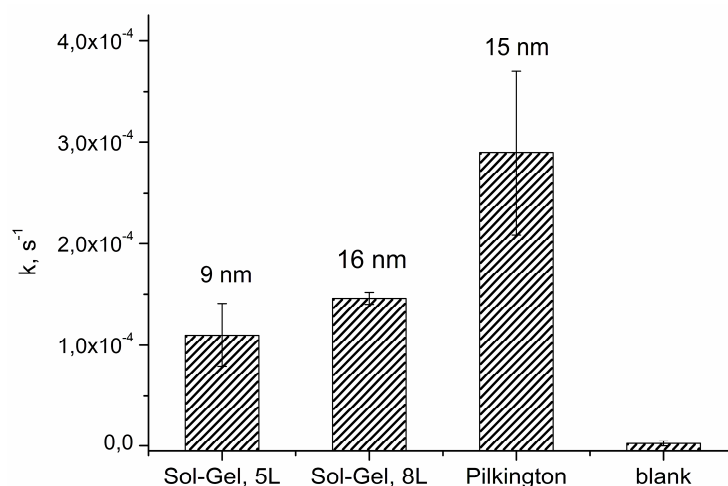


Figure 3-8: Photocatalytic activity of titanium dioxide films with different thickness on glass substrate.

Pilkington glass is obtained by atmospheric pressure chemical vapor deposition (APCVD) using TiCl_4 and ethyl acetate as precursors. Before deposition of the photocatalytic film, a silicon oxide layer is deposited on the glass surface in order to prevent the migration of alkaline metal ions into the TiO_2 coating. Decreased efficiency of photocatalytic coatings has been observed by Heller and coworkers on soda-lime glass compared to quartz glass.²⁷¹ They assigned this effect to the introduction of recombination centres by alkaline metal ions. Films of TiO_2 particles deposited by APCVD have been reported to exhibit a thickness of 15 nm, while SEM investigations revealed particle sizes of 30 nm. It has been concluded that the particles are consequently broad domes rather than spherical particles.⁶⁵ Pilkington ActiveTM TiO_2 films have been reported to consist of anatase and rutile.²⁷² Hence, the lower photocatalytic activity of films of sol-gel TiO_2 nanoparticles compared to Pilkington ActiveTM glass can be ascribed to inhibition by alkaline metal ions. Moreover, owing to larger particle sizes, a higher surface roughness is likely for Pilkington glass, leading to a higher surface area available for photocatalysis.⁶⁵

Unfortunately, due to different experimental conditions the photocatalytic activity of films cannot be compared to the results obtained for particle dispersions.

It is concluded that the prepared sol-gel TiO_2 nanoparticles are suitable for the formation of photocatalytic films. The particles exhibit significant photocatalytic activity and show good film formation behaviour.

3.1.3 Conclusions

TiO₂ nanoparticles with diameters ranging from 4 to 10 nm have been prepared by a straightforward low-temperature synthesis method. The particles are nicely redispersible in water owing to nitrate on their surface and show spherical shape. The phase composition of the particles can be tuned between pure anatase and 4:6 anatase/brookite by adjusting the precursor concentration. Investigations on the photocatalytic activity of the particles in suspension and as films on glass substrates revealed significant photocatalytic activity, even if commercially available systems could not be surpassed. The high amount of surface hydroxyl groups available for subsequent modification reactions and the spherical shape of the obtained particles render the obtained particles appropriate for further modification reactions.

3.2 Stability of Organophosphonates under Photocatalytic Conditions

In order to achieve interaction of photocatalytic titanium dioxide nanoparticles with organic substrates, coupling agents are required. Highly stable coupling molecules are needed which should anticipate release of particles and degradation of the organic substrate. It is well known that organophosphonates exhibit a stable interaction with titanium dioxide surfaces as discussed in the introduction. Hence, the above prepared sol-gel TiO₂ nanoparticles (7 nm diameter) were modified with different organic phosphonates and phosphates and the UV stability of different organic moieties under various conditions was investigated in order to elucidate the mechanism of degradation. The photocatalytic degradation behaviour of organic molecules in the presence of TiO₂ nanoparticles has been investigated thoroughly recently in order to exclude the formation of toxic intermediates when photocatalytic degradation is applied for wastewater treatment or self-cleaning surfaces.^{1, 32, 273-276} It is nowadays well known that in the presence of water hydroxyl radicals are created on the surface of photocatalytic particles, which can initiate the degradation of any organic compound.³² However, the degradation of substances that bind to the surface of the photocatalyst has hardly been investigated up to now as discussed in the introduction. It is assumed that in the degradation of such molecules direct hole oxidation and oxidation by surface trapped holes might play a major role, owing to the steric proximity to the photocatalyst.³⁶ However, as elucidated in the introduction, these processes have been reported to be hindered in the presence of phosphonate.¹⁴⁷ Moreover, as discussed above the P-O-Ti bond was found to be photocatalytically stable. Thus, only the organic part is degraded, for which two possibilities exist: either (i) the P-C bond breaks or (ii) the organic moiety is degraded sequentially. This mechanism can be different for unequal organic moieties. For this reason, phosphonates with different organic moieties were investigated regarding their photocatalytic degradation. Another question that arises is, what species is left on the surface if the P-O-Ti bond is not broken. Eventual phosphate remaining on the particles' surface might lead to increased photocatalytic activity, as found in earlier investigations.^{147, 148} Such phosphate doped photocatalysts are obtained by calcination of titanium dioxide photocatalysts modified with organophosphonates.¹⁴⁸ Taking into account that the organic moieties are degraded upon UV illumination, it might be possible to prepare phosphate enhanced photocatalysts in-situ upon

illumination, which would render the calcination step unnecessary. Thus, the particles were investigated thoroughly after complete degradation of the organic moieties. Furthermore, it is assumed that the degradation of organic phosphates and phosphonates might exhibit unequal reaction kinetics, due to the different stabilities of P-C and P-O-C bonds and different electronic properties. In addition to that, surface coverage is believed to play a key role for the degradation kinetics due to shielding of the surface against the species required for photocatalysis: photons, water and oxygen. For this reason, degradation kinetics was studied for different organic moieties under different conditions.

Thus, the degradation behaviour of organic phosphonates and phosphates bound to the surface of titanium dioxide nanoparticles under illumination with two 9 W UVA black light lamps was investigated. Sol-gel TiO₂ nanoparticles (10 nm) were prepared and modified with phenylphosphonic acid (PPA), phenylphosphoric acid (PPoA) and DPA by stirring for 3 days in methanol/water 3:1 mixtures containing 3 mM coupling agent according to a procedure by Ivanovici.²⁵² After centrifugation, the modified particles were washed thoroughly with ethanol to remove unreacted coupling agent, dried and analyzed by ³¹P MAS NMR, ¹³C CPMAS NMR, FT-IR, TGA and elemental analysis. Titanium dioxide nanoparticles modified with different phosphonic and phosphoric acids were investigated regarding degradation intermediates and product. Furthermore, the influences of different parameters and coupling molecules on the kinetics of the degradation reaction were investigated. In order to study differences in the degradation of phosphates and phosphonates, PPA@TiO₂ and PPoA@TiO₂ were compared regarding the kinetics of their degradation under UVA illumination. In a subsequent study, the degradations of PPA@TiO₂ and DPA@TiO₂ were compared regarding their kinetics in order to elucidate the degradation mechanism of organic compounds that exhibit a covalent connection to the photocatalyst. In addition, the degradation kinetics of modified particles exhibiting different surface coverage were investigated. Moreover, the photocatalytic activity of the degradation products was investigated and compared with the unmodified titanium dioxide nanoparticles.

3.2.1 Degradation of Phenylphosphonic acid

Realistic conditions for the investigations on the photocatalytic stability include the presence of water. Thus, for first investigations particles modified with moderately hydrophobic PPA were applied due to their water-dispersibility and easy accessibility.

The degradation experiments were conducted in an experimental setup similar to the one presented in section 3.1.2.1. PPA@TiO₂ was dispersed in water at a concentration of 2 wt% applying an ultrasonic finger and subsequently exposed to UV light in an illumination chamber. In Figure 3-9 the FT-IR spectra after different times of illumination are presented.

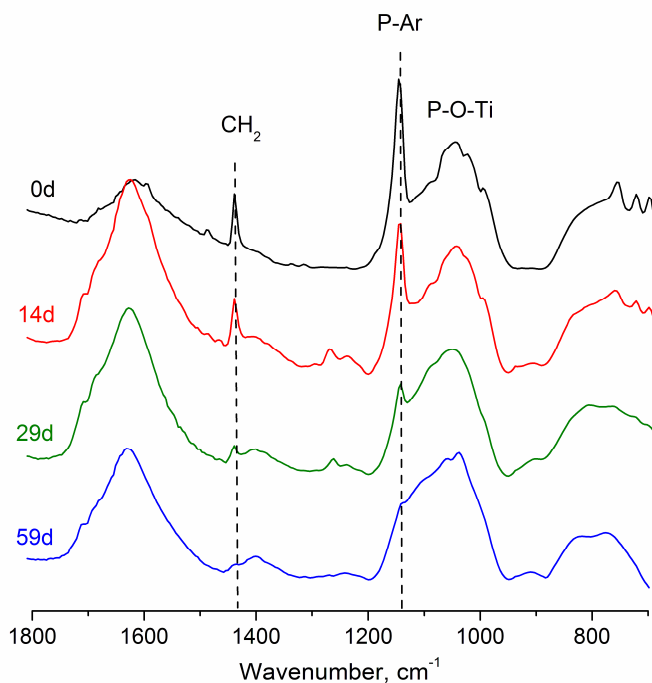


Figure 3-9: FT-IR spectra of PPA@TiO₂ after different times of UV-illumination.

The P-O-Ti signal between 970 and 1150 cm⁻¹ maintained its intensity throughout the illumination process. Thus, it is assumed that the P-O-Ti bond is stable which is in agreement with earlier investigations on the degradation of DMMP.^{158, 159} However, the P-Ar (1150 and 1450 cm⁻¹) vibration was decreasing with illumination time compared to the Ti-O and the P-O-Ti signal. From this observation it can be concluded that the organic moiety was degraded. However, from FT-IR a breakage of the P-C bond cannot be verified due to overlapping of an eventually arising P-aliphatic/olefinic signal with the broad P-O-Ti band. Intermediately arising weak signals at 1220 and 1400 cm⁻¹ are assigned to olefinic or alcoholic degradation intermediates. In order to identify such intermediates, the degradation was also tracked with ¹³C CPMAS NMR. From FT-IR, a phosphate species seemed to be left on the surface of the particles after degradation of the organic moiety. However, incomplete degradation would also present phosphonates

on the surface. Thus, the reaction was also tracked with ^{31}P MAS NMR, which allows to distinguish between phosphate and phosphonate species.

Figure 3-10 presents ^{31}P MAS NMR collected after different times of illumination. While the phosphonate was identified at 15 ppm before illumination, a second signal at -2 ppm was arising upon illumination which could be assigned to a phosphate species. After 95 days of illumination the degradation was complete and only phosphate was left on the surface.

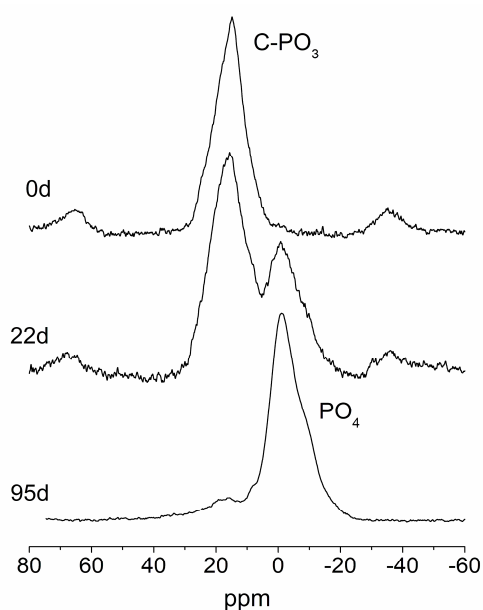


Figure 3-10: ^{31}P MAS NMR of PPA@TiO₂ after different times of illumination at 2 wt%.

Figure 3-11 presents the ^{13}C CPMAS NMR spectra measured after different times of illumination of PPA@TiO₂. The spectrum without illumination exhibited an intense aromatic signal for the phenyl ring and a sharp signal in the CH₃ region. While the aromatic band was decreasing with illumination time, the CH₃ signal was increasing. Moreover, after 22 days of illumination minor peaks were observed between 50 and 70 ppm (alcohol), at 110 ppm (olefin) and between 150 and 170 ppm (aldehyde or carboxylate). However, these signals have disappeared after 95 days of illumination indicating degradation intermediates. Thus it is concluded that the degradation proceeds rather sequentially than via breakage of the P-C bond.

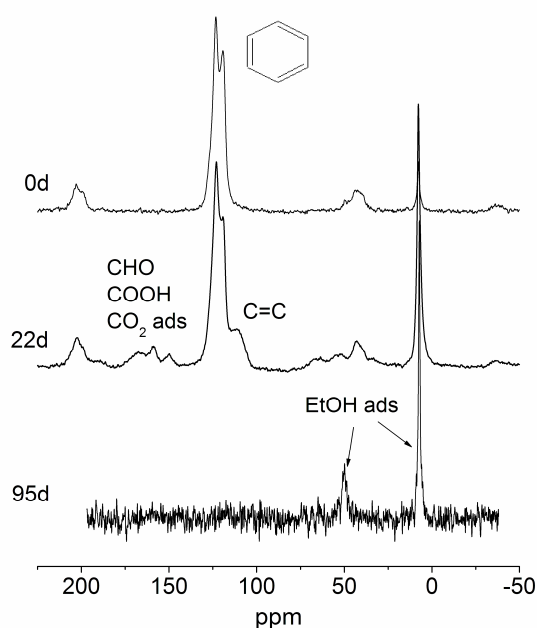


Figure 3-11: ^{13}C CPMAS NMR of PPA@TiO₂ after different times of illumination at 2 wt%.

The methyl signal on the other hand did not disappear upon illumination. Non-spinning ^{13}C HPDEC NMR of the illuminated sample (Figure 3-12) revealed a second signal at 55 ppm, indicating that the signals can be assigned to ethanol, which might exhibit hydrogen bonds to Ti-OH groups on the TiO₂ surface.

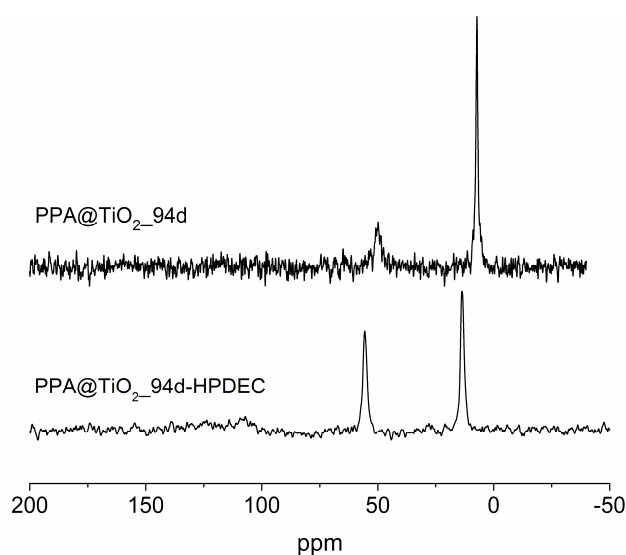


Figure 3-12: ^{13}C CPMAS NMR and non-spinning ^{13}C HPDEC NMR of PPA@TiO₂ after 94 days of illumination and ^{13}C HPDEC NMR of TiO₂ after stirring in MeOH/water and washing with ethanol.

In CPMAS NMR spectroscopy the magnetization is transferred from protons to a carbon nucleus. Hence, the methyl carbon appears more intense compared to the methylene group. The adsorbed ethanol originates from washing of the particles after illumination. Ethanol has been shown to adsorb on titanium dioxide surfaces in different ways, including molecularly adsorbed ethanol and ethoxy species.²⁶⁵ Molecularly adsorbed ethanol is adsorbed via hydrogen bonds and has been found to be released upon drying at 200°C.²⁷⁷

In order to prove the presence of ethanol that interacts with the TiO₂ surface by hydrogen bonding, the particles were dispersed in d⁶-DMSO and sonicated in an ultrasonic bath for 3 days to assure quantitative extraction of ethanol. The DMSO was able to break the hydrogen bonds and HSQC NMR (Figure 3-13) of the liquid confirmed that ethanol was in the system. Moreover, ¹³C HPDEC NMR after the extraction of ethanol revealed no other carbon species on the particles.

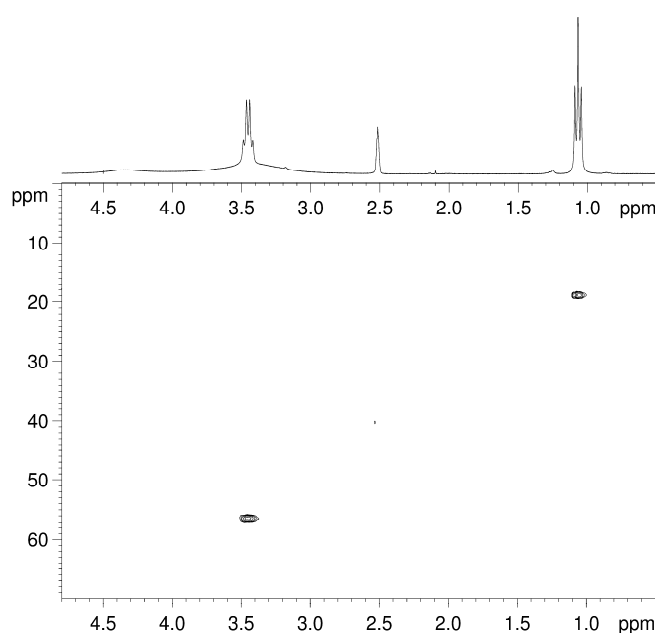


Figure 3-13: HSQC NMR spectrum of d⁶-DMSO with which TiO₂ particles have been extracted.

Thermogravimetric analysis of PPA@TiO₂ shown in Figure 3-14 revealed a decrease in mass loss between 250 and 600 °C of the illuminated samples compared to the not illuminated particles. Moreover, no defined onset temperature was observed for the samples illuminated for 29 and 94 days, but a rather diffuse mass loss over the whole temperature range between 100 and 500 °C was monitored. This continuous mass loss can be assigned to water as well as hydrogen bonded ethanol (identified by NMR)

which desorb from the surface. For particles illuminated for 29 days the diffuse mass loss is ascribed to various different degradation intermediates and volatile compounds (similar as after 94 days of illumination) concurrently.

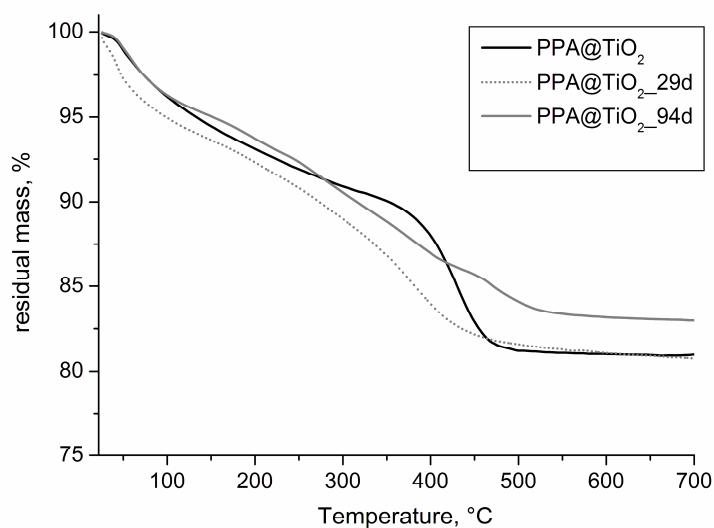


Figure 3-14: TGA plots of PPA@TiO₂ without illumination and after 94 days of illumination of 2 wt% particle dispersions with 9W UVA light.

Elemental analysis presented in Figure 3-15 confirmed the stability of the P-O-Ti bond showing a constant phosphorus content (●), while the carbon content (■) was decreasing.

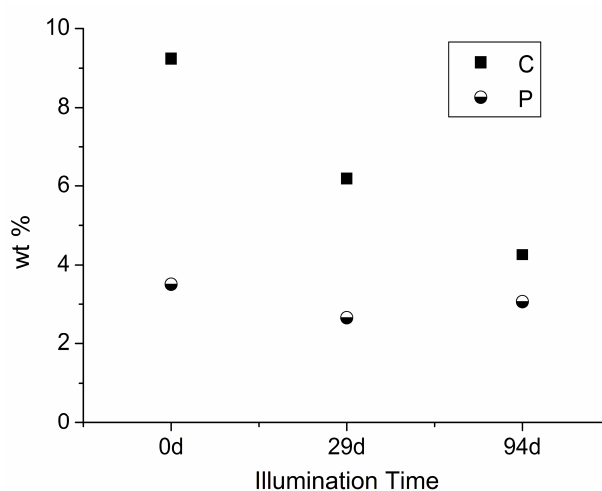


Figure 3-15: Elemental analysis of PPA@TiO₂ after different times of illumination: wt% C: ■ and wt% P: ●.

Hence, the degradation of the organic moiety as well as the stability of the P-O-Ti bond is confirmed. However, due to adsorbed ethanol and CO₂, the sample still contained between 3 and 4 wt% carbon after organics were no more detectable by means of NMR (94d).

The discussed investigations on the UV stability of PPA@TiO₂ revealed that the organic moiety cannot be protected from degradation by a phosphonate intermediate layer. Complete degradation of the organic moiety was confirmed by FT-IR and NMR. The degradation was found to proceed rather sequentially than via breakage of the P-C bond as detected by ¹³C CPMAS NMR and FT-IR. Organic species left on the surface of the illuminated particles could be assigned to hydrogen-bonded ethanol. The P-O-Ti bond is stable upon UV-illumination and upon degradation of the aromatic moiety a phosphate species is formed on the particles' surface as shown by FT-IR, ³¹P NMR and elemental analysis. In order to elucidate the mechanism of degradation, the degradation kinetics were investigated varying different parameters.

3.2.2 Kinetics and Mechanism

In order to determine the rate constant *k* of the degradation reactions, a first-order kinetic is assumed and the rate law is thus the same as for the photocatalytic degradation of methylene blue discussed in section 3.1.2.1 (Equation 11).

Plotting ln(*A*₀/*A*) versus time the rate constant *k* can be determined from the slope in the graph. As discussed above, the rate constant *k* was determined varying different parameters in order to elucidate the degradation mechanism as well as differences in the stability of different coupling agents.

The reproducibility of the method was proven using 0.2 wt% dispersions of PPA@TiO₂ with a surface coverage of 4.3 molecules/nm² - corresponding to full surface coverage¹⁴³ - in ethanol/water 4:1. The degradation was tracked by monitoring the absorption of the P-Ar vibration at 1143 cm⁻¹. In Figure 3-16 the kinetic plots of the reproducibility experiments are presented. It is concluded that minor deviations can occur and the reproducibility is limited to ± 0.009 d⁻¹ for the rate constant *k*.

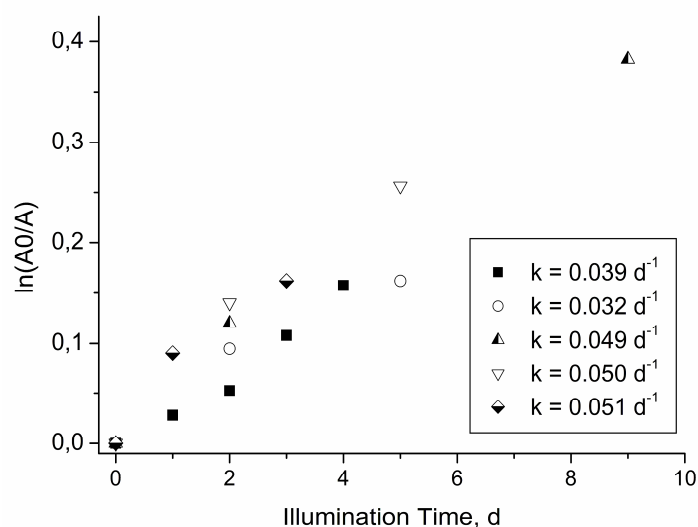


Figure 3-16: Kinetic plots and k-values of various illumination experiments of PPA@TiO₂ under similar conditions.

Thus, the accuracy of the method was determined and allows correct interpretation of the data discussed on the following pages.

3.2.2.1 Phosphonate versus Phosphate

It is assumed that the different charge distribution in phosphonates and phosphates might lead to unequal kinetics of degradation. Thus, the rate constants k of degradation of PPA@TiO₂ and PPOA@TiO₂ were investigated under similar conditions. 0.2 wt% of modified particles exhibiting 4.4 molecules/nm² surface coverage were dispersed in a mixture of ethanol and water (4:1) applying an ultrasonic bath. FT-IR spectra of both compounds after different times of illumination are presented in Figure 3-17. For PPA@TiO₂ the vibrational absorption at 1143 cm⁻¹ (P-C) was monitored while the degradation kinetics of PPOA@TiO₂ was determined by tracking the absorption at 1222 cm⁻¹ (P-O-C). It is observed from Figure 3-17 that the tracked vibrations were decreasing with illumination time for both compounds compared to the stable P-O-Ti bond.

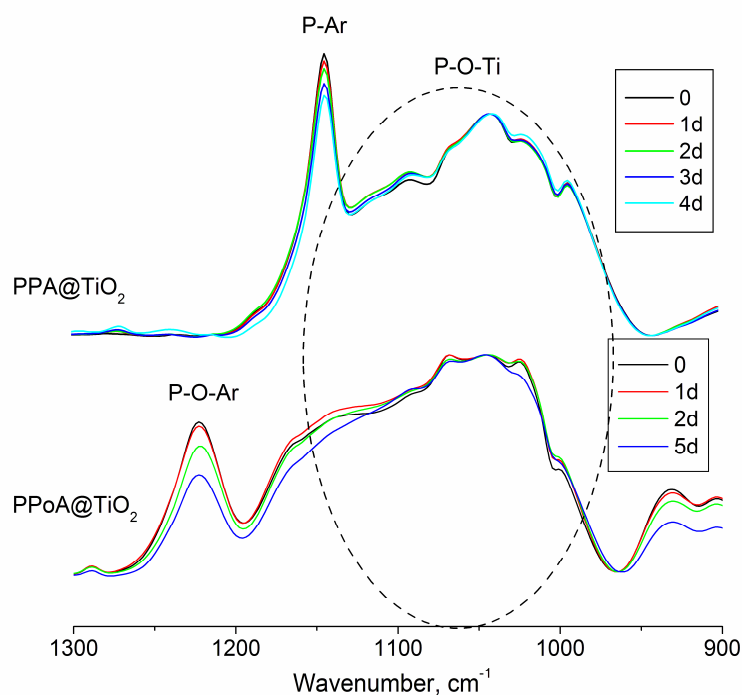


Figure 3-17: FT-IR spectra of PPA@TiO₂ and PPoA@TiO₂ after different times of illumination.

The kinetic plots for the degradation of both compounds were created from the absorptions at the respective wavenumber after different illumination times (Figure 3-18). A_0 is the absorption (peakmaximum) before illumination and A describes the absorption after the respective illumination time.

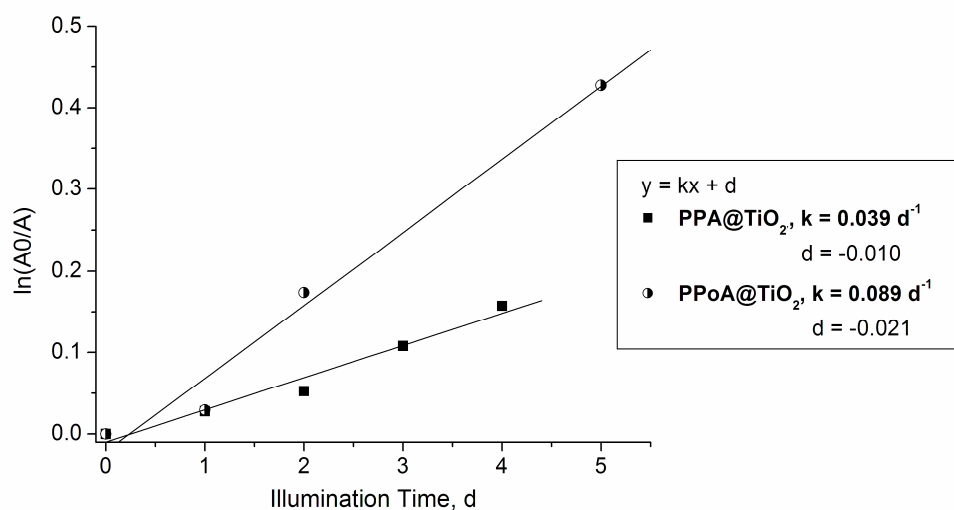


Figure 3-18: Kinetic plots of PPA@TiO₂ and PPoA@TiO₂ illuminated under equal conditions.

In both cases the degradation can be described as linear. Applying a linear fit, it is observed that the P-O-Ar vibration was decreasing faster compared to the P-C vibration. The difference between the two rate constants k significantly exceeded the error range of 0.009 d^{-1} .

Thus it is concluded that the phosphonate moiety is more stable upon UV illumination than the phosphate. This might be attributed to the fact that the P-C bond exhibits higher stability than the P-O-C bond. However, this would mean that – at least for the phosphate – the degradation proceeds via cleavage of these bonds rather than via sequential degradation. For this reason, ^{13}C CPMAS NMR was applied to elucidate the mechanism of degradation of PPOA (Figure 3-19).

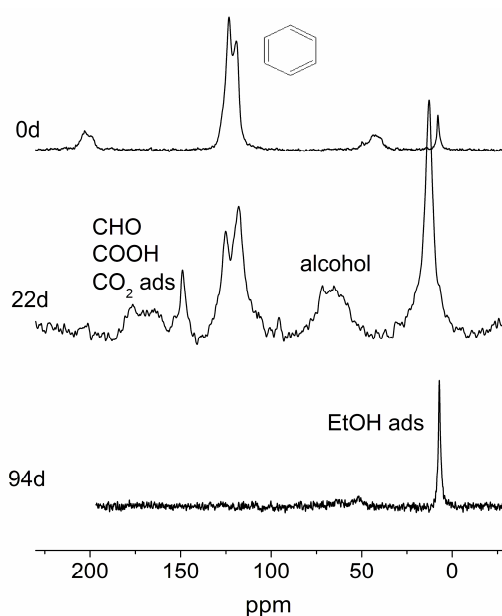


Figure 3-19: ^{13}C solid state NMR of PPOA@TiO₂ after different times of illumination at 2 wt% (CPMAS for 0 and 94 days, 22 days: HPDEC).

As seen from Figure 3-19, various degradation intermediates were identified in the alcoholic and carboxylic region, suggesting a sequential degradation also for the phosphate. Degradation intermediates observed from ^{13}C NMR may also be ascribed to species adsorbed physically from the solution. However, owing to the high amount of intermediate species present on the titanium dioxide surface, a sequential degradation is rather suggested than cleavage of the P-O-Ti bond. A possible explanation for the unequal degradation kinetics of PPA and PPOA is a facilitated hydroxyl radical formation owing to hydrogen bond formation between the phosphate group and water,

enabled by the free lone pairs of the bridging oxygen. As discussed in the introduction, the photocatalytic activity of TiO_2 can be enhanced by phosphate-doping. As stated by Zhao et al.¹⁴⁷ the increased photocatalytic activity is assigned to facilitated hydroxyl radical formation owing to hydrogen bond formation between the phosphate group and water. However, not only ionic phosphate species form hydrogen bonds with water, but also the additional lone pairs of the bridging oxygen in organophosphates might enable hydrogen bond formation. Indeed several theoretical studies confirm the hydrogen bond acceptor nature of the phosphoester oxygen.^{278, 279}

The investigations on the degradations of PPA@TiO_2 and PPoA@TiO_2 revealed a sequential degradation of the aromatic moieties for both compounds. This decomposition can either (i) be a consequence of the UV absorption of the organic moiety itself or (ii) be initiated by radicals. In order to study the influence of direct photolysis on the degradation, the degradation kinetics and mechanism of an alkylphosphonic acid is investigated. However, if radical species originating from the titanium dioxide photocatalyst are responsible for the degradation, two different possibilities exist for the nature of such radicals. As discussed above, owing to the steric proximity of the organic moiety to the TiO_2 surface, a direct degradation via surface trapped holes might be possible. Moreover, the formation of hydroxyl radicals in the presence of water is possible. The role of direct hole oxidation was investigated by studying the degradation of organic phosphonates in a water free environment where the formation of hydroxyl radicals is limited.

3.2.2.2 Arylphosphonate versus Alkylphosphonate

The degradation of an alkylphosphonic acid was investigated in order to study the influence of direct photolysis on the degradation. Furthermore, pure PPA was illuminated under similar conditions. The latter investigations did not reveal any decomposition of PPA after 30 days of illumination. Hence direct photolysis was assumed to play no role in the degradation of PPA@TiO_2 . Nevertheless the degradation of DPA@TiO_2 was monitored in order to gain further insight in the mechanism of decomposition. Comparing the degradation of DPA@TiO_2 with PPA@TiO_2 , two major problems arise: First, no vibrational absorption for the P-C bond can be identified in the infrared spectra of DPA. Thus, the absorption at 2921 cm^{-1} was monitored, which is assigned to the aliphatic CH stretching vibration. However, the changes of this CH vibration cannot be compared with the decrease of P-Ar vibration of PPA, because due

to sequential degradation, a faster decrease of the CH vibrations is expected compared to the P-C signal. Hence, the CH stretching vibrations of PPA need to be compared with the CH stretching vibrations of DPA. Thus, the decomposition of the aromatic ring was tracked by monitoring the absorbance change at 3056 cm^{-1} . However, the CH stretching vibration was shifted slightly upon increasing decomposition as seen from Figure 3-20 which is assigned to an increased force constant of the C-H bond owing to reduced π - π stacking. Thus, the absorption was not tracked at a fixed wavenumber, but the maximum of the CH vibrational signal was monitored.

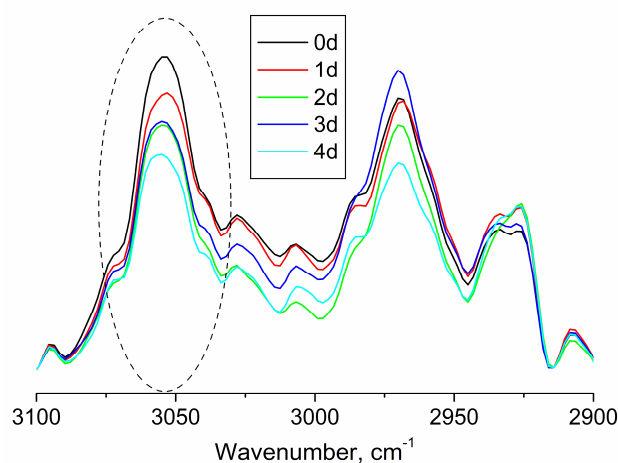


Figure 3-20: CH stretching region of the FT-IR spectra of PPA@TiO₂ after different times of illumination.

In Figure 3-21 the k-values calculated from the degradation of the P-C bond are compared with the k-values obtained by tracking the absorption in the aromatic region.

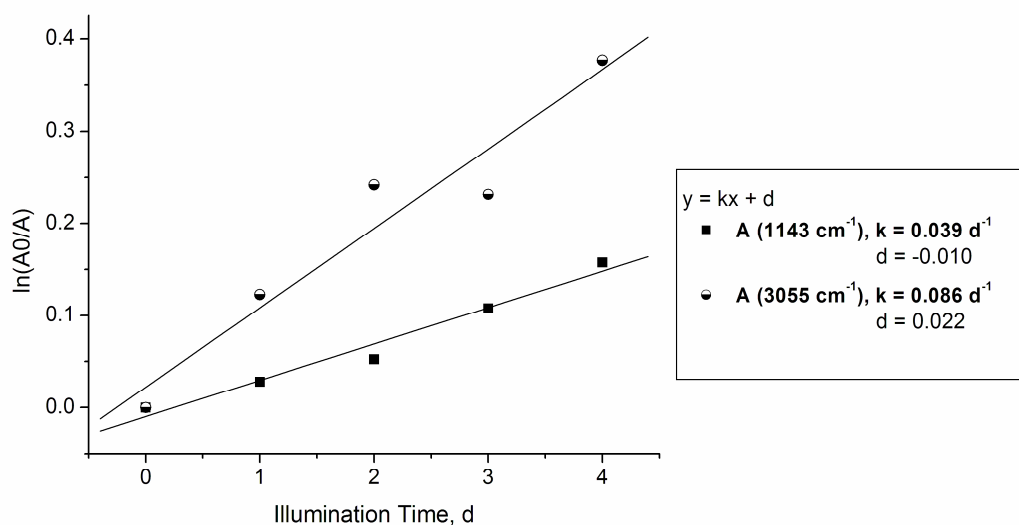


Figure 3-21: Kinetic plots of PPA@TiO₂ monitoring the absorptions at 1143 cm⁻¹ and 3055 cm⁻¹.

It is observed from Figure 3-21 that the aromatic CH vibration was decreasing significantly faster compared to the P-Ar signal. Thus, it was shown that a comparison of the CH vibration of DPA with the CH vibration of PPA is more reasonable than with the P-Ar vibration of PPA. Moreover, this result could be another evidence for a sequential degradation of the organic compound.

The second problem that arises is the limited surface coverage obtainable with DPA. While previously prepared PPA@TiO₂ exceeds 4 molecules/nm², for DPA only 3 molecules/nm² could be achieved. The higher surface coverage obtained for PPA is in agreement with literature reports²⁸⁰ and is ascribed to π - π stacking of the aromatic moieties on the TiO₂ surface. It is assumed that surface coverage plays an important role in the degradation kinetics, not only because surface hydroxyl groups act as traps for holes but also due to steric effects that inhibit the contact of species required for photocatalysis to the particles' surface. Thus, PPA@TiO₂ and DPA@TiO₂ exhibiting similar surface coverage (3.4 and 3.1 molecules/nm² respectively) were prepared by adjusting the concentration of PPA and DPA used for modification. The modified particles were dispersed at 0.2 wt% in ethanol/water 4:1 and illuminated in the experimental setup described in section 3.1.2.1. Samples taken after certain time intervals were centrifuged and washed with ethanol. Quantitative IR spectra of DPA@TiO₂ after different times of illumination are presented in Figure 3-22. From the recorded spectra, also for DPA a shift of the CH stretching vibrations to higher wavenumbers was observed upon degradation. This effect is assigned to less ordering and conformational changes as found by Snyder et al..²⁸¹

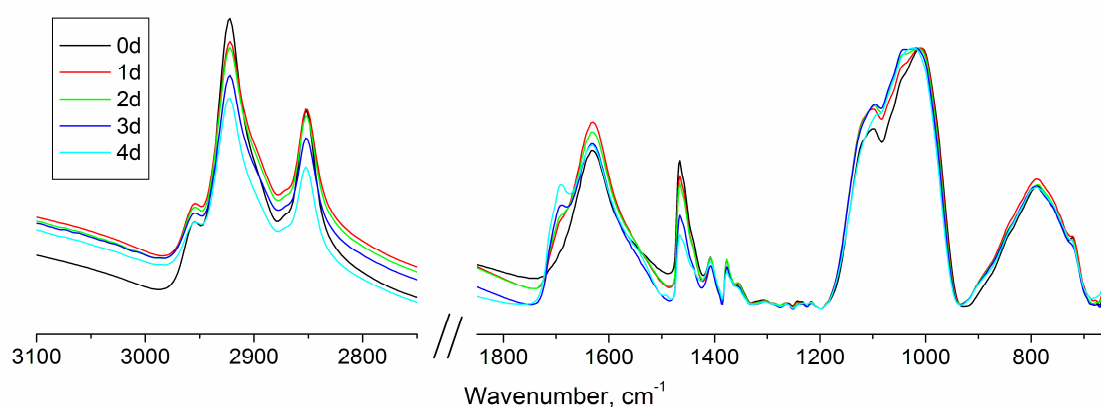


Figure 3-22: FT-IR spectra of DPA@TiO₂ after different times of illumination.

While the broad P-O-Ti signal between 930 and 1180 cm⁻¹ was stable, a decrease of the CH stretching (2921 cm⁻¹) and bending (1460 cm⁻¹) was observed. Thus it is concluded that the organic moiety was degraded while a phosphate species remained on the particles' surface. The presence of a phosphate species was confirmed by a signal at 0 ppm in the ³¹P MAS NMR (Figure 3-23). For NMR investigations, the modified particles were illuminated at a concentration of 2 wt% in ethanol/water mixtures because larger amounts of particles were required for solid state NMR.

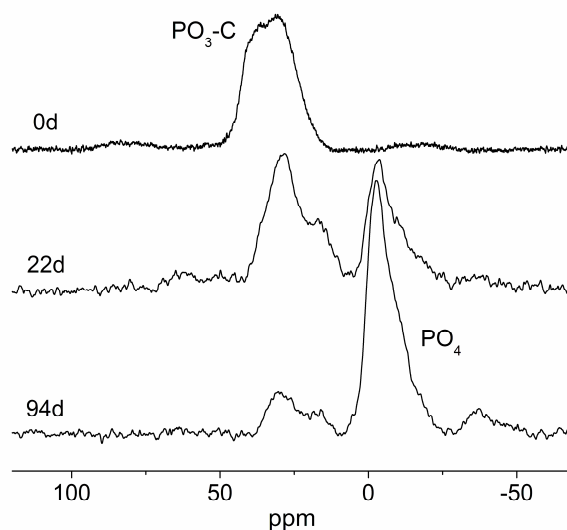


Figure 3-23: ³¹P MAS NMR spectra of DPA@TiO₂ after different times of illumination.

Moreover, intermediately arising C=O vibrations (1700 cm^{-1}) observed in the FT-IR spectra in Figure 3-22 confirmed the assumption that the degradation does not proceed via breakage of the P-C bond but is rather sequential via formation of alcohol, aldehyde and acid to CO_2 . These findings are in agreement with the results obtained upon illumination of PPA@TiO_2 (vide supra).

The kinetic plots of DPA@TiO_2 and PPA@TiO_2 are compared in Figure 3-24.

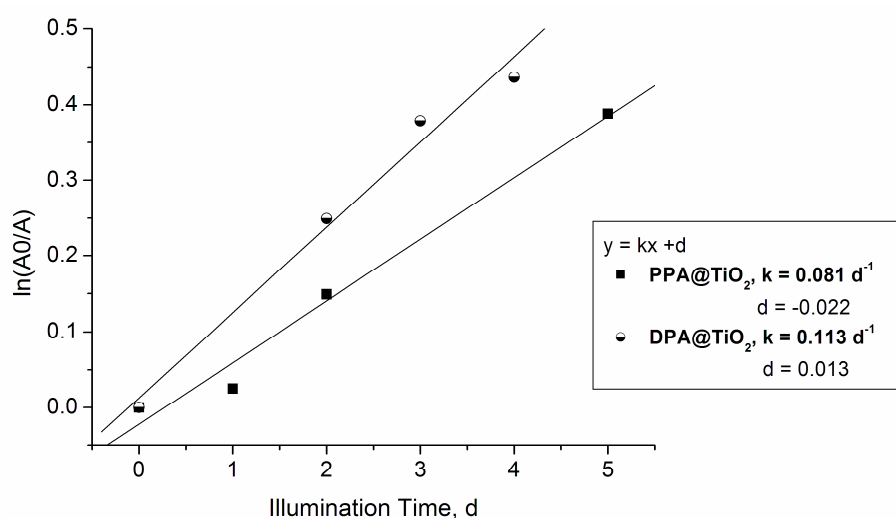


Figure 3-24: Kinetic plots of PPA@TiO_2 and DPA@TiO_2 illuminated under equal conditions.

The degradation of DPA@TiO_2 proceeded significantly faster compared to the degradation of PPA@TiO_2 (Figure 3-24). This result is assigned to worse stabilization of radicals by the alkyl chain compared to the aromatic ring, where the radicals can encounter mesomeric stabilization.

These results show insistently that the degradation via direct UV absorption of the aromatic ring does not exhibit a reaction rate in the same regime as the photocatalytic degradation. Thus, the degradation is initiated by a radical species which can either be a hole or a hydroxyl radical. For the formation of hydroxyl radicals the presence of water is required. Thus, the mechanism can be elucidated by investigation of the degradation kinetics in dependence of the water present in the system as discussed in section 3.2.2.3.

3.2.2.3 Solvent

The effect of water on the degradation rate of PPA@TiO₂ was investigated using different solvents ranging from water over ethanol/water (1:1) to dry n-heptane. 0.2 wt% suspensions of PPA@TiO₂ exhibiting a surface coverage of 4.5 molecules/nm² in the respective solvents were prepared by ultrasonication and illuminated in an experimental setup described in section 3.1.2.1. For illumination experiments in dry n-heptane the relative humidity was kept below 20%. Figure 3-25 shows the kinetic plots of PPA@TiO₂ illuminated in different solvents. It is observed that the degradation kinetics were the same for a water-free environment as for ethanol/water mixtures.

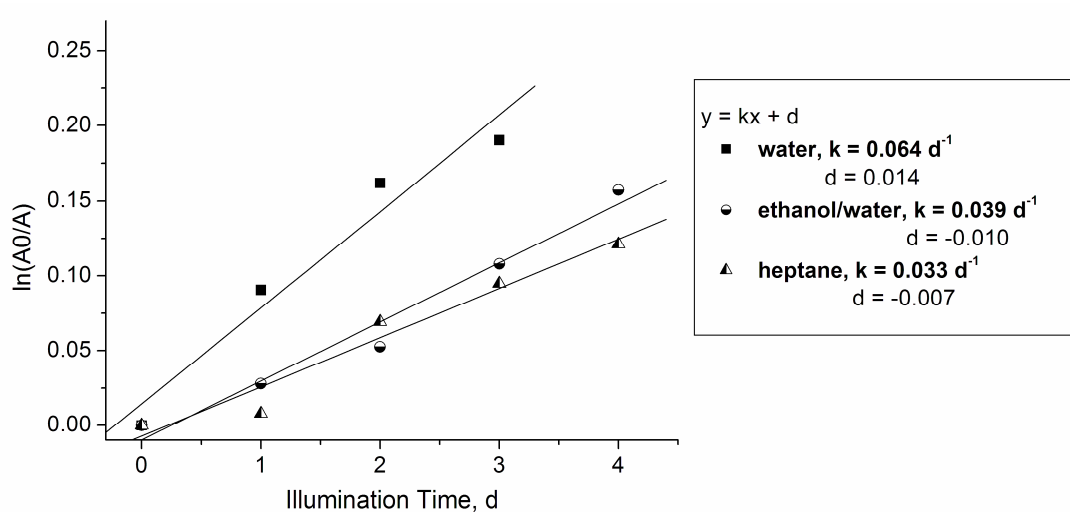


Figure 3-25: Kinetic plots of PPA@TiO₂ illuminated in different solvents.

It can be concluded that the degradation of PPA@TiO₂ does not only proceed via hydroxyl radicals, but also via hole oxidation (valence band or surface trapped hole), because the degradation reaction was not slowed down in the absence of water. Hence, it is assumed that the degradation is initiated by the transfer of electrons from the organic moiety to surface trapped holes and is thus not affected by the presence of water. However, when illuminated in pure water, the degradation proceeds significantly faster than for all other solvent mixtures. This result can be explained by the fact that both mechanisms – hole oxidation and degradation via hydroxyl radicals – are co-existent and when the amount of water is increased above a certain ratio, the degradation via hydroxyl radicals can proceed faster and thus accelerate the whole degradation process.

Due to the different reactivity of aliphatic and aromatic moieties with the two radical species it is possible that the degradation kinetics of DPA@TiO₂ exhibit unequal dependence on the solvent compared to PPA@TiO₂. Thus, also DPA@TiO₂ was studied regarding its degradation in the presence and absence of water. However, the degradation in pure water could not be investigated because the hydrophobic particles are not wetted by water. From the kinetic plots presented in Figure 3-26 it is shown that the degradation rate was slightly inferior in the absence of humidity.

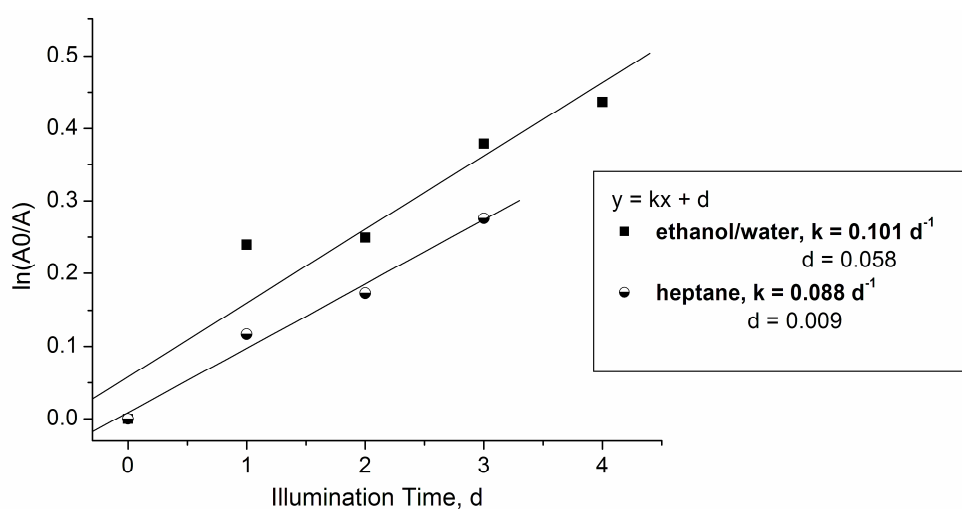


Figure 3-26: Kinetic plots of DPA@TiO₂ illuminated in different solvents.

However, the decrease in the rate constant was quite low, indicating that the direct hole degradation constitutes a considerable part of the degradation also for DPA.

In order to intensify the study on the dependence of the degradation of PPA@TiO₂ on the solvent, the particles were illuminated without solvent at different relative humidity. Samples taken after 2, 5 and 9 days were compared with the results after the same time in 0.2 wt% ethanol/water mixtures (Figure 3-27). The rate of degradation was significantly decreased for illumination of the dry samples compared to degradation in suspension. However, degradation took place and was accelerated with increasing relative humidity.

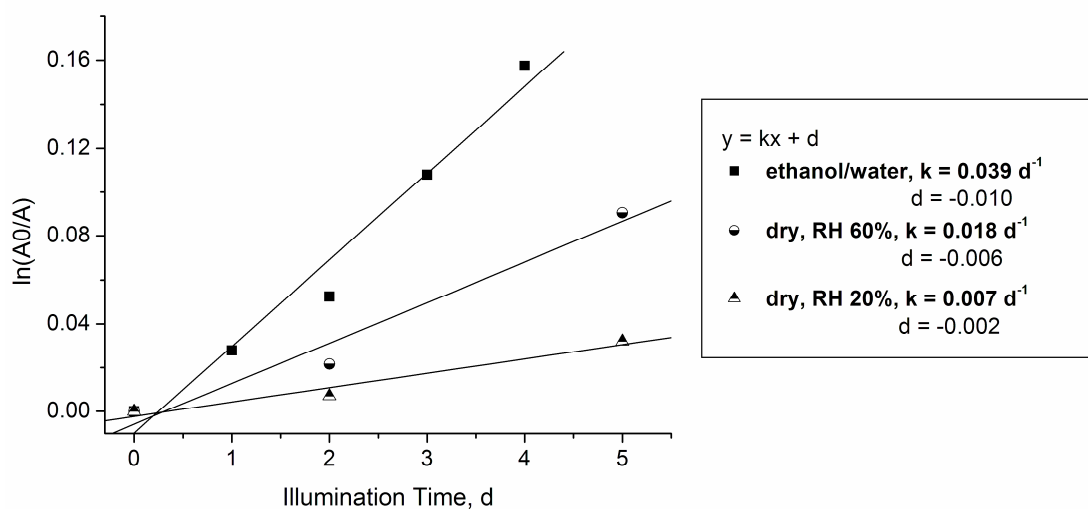


Figure 3-27: Kinetic plots of PPA@TiO₂ illuminated in ethanol/water 4:1 (0.2 wt%) and dry with 20% and 60% relative humidity.

The study on the different humidities might not be unambiguous and reproducible because a homogeneous illumination of the powder is experimentally challenging due to varying thickness of the powder film. Nevertheless, it could be revealed that both compounds are also degraded in dry state at low relative humidity. Hence, it is emphasized that the degradation mechanism depends strongly on the conditions. In dry state the degradation is assumed to proceed via direct hole oxidation while in the presence of water both degradation mechanisms – hole oxidation and degradation via hydroxyl radicals – occur at the same time. Which mechanism is dominant depends on the conditions – in particular on the water present in the system. This confirms the results obtained from the investigations in different solvents.

Thus it was found that the degradation is initiated by hydroxyl radicals to a large extent. It is assumed that oxidation by valence band holes or surface trapped holes contributes considerably to the degradation due to only slightly lower degradation rates in the absence of water. However, no definite conclusion can be drawn from the described investigations as water is adsorbed on the particles' surface even after vigorous drying. Despite drying at 100°C in vacuo the presence of hydrogen bonded water on the surface cannot be precluded. However, earlier investigations on the degradation of organic compounds without covalent connection to the titanium dioxide surface revealed no degradation in organic solvents.²⁸² Thus it is concluded that organic phosphonates on titanium dioxide can in contrast to organic species without covalent

connection be degraded by direct hole oxidation, despite the results by Zhao and coworkers, indicating an obstruction of direct hole oxidation by the presence of phosphate.¹⁴⁷

3.2.2.4 Surface Coverage

It is assumed that the titanium dioxide surface can be shielded against species required for photocatalysis – photons, water and oxygen – by coupling agents present on the surface of the particles. Therefore, the degradation kinetics might depend on the surface coverage with organic phosphonate. For this reason, PPA@TiO₂ was prepared at three different coverage grades - 3.4, 3.8 and 4.5 molecules/nm² - by adjusting the concentration of PPA used for the modification reaction. The particles were dispersed at 0.2 wt% in ethanol/water 4:1 and illuminated similar to previous experiments. Figure 3-28 presents the kinetic plots of PPA@TiO₂ exhibiting different surface coverage.

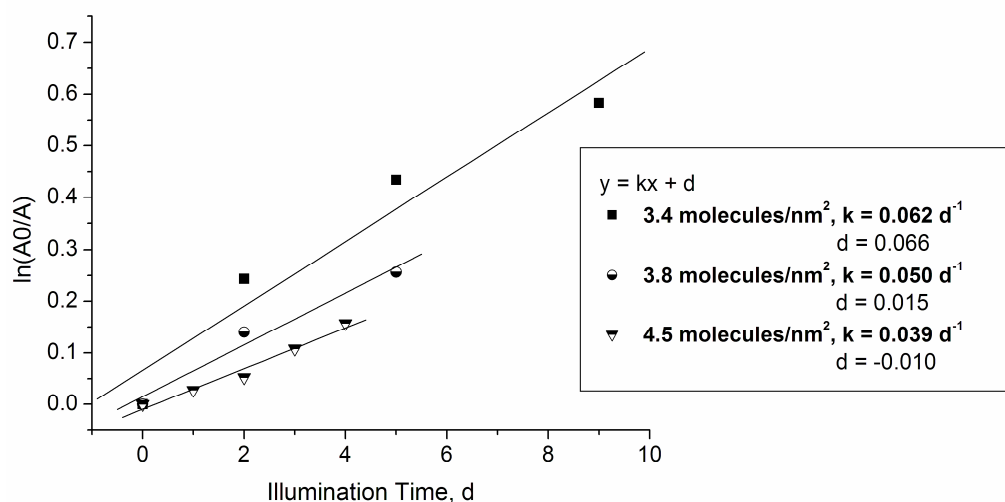


Figure 3-28: Kinetic plots of PPA@TiO₂ with different surface coverage illuminated at 0.2 wt% in 4:1 ethanol/water with two 9 W UVA lamps.

As displayed in Figure 3-28, the rate constant k for the photocatalytic degradation of PPA was increasing with decreasing surface coverage. This result approves the assumption that the modification of the particles' surface can inhibit the photocatalytic processes. As discussed above, it is assumed that at least part of the species required for photocatalysis are sterically shielded from the surface. Thus, it is suggested that at high

surface coverage the main degradation mechanism occurs via direct hole oxidation, while at low coverage the degradation via hydroxyl radicals can enhance the rate. However, it is concluded from the rate constants that the influence of the surface coverage on the degradation kinetics is limited. Hence, the comparison of PPA@TiO₂ exhibiting 3.4 molecules/nm² with DPA@TiO₂ having 3.1 molecules/nm² has been proven to be feasible.

3.2.2.5 Particle Concentration

The degradation kinetics of PPA@TiO₂ were investigated at different particle concentrations in order to investigate the effect of dispersibility on the degradation kinetics. From the kinetic plots presented in Figure 3-29 it can be concluded that the photocatalytic degradation rate was drastically decreased at higher particle concentration. This effect is mainly ascribed to worse dispersibility as seen from Figure 3-30.

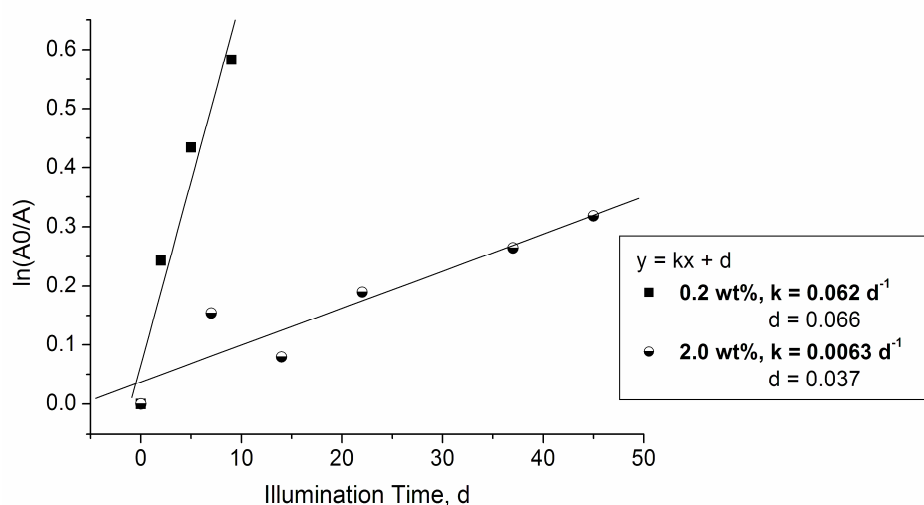


Figure 3-29: Kinetic plots of PPA@TiO₂ illuminated at different particle concentrations in water with two 9 W UVA lamps.

It is assumed that the degradation was slowed down at high particle concentration due to the lower transparency of the dispersion caused by agglomeration of particles. Thus, particles modified with PPA@TiO₂ were dispersed in ethanol/water 4:1 at 0.2 wt% and 2 wt% and investigated optically and by DLS. From the DLS plots presented in Figure

3-30 it could be observed that the dispersibility of modified particles was strongly decreased at high concentrations. Moreover, the photograph image presented in Figure 3-30 illustrates that a 2 wt% suspension exhibits much lower transparency than a 0.2 wt% suspension. Thus, it is assumed that the majority of particles is inaccessible for UV light due to larger agglomerates which lead to a lower active surface as well as absorption and scattering of the irradiated UV light.

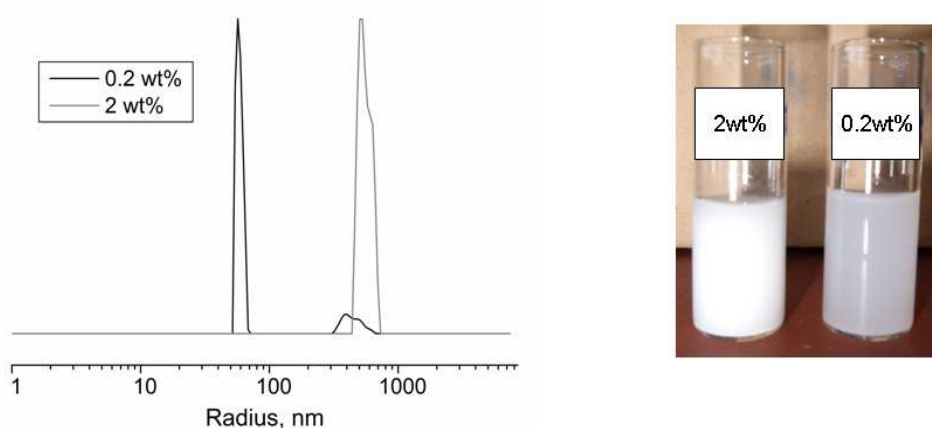


Figure 3-30: DLS plot and optical photograph image of DPA@TiO₂ dispersed in ethanol/water (4:1) at 0.2 wt% and 2 wt%.

3.2.2.6 Degradation of the Solvent

Owing to the formation of hydroxyl radicals on the surface of TiO₂ nanoparticles in the presence of water any organic compound can be degraded photocatalytically.³² Thus, also the solvent might be degraded, which may influence the degradation of organic phosphonates present on the surface. If radicals are consumed for the degradation of the solvent, the degradation rate of the phosphonates might be decreased. Hence, the degradation of n-heptane was studied in the presence of unmodified titanium dioxide nanoparticles as well as PPA@TiO₂ and DPA@TiO₂. The respective particles were dispersed in n-heptane and illuminated for 3 days in the experimental setup described in section 3.1.2.1. From the NMR spectra presented in Figure 3-31 no degradation products were identified. However, a volume change of the dispersion was observed, which can either be ascribed to the degradation of heptane or to its high volatility.

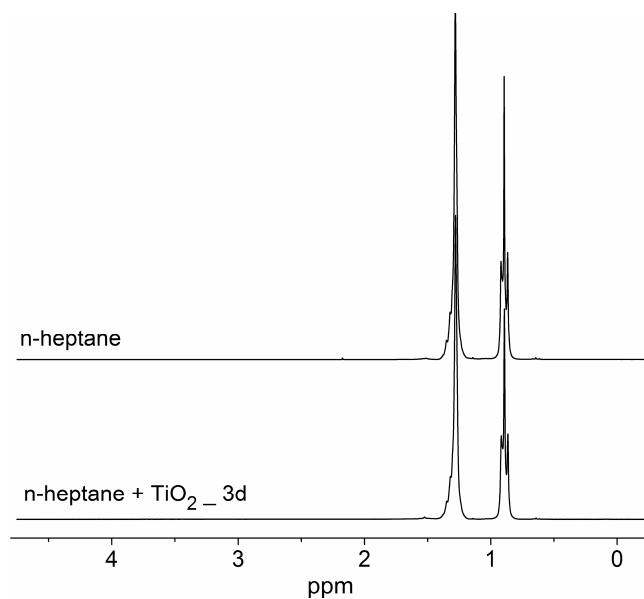


Figure 3-31: ^1H NMR of n-heptane and n-heptane illuminated for 3 days in the presence of DPA@TiO₂.

In order to elucidate whether n-heptane was degraded or evaporated, the stability of dodecane was investigated. As dodecane exhibits a low volatility an eventual volume change can only be attributed to its degradation. When dodecane was illuminated for 4 days, no volume change was observed. Furthermore, from ^1H NMR no degradation products were detected.

Thus, the solvent was not degraded and the volume change observed for n-heptane can be assigned to evaporation. Hence it was shown that degradation of the solvent does not take place in the same time scales as the degradation of the surface-bound species does.

3.2.3 Characterization of Illumination Products

The products obtained after degradation of the organic moieties were characterized by FT-IR, ^{13}C CPMAS NMR, ^{31}P MAS NMR, TGA, XRD and elemental analysis. As discussed in sections 3.2.1 and 3.2.2, the FT-IR spectra after different times of illumination revealed a decrease of the signals which can be assigned to organic moieties, while the P-O-Ti bond was stable. The spectra obtained after illumination were similar for all investigated coupling agents and show a phosphate signal (Figure

3-32). A similar signal was obtained after temperature treatment of particles modified with organophosphonates as observed from Figure 3-32.

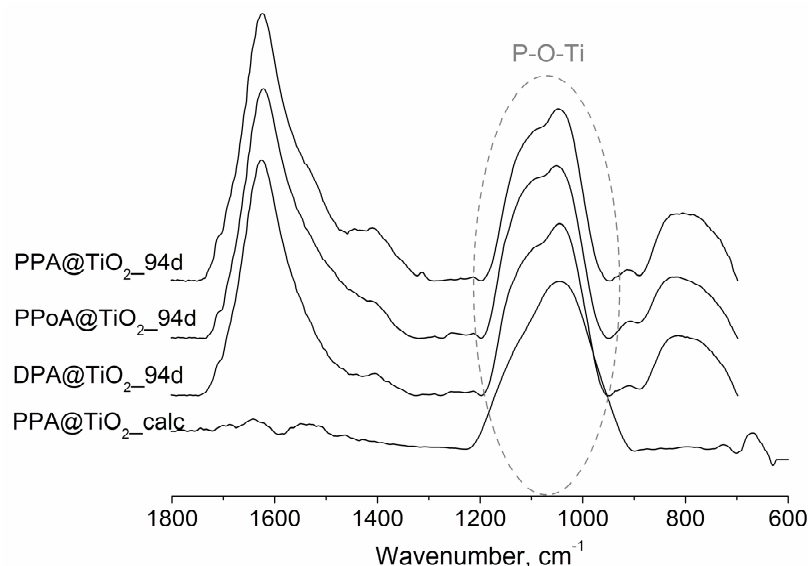


Figure 3-32: FT-IR spectra of PPA@TiO₂, PPOA@TiO₂ and DPA@TiO₂ after illumination and PPA@TiO₂ after calcination at 500°C.

From the stable P-O-Ti vibration it is assumed that a phosphate species remained on the particles' surface. ³¹P MAS NMR spectra (Figure 3-10 and Figure 3-23) confirmed this assumption by the presence of a signal in the PO₄³⁻ region. No other phosphorus species were detected for all samples. Again, a similar spectrum was obtained after calcination of the modified particles and no salt phase was observed. ¹³C CPMAS NMR spectra for PPA@TiO₂ and PPOA@TiO₂ revealed the presence of ethanol after illumination as discussed in section 3.2.1, while for DPA@TiO₂ no organic species were found after illumination. It is assumed that the highly hydrophobic surface of DPA@TiO₂ does not allow the formation of hydrogen bonds with ethanol. Thermogravimetric analyses of the modified particles after illumination exhibited a continuous mass loss over the measured temperature range similar to PPA@TiO₂ after illumination (Figure 3-14). The observed mass loss is assigned to desorption of volatile compounds and condensation of surface hydroxyl groups. Elemental analysis revealed a decrease in carbon content throughout the illumination process due to degradation of the organic compound to CO₂ and water (Figure 3-33). However, a small carbon content was also observed on the particles after illumination owing to adsorbed ethanol. The phosphorus content on the other hand was

constant for all investigated samples which confirms the UV stability of the P-O-Ti bonds.

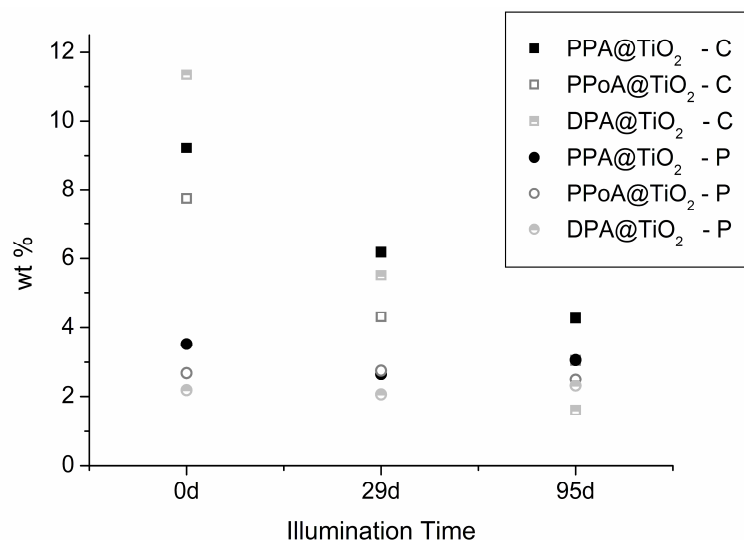


Figure 3-33: Elemental analysis of PPA@TiO₂, PPOA@TiO₂ and DPA@TiO₂ after different times of illumination at 2 wt% with two 9 W UVA lamps.

The degradation product was thus found to be a phosphate species remaining on the TiO₂ surface. A similar product can be obtained by calcination of the same modified particles. However, it is assumed that temperature treatment, in contrast to UV treatment, might lead to modification changes of the titanium dioxide. Moreover it is possible that upon temperature treatment phosphate can migrate inside the TiO₂ matrix and act as a dopant and in addition a titanium phosphate phase might be formed on the surface on the particles.¹³⁴ For this reason, DPA@TiO₂ and PPA@TiO₂ were calcined at 500°C for 24 hours and the X-ray diffraction patterns of illuminated and calcined particles were compared. The phase contents obtained by Rietveld refinement of illuminated and calcined particles are compared with bare sol-gel TiO₂ nanoparticles in Figure 3-34. Crystallite sizes of the different phases are presented in the respective columns. It is concluded that no phase transformations took place upon illumination, while upon calcination the anatase content was increasing significantly upon decreasing brookite content. Furthermore, the crystallite sizes of brookite were growing upon calcination. Additional reflexions present in the diffraction patterns of illuminated samples, which cannot be assigned to a titanium oxide phase, could be assigned to

sodium ethanolate. However, this assignment is ambiguous due to the instability of sodium ethanolate to hydrolysis.

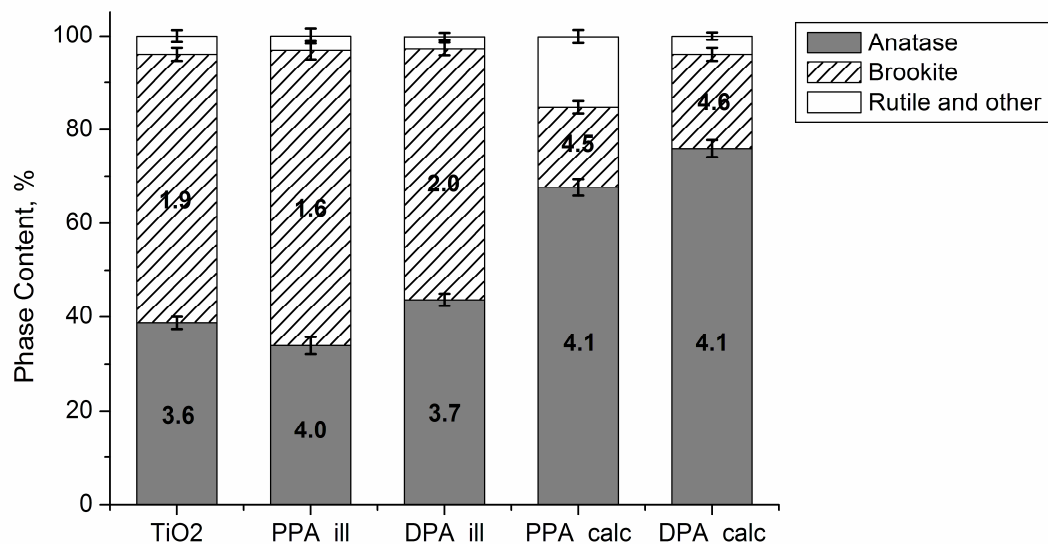


Figure 3-34: Composition of illuminated and calcined PPA@TiO₂ and DPA@TiO₂ calculated from XRD patterns by Rietveld refinement.

Thus it was found that the phase composition of TiO₂ nanoparticles did not change upon illumination, while upon calcination a higher anatase content was obtained. Moreover, crystallite sizes were not changed by illumination, while upon calcination crystallite sizes of brookite were increasing drastically from 1.9 to 4.5 nm.

As reported by several groups, the photocatalytic activity of titanium dioxide nanoparticles is enhanced by the presence of phosphate species on the surface.^{135, 147, 148} Several investigations involved temperature treatment when organic phosphonates were applied,¹⁴⁸ which does not only generate phosphate on the surface of the particles, but also induces a migration inside the particles. However, Zhao and coworkers found an enhanced photocatalytic activity after immersion of TiO₂ in H₃PO₄ even without calcinations.¹⁴⁷ Thus, it is concluded that the activity enhancement is caused by a facilitated hydroxyl radical formation owing to hydrogen bond formation between the phosphate anions and water. Hence, the photocatalytic activity cannot only be increased by doping phosphorus into the TiO₂ framework, but also by surface modification with PO₄³⁻. For this reason, the activity of the UV treated particles in degrading methylene blue under UV irradiation was investigated and compared to bare titanium dioxide

particles as well as modified particles and calcined particles. The photocatalytic activity was tested following the procedure described in section 3.1.2.1.

In order to determine an eventual change in the photocatalytic activity of the modified and UV degraded particles compared to the unmodified TiO₂ nanoparticles, the particles were tested at various stages of preparation. Thus, bare TiO₂ nanoparticles were tested as well as particles modified with phosphonic and phosphoric acids (PPA, PPA and DPA) and illuminated particles. Furthermore, the modified particles were calcined at 500 °C for 10 hours in order to degrade the organics and generate phosphate species. The photocatalytic activity of thus obtained phosphate doped particles was compared to the ones obtained by UV degradation.

In Figures 3-35-37 the k-values of the different samples are presented.

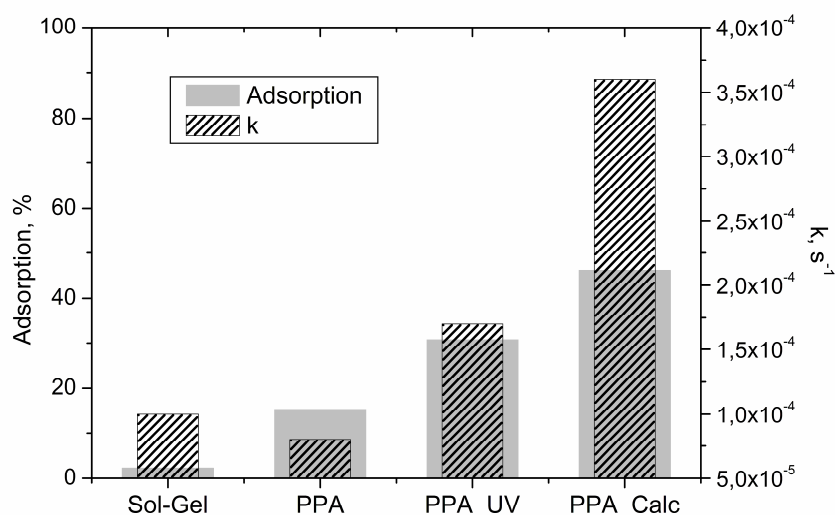


Figure 3-35: K-values and adsorption behaviour of the bare particles compared to differently treated PPA@TiO₂.

It is seen that the photocatalytic activity decreased when the particles were modified. This is assigned to the fact that the adsorption of dye on the particles' surface is reduced when the surface is covered by hydrophobic moieties (Figure 3-35).

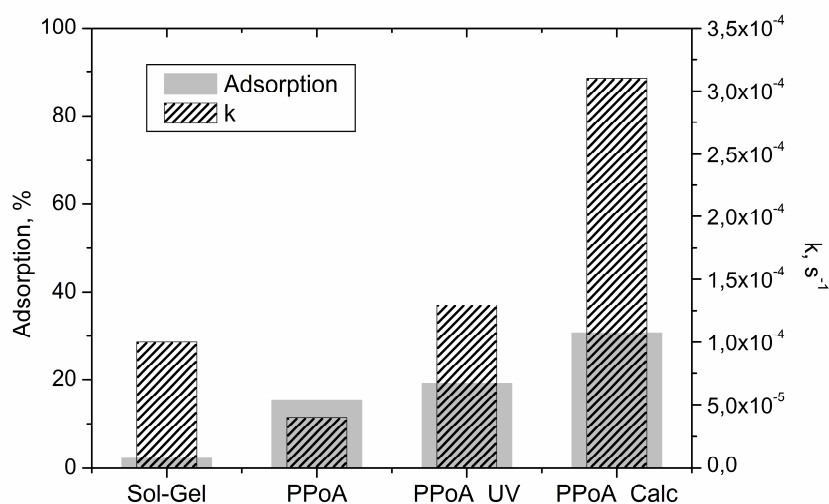


Figure 3-36: K-values and adsorption behaviour of the bare particles compared to differently treated PPOA@TiO₂.

It is well known, that the adsorption of the organic species on the photocatalysts' surface plays an important role in photocatalytic degradation process. From Figures 3-35-37 it is seen that generally the photocatalytic activity was higher when the adsorption of the dye was improved. The adsorption was enhanced when phosphate species were present on the surface of the particles owing to charge accumulation on the surface. However, as seen from the Figures, the adsorption of dye on PPA@TiO₂ and PPOA@TiO₂ was higher compared to bare particles, which exhibit nevertheless higher photocatalytic activity. Thus, the bad activity of the modified particles is rather assigned to the consumption of electrons and holes for the degradation of the organic coupling molecules. Moreover, as stated above (section 3.2.2.4) the modification with coupling molecules makes the titanium dioxide surface sterically inaccessible for species required for photocatalysis. Another explanation might be the deceleration of hole initiated oxidation in the presence of phosphonates and phosphates as stated by Zhao and coworkers.¹⁴⁷

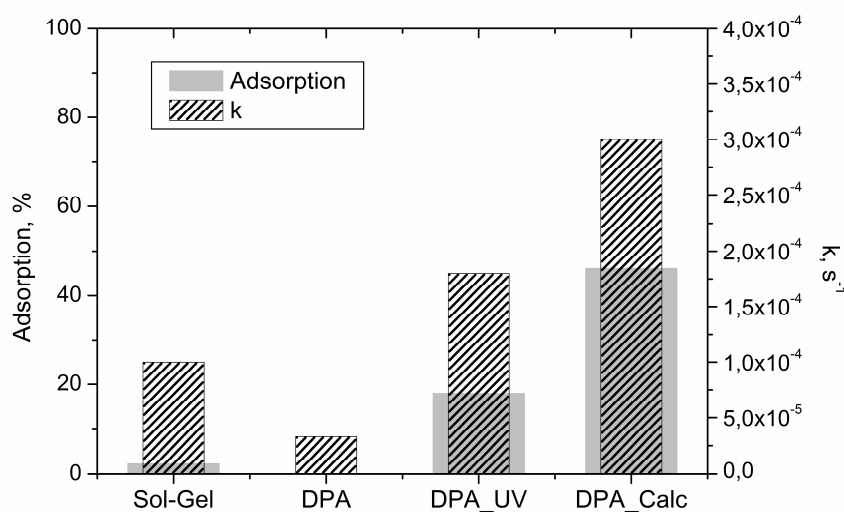


Figure 3-37: K-values and adsorption behaviour of the bare particles compared to differently treated DPA@TiO₂.

Comparing Figures 3-35 and 3-37, it is seen that the photocatalytic activity was higher for PPA@TiO₂ than for DPA@TiO₂, which is in concordance with the above mentioned theory of worse adsorption of dye due to a more hydrophobic moiety present on the surface. However, after degradation of the organics by UV illumination, the samples exhibited again higher photocatalytic activity, which did not depend on the type of phosphonate they had been modified with. Moreover, the illuminated samples showed higher photocatalytic activity compared to bare TiO₂ nanoparticles. This result converges with literature reports on the enhancement of the photocatalytic activity by phosphate doping.^{135, 147, 148} However, the calcined particles exhibited a significantly higher photocatalytic activity compared to illuminated particles. It is assumed that phosphate can migrate into the bulk titanium dioxide nanoparticles at elevated temperatures, whereas upon illumination the created phosphate stays on the surface of the particles. However, it is possible that the organics were not yet fully degraded and inhibited the MB degradation. For this reason, titanium dioxide nanoparticles were modified with phosphoric acid and the photocatalytic activity of thus obtained particles was compared to the illuminated samples.

In Figure 3-38 the photocatalytic activities of the illuminated and calcined particles and the activity of particles treated with phosphoric acid (PA) are presented. It is seen that after illumination the samples were slightly less photocatalytically active than PA@TiO₂. The absence of an organic moiety in phosphoric acid compared to organophosphonates and phosphates is assumed to make a higher surface coverage

possible, which can lead to a higher photocatalytic activity. However, it is also possible that traces of organics that could not be detected by spectroscopic methods are left on the particles' surface, decreasing the degradation rate of methylene blue.

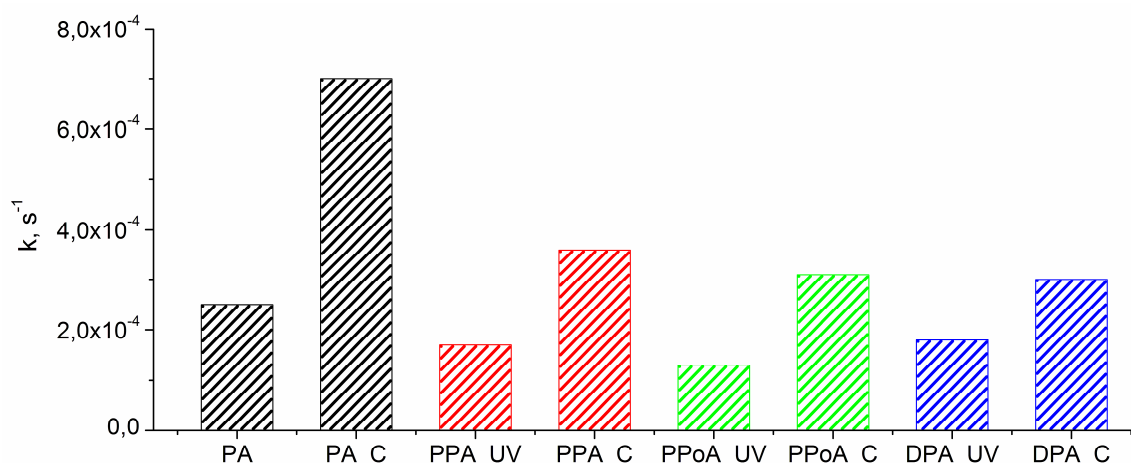


Figure 3-38: K-values of PA@TiO₂ without and with calcination compared to differently treated PPA, PPOA and DPA@TiO₂.

Moreover, it is seen that the photocatalytic activity increased drastically upon calcination also for PA@TiO₂. Thus, it is assumed that during calcination not only the organic compounds were degraded as upon illumination, but in addition to that side reactions occurred. As elucidated above, from XRD measurements including Rietveld analysis higher amounts of anatase were observed for calcined samples compared to illuminated particles. Anatase is known to exhibit best photocatalytic activity among the different phases of titanium dioxide as elucidated in the introduction. As mentioned in the introduction, phosphorus might migrate into the titanium dioxide matrix upon temperature treatment, be doped into the framework and cause a band gap shortening. However, it is interesting, that the photocatalytic activity of calcined PA@TiO₂ was significantly higher than the activities of the calcined particles modified with organophosphonates and phosphates. Calcined PA@TiO₂ was calculated to consist of 60% anatase and 34% brookite. This composition might be optimal for photocatalytic activity. However, the increased activity might also be attributed to a higher surface coverage achieved with phosphoric acid.

3.2.4 Conclusions

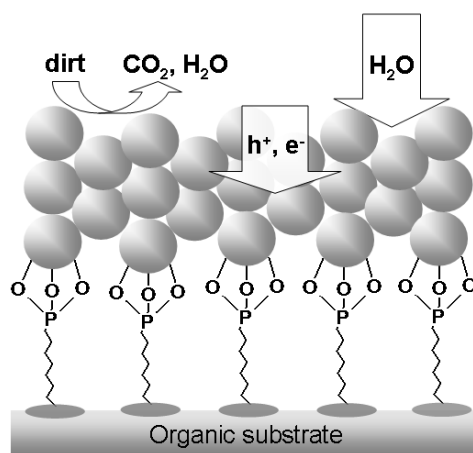
The degradation of organic phosphonates and phosphates on photocatalytic titanium dioxide nanoparticles was investigated. The organic moieties were found to be completely degraded while the P-O-Ti bond is photocatalytically stable and a phosphate species remains on the particles' surface. This phosphate species was found to enhance the photocatalytic activity significantly compared to bare TiO₂ nanoparticles, even if a calcination step is more effective to obtain increased photocatalytic activity. Moreover, the degradation of the organic moieties was found to proceed sequentially via addition of hydroxyl radicals as well as by electron transfer from the organic compound to surface trapped holes. The degradation reaction rate of phosphate was shown to be faster compared to phosphonate which is assigned to facilitated hydroxyl radical formation due to the accessory lone pair of the additional oxygen, which is a hydrogen bond acceptor. Furthermore, the degradation rate of alkylphosphonate was found to be faster compared to aromatic phosphonates owing to worse stabilization of radicals.

Hence, the phosphonate bridge cannot protect the organic species from degradation. This finding makes such modified particles unsuitable for monolayer coatings on organic substrates. However, as found by Lorret et al.²⁹⁷ for an optimal photocatalytic activity the film thickness of such coatings should be in the range of 100 nm. Thus, multilayer coatings are required. Such coatings should be prepared in such a way that the first layers exhibit functional groups for the interaction with the substrate. Subsequent layers should be composed of bare TiO₂ nanoparticles. Due to the short lifetime and diffusion length of photogenerated electrons and holes,³² it is assumed that the substrate and the first layers of functionalized particles can thus be protected from degradation. Nevertheless, the particles in the first layers need a bare surface for interaction with subsequent layers of bare TiO₂ nanoparticles.

Two different possibilities exist for the connection of titanium dioxide nanoparticles to an organic substrate when the particles should exhibit one bare side for photocatalysis: First, the coupling agent can be deposited on the substrate before subsequently depositing the particles. The second possibility is an anisotropic surface modification of the particles and subsequent deposition of the modified particles on the substrate. Since a one-step coating process was desired, anisotropic surface modification was investigated.

3.3 Anisotropic Modification of TiO₂ Nanoparticles

As found by Lorret et al., for optimal photocatalytic activity the film thickness should be in the range of 100 nm.²⁹⁷ Thus, multilayers of titanium dioxide nanoparticles are required. However, for interaction with the substrate modification with organic molecules is necessary, while on the other hand a bare titanium dioxide surface is needed for high photocatalytic activity. For economic reasons, only the first layers should involve modified particles, while the main coating consists of bare TiO₂ nanoparticles. Owing to the short diffusion length of photogenerated charge carriers, the substrate and coupling agents should be protected from degradation by this approach (Scheme 3-4). However, interaction of modified particles with bare TiO₂ particles is only possible, if the modification is anisotropic, so that the interface layer of particles can interact with both, the substrate and the bare particles.



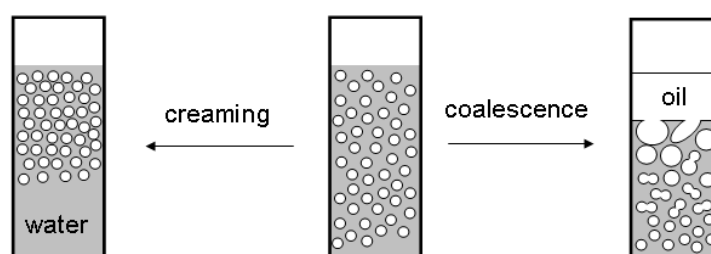
Scheme 3-4: Schematic representation of a multilayer film composed of one layer of anisotropically modified particles and subsequent layers of unmodified particles.

Anisotropic surface modification can be achieved by various different methods as discussed in the introduction. Due to the fast reaction kinetics between phosphonates and TiO₂ surfaces, modification in Pickering emulsion¹⁹¹ was assumed to be adequate for the anisotropic modification of titanium dioxide nanoparticles with organic phosphonates.

3.3.1 Pickering Emulsions Stabilized by TiO₂ Nanoparticles

Numerous investigations on the stability of Pickering emulsion have been conducted applying various kinds of particles as stabilizers^{195, 198, 211} as discussed in the introduction. The stability of such particle stabilized emulsions was found to depend on the wettability of the particles as well as interactions between the particles.^{193, 196} The wettability is influenced by surface properties and the polarity of the oil phase, while interactions between the particles can be determined by adjusting pH, electrolytes and particle concentration. All of these factors were investigated and optimized for TiO₂ nanoparticles prepared according to the above described sol-gel method.

Particle stabilized emulsions were prepared by addition of 20 vol% oil phase to a suspension of the particles in water under agitation with an IKA[®] T25 Ultra Turrax[®] dispenser. Investigations on the stability of Pickering emulsions were conducted according to a procedure by Binks and Lumsdon.¹⁹⁷ After agitation the emulsions were stored in closed vessels with a small diameter. Height changes of the oil/emulsion and emulsion/water interfaces were tracked and the total volumes of oil and water released from the emulsion were calculated. Upon creaming continuous phase (water) is released while coalescence describes the release of dispersed phase (oil). When the amount of released phase is related to the totally added amount of the respective phase, a value for the stability to creaming/coalescence is obtained. As all emulsions were found to be extremely instable to creaming, only the stability to coalescence will be discussed on the following pages. However, as seen from Scheme 3-5, upon creaming the emulsion droplets pack more closely by releasing continuous phase and no destruction of droplets occurs. For this reason, the stability to creaming is not crucial if modification of the particles with coupling agents present in the oil phase is aimed.



Scheme 3-5: Stability of emulsions measured by tracking the change of the water-emulsion (creaming) and the emulsion-oil (coalescence) interfaces.

In Figure 3-39 optical photographs of a typical emulsion immediately after agitation and 30 minutes after agitation are presented.

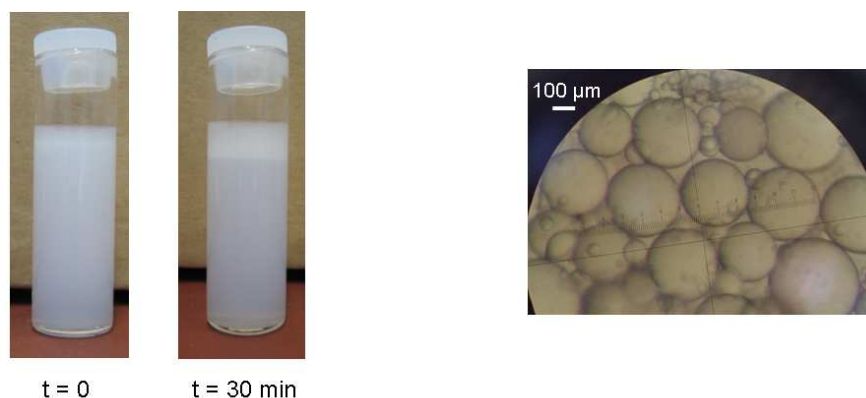


Figure 3-39: Photograph image (left) and optical microscope image (right) of a typical emulsion (1 wt% particle concentration, pH = 3, no salt, cyclohexane) immediately after agitation and 30 minutes after agitation.

While the emulsion droplets are dispersed in the whole water phase in picture **a**, they are packed in the upper part in picture **b**. Thus, the emulsion is instable to creaming but stable to coalescence as no oil phase is emerged from the emulsion. The optical microscope image taken immediately after agitation presented in Figure 3-39 exhibits droplet sizes of 50-500 μm .

The stability and the type of emulsion that is formed depends on the wetting behaviour of the particles. For a stable emulsion the particles need to be wetted by both liquids, which means that the oil-water-solid angle of contact needs to be near 90° . As discussed in the introduction, for contact angles slightly below 90° , oil-in-water emulsions are stabilized, while for contact angles above 90° water-in-oil emulsions are formed.¹⁹⁴

Titanium dioxide nanoparticles exhibit a high wettability with water due to their hydrophilic surface. Thus it is assumed that oil-in-water emulsions are stabilized by TiO_2 nanoparticles. Conductivity measurements were performed in order to determine the type of emulsion. High conductivities in the range of several $\mu\text{S}/\text{cm}$ to mS/cm indicated a conducting continuous phase (water) and thus the formation of o/w emulsions was confirmed. Moreover the polarity of the oil phase influences the oil-water-solid angle of contact and plays an important role when the stability of a Pickering emulsion is optimized. For this reason the stability of emulsions with different oil phases were

investigated. It was found that emulsions with highly apolar cyclohexane as the oil phase exhibited higher stability compared to emulsions with the more polar oil phase toluene. Obviously an optimal oil-water-solid angle of contact (slightly below 90°) is obtained for highly polar oil phases. For this reason cyclohexane was used for further investigations.

Surface properties and especially ionic species present on the particles' surface have a high impact on the stability of emulsions. The surface charge can be regulated by adjusting the pH or electrolyte concentration. To form a stable interfacial film it is necessary that the particles show interactions with each other without being flocculated.¹⁹⁶ For this reason the stability of the emulsions is expected to be highest at a pH slightly below the flocculation point. The pH of flocculation was investigated for various particle and salt concentrations. In Figure 3-40 the pH of coagulation for different NaCl and particle concentrations with cyclohexane as the oil phase is presented. This graph makes a prediction of the optimal pH for stable emulsions possible.

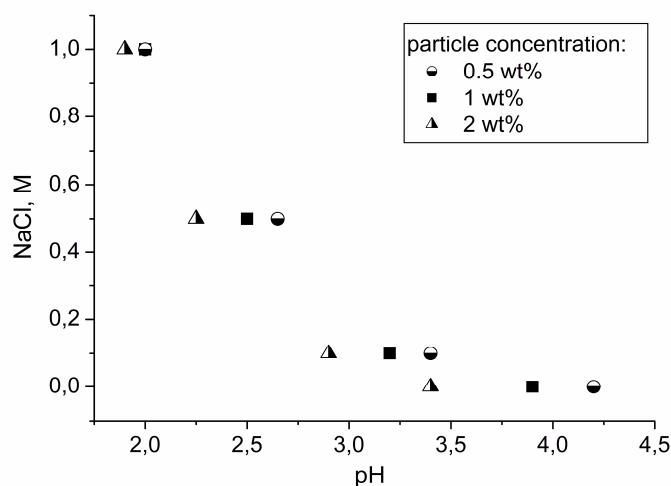


Figure 3-40: Critical coagulation pH for different salt and particle concentrations.

The coagulation point describes the pH where the suspension starts to be non-transparent for visible light, but no sedimentation occurs. It is seen from Figure 3-40 that the pH of flocculation is decreasing with increasing salt and particle concentration.

For emulsions without salt and 1 wt% particles most stable emulsions are assumed to be obtained at pH values around 3.7. For 0.5 wt% on the other hand the particles start to

flocculate at a pH of 4.2 which leads to the assumption that emulsions might be stable at pH values around 4.

In Figure 3-41 the stability of emulsions without salt and 1 wt% particle concentration to coalescence at different pH values is presented as a function of time.

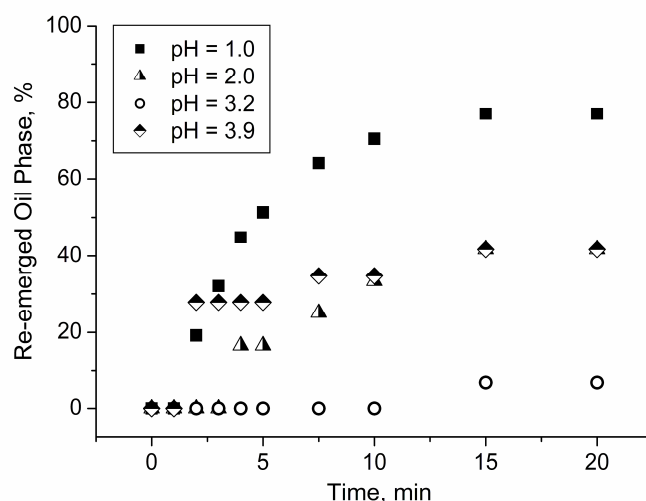


Figure 3-41: Stability of emulsions without NaCl and with 1 wt% particles to coalescence depending on the pH: re-emerged oil phase as a function of time.

After 20 minutes the lowest amount of emerged oil phase was distinguished at pH 3.2. Moreover, it is seen from Figure 3-41 that no coalescence was observed for 10 minutes for this sample, while at pH 1.0 the emulsion started to coalesce already after 2 minutes.

Figure 3-42 compares the stability of emulsions depending on pH and salt concentration. Similar trends were observed for emulsions with or without salt. Regardless the addition of electrolyte, the emulsions exhibited a minimum for the amount of re-emerged oil phase and thus maximum stability at a certain pH. However, the minimum was shifted to lower pH for samples with salt.

For emulsions without salt, highest stability was obtained at pH values slightly above 3 (3.2), whereas for emulsions with 0.1 M NaCl concentration the highest stability was gained for pH 2.8. As explained above, optimal film formation at the o/w interface is obtained in a state of incipient flocculation, where the particles exhibit significant attractive interaction but do not agglomerate. Thus, most stable emulsions were expected at pH values slightly below the flocculation point. These results are in concordance with the measured flocculation points of 1 wt% suspensions without NaCl (3.9) and with 0.1 M NaCl (3.4).

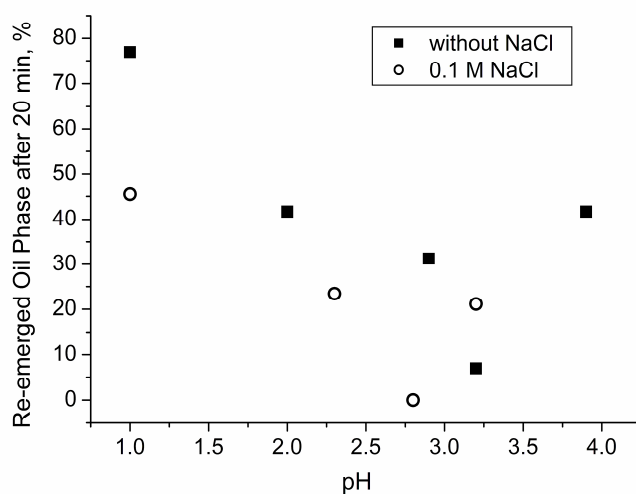


Figure 3-42: Stability of emulsions with 1 wt% particles to coalescence depending on pH and addition of NaCl.

Moreover, it is observed that the stability of emulsions can be enhanced by addition of NaCl if the pH is slightly below the flocculation point of the respective salt concentration. This finding is in concordance with investigations by Binks et al.¹⁹⁷ on emulsions stabilized by silica particles. They found that the addition of electrolytes can enhance the stability of emulsions. However, the point of zero charge (pzc) for silica is around pH 2, whereas the pzc of titanium dioxide is close to pH 6. For this reason, the negative surface charge on silica is increasing with increasing pH (above pH 2), while for titanium dioxide the positive surface charge is decreasing with increasing pH (up to pH 6). Hence the critical coagulation concentration increases with increasing pH for silica, but it decreases for TiO₂. These observations are in concordance with the DLVO theory,^{283, 284} which combines the effects of the van der Waals attraction and the electrostatic repulsion forces as charged particles approach each other.

As discussed above, the pH of flocculation depends on the particle concentration (Figure 3-40). Thus, when the stabilities of emulsions exhibiting different particle concentrations are compared, the pH needs to be optimized for every concentration. In Figure 3-43 the time-dependent stabilities of emulsions with different particle concentrations are compared. The stability to coalescence was increasing from 0.5 to 1 wt%, but did not increase significantly when the particle concentration was elevated above 1 wt%. Therefore, all subsequent investigations were carried out at 1 wt% of particles.

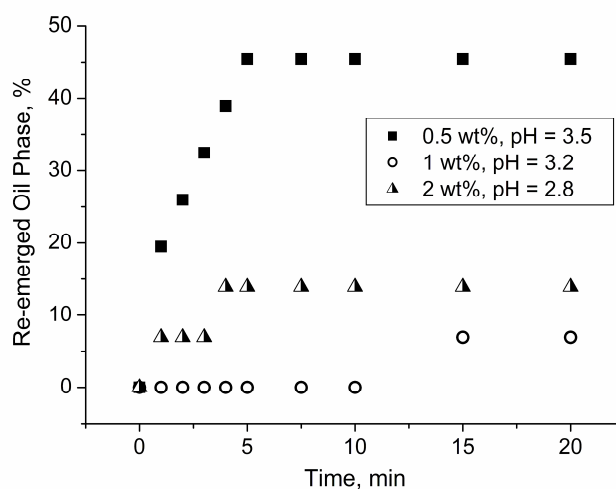


Figure 3-43: Stability of emulsions without salt to coalescence depending on the particle concentration as a function of time.

The following conclusions can be drawn from the investigations on the stability of Pickering emulsions stabilized by sol-gel TiO_2 nanoparticles: The pH of coagulation decreases with increasing particle and salt concentration. This behaviour is assigned to the decreasing positive surface charge of titanium dioxide nanoparticles with increasing pH (until pH 6 – point of zero charge) and is in concordance with the DLVO theory. Most stable Pickering emulsions are obtained at pH values slightly below the critical coagulation point – where the particles are in a state of incipient flocculation. The stability of the emulsions can be enhanced by addition of salt in the water phase. Furthermore, the efficiency of titanium dioxide particles in stabilizing Pickering emulsions is increasing with particle concentration. The investigated particles are efficient in stabilizing emulsions at pH values near 3. This finding is very promising for this work, taking into account that the phosphonic acid derivatives at this pH value are dissociated, favoring the reaction with the positively charged titania surface.

3.3.2 Modification in Pickering Emulsion

The addition of hydrophobic coupling agents to the oil phase of a Pickering emulsion provides a straightforward route to Janus nanoparticles. As discussed above, it is assumed that this method can be applied for the anisotropic modification of metal oxide surfaces with phosphonates due to the fast reaction kinetics.²⁸⁵ Modified particles are assumed to be immobilized at the interface of the emulsion owing to

hydrophilic/hydrophobic interactions with the solvents. For this reason an increased stability of emulsions containing organic phosphonates is expected.

Pickering emulsions were prepared by addition of 20 vol% cyclohexane containing 3 mM dodecylphosphonic acid (DPA) to a 1 wt% suspension of TiO₂ nanoparticles in water upon agitation with an IKA[®] T25 Ultra Turrax[®] disperser. In Figure 3-44 the stability of such emulsions to coalescence is presented as a function of time compared to a similar emulsion without phosphonate. It is seen that the stability was enhanced drastically upon addition of DPA. No coalescence was observed for several days.

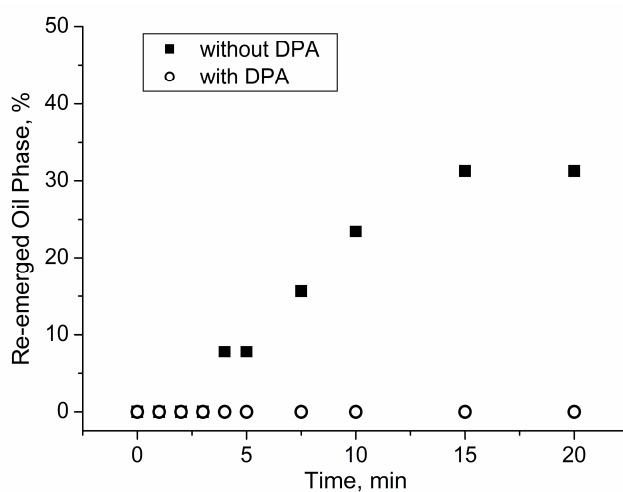


Figure 3-44: Stability of emulsions with 1 wt% particles, no salt and pH = 2.9 to coalescence, without and with DPA.

The significantly increased stability of emulsions with DPA suggests that the particles are immobile at the o/w interface. Such drastically decreased mobility of the particles can only be ascribed to a differentiated surface, one hydrophilic and one hydrophobic side.

The Pickering emulsion was broken by centrifugation and the obtained particles were washed thoroughly with ethanol. Thus obtained Janus nanoparticles were characterized by FT-IR, TGA and NMR. Thermogravimetric analysis presented in Figure 3-45 revealed similar onset temperatures for anisotropically modified particles and particles modified in suspension. Both TG plots showed a continuous mass loss at low temperatures which is assigned to the release of volatile compounds due to desorption and condensation of surface hydroxyl groups. At low temperatures the release of adsorbed species (water, ethanol) and the condensation of Ti-OH groups was

observed. Due to higher free surface area the mass loss at low temperatures was higher for particles modified in emulsion. In the temperature range between 260 and 600 °C a lower mass loss was observed for particles modified in emulsion, indicating lower surface coverage due to anisotropic modification.

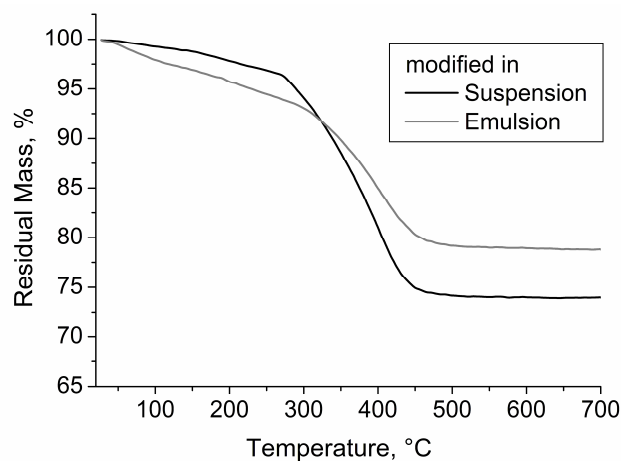


Figure 3-45: TGA plots of particles modified with DPA in suspension and emulsion.

In Figure 3-46 the FT-IR spectra of particles modified with DPA in suspension and in emulsion are presented.

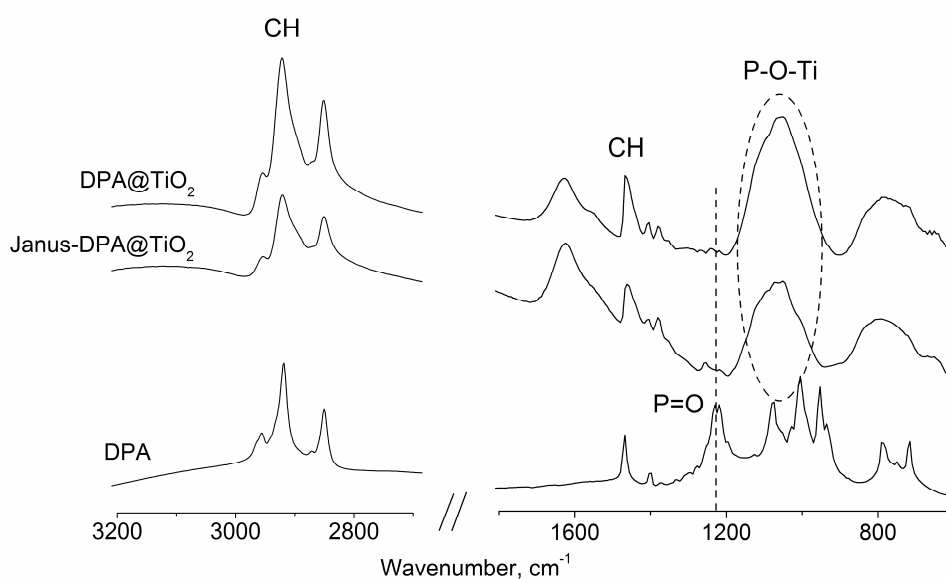


Figure 3-46: FT-IR spectra of DPA and particles modified in suspension and emulsion.

For both compounds the formation of P-O-Ti bonds could be proven by a broad signal observed between 970 and 1150 cm^{-1} . Moreover, the presence of characteristic CH stretching vibrations at 2850 and 2920 cm^{-1} proved the successful modification with DPA. The disappearance of the P=O signal at 1220 cm^{-1} is in concordance with literature reports on isotropic modification and indicated similar bonding modes of particles modified in suspension and in emulsion.¹³⁴

^{31}P NMR spectra of DPA and particles modified with DPA in emulsion are presented in Figure 3-47. The phosphorus signal was shifted highfield and broadened when particles were modified with DPA.

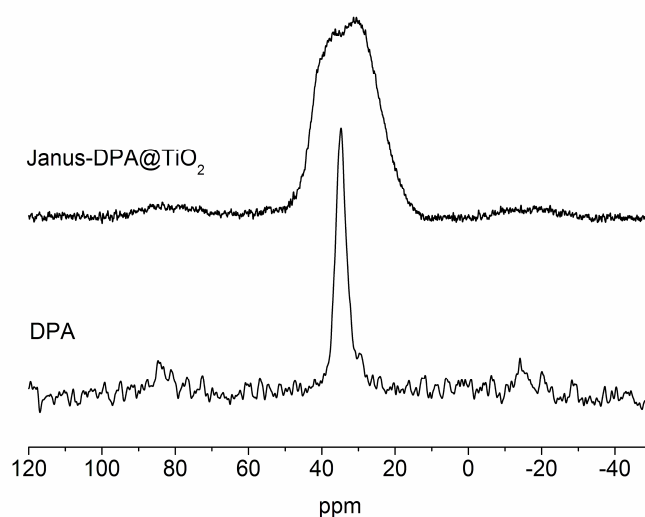
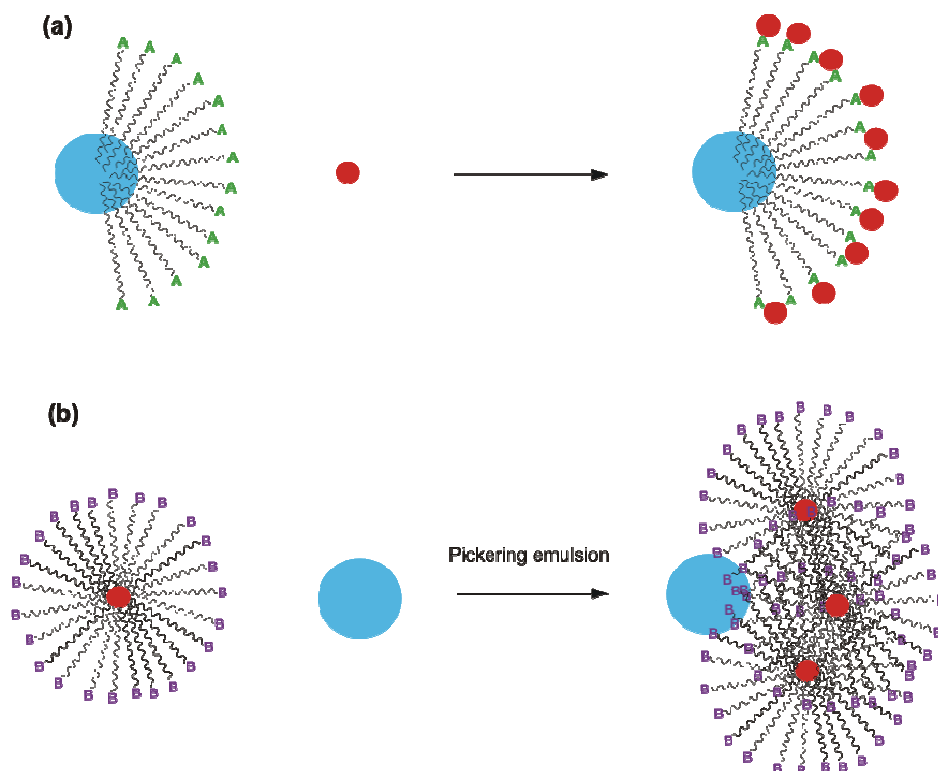


Figure 3-47: ^{31}P NMR spectrum of DPA and ^{31}P MAS NMR spectrum of particles modified with DPA in emulsion.

The ^{31}P NMR signal shift and shape was similar to the one observed for particles modified in suspension (Figure 3-23 – section 3.2.2.2) and can be assigned to P-O-Ti bonds. Unfortunately, due to the influence of numerous factors on the ^{31}P NMR shift, the content of P-O-Ti bonds could not be quantified. However, ^{17}O MAS NMR investigations on titanium dioxide modified with different organic phosphonates by Brodard-Severac et al.¹⁴⁵ revealed the presence of several different binding modes.

3.4 Proof of the Anisotropy

A drastically increased stability of Pickering emulsions was achieved upon addition of hydrophobic coupling molecules to the oil phase. This fact can be considered as an evidence for a differentiated surface of the particles. In addition, a direct proof by an electron microscope technique was aimed. However, in electron microscopy the organic coupling agents cannot be identified owing to their transparency for the electron beam. Thus, the decoration of the modified side of the particles with metal nanoparticles, which exhibit high contrast in electron microscopy, seemed to be a straightforward technique to make the anisotropy visible in TEM. Literature reports on selective labeling of one hemisphere of Janus particles with metal nanoparticles usually involve gold nanoparticles as discussed in the introduction.^{170, 223} Hence phosphonates that exhibit organic groups capable for interaction with gold are required. For this reason, poly(ethylene glycol) (PEG) with one phosphonate end group was prepared and used for the anisotropic modification of titania nanoparticles. Interaction between the hydrophilic polymer chain and gold nanoparticles exhibiting citrate groups on their surface was assumed to make a selective labeling of the PEG-modified side of the particles possible (Scheme 3-7, page 87). In another approach, the interaction between the alkyl chains of dodecylphosphonic acid and a hydrophobic stabilizing agent on the gold nanoparticles was utilized (Scheme 3-11, page 97). Covalent interaction was aimed when mercapto undecylphosphonic acid (MPA) was used. The decoration of Janus particles exhibiting MPA on one side with gold nanoparticles was hoped to be achieved by exchange of the stabilizing agent on the gold surface with the thiol group of MPA (Scheme 3-6). For creating covalent interaction, two approaches are possible: The first possibility involves the modification of TiO₂ nanoparticles with the respective phosphonate and then gold nanoparticles are added in a second step. In this approach the exchange reaction is highly diffusion limited due to immobilization of the phosphonate on TiO₂ nanoparticles. Thus, a second approach was investigated where the stabilizing agent of gold nanoparticles was exchanged with MPA in a first step followed by anisotropic modification of titanium dioxide nanoparticles with such modified gold particles (Scheme 3-6). Owing to the fast reaction of phosphonates with metal oxide surfaces²⁸⁵ this approach was assumed to be highly promising.



Scheme 3-6: Schematic representation of different approaches for the anisotropic decoration of Janus particles with colloidal gold. (a) Anisotropic modification of TiO₂ particles with functional group A (thiol) that can interact with gold or (b) Modification of gold nanoparticles with functional group B (phosphonate) that can interact with TiO₂.

Gold nanoparticles exhibiting different stabilizing agents on their surface were required to address the various interactions. Hence, colloidal gold was prepared by different methods involving hydrophilic and hydrophobic stabilizing agents. Furthermore, the influence of size and surface properties of titanium dioxide nanoparticles as well as different modification methods were investigated regarding the applicability for proving the anisotropic nature of the titanium dioxide nanoparticles.

3.4.1 Synthesis of Gold Nanoparticles

Gold nanoparticles exhibiting different stabilizing agents on their surface were required in order to achieve different interactions with Janus nanoparticles. Various literature known approaches for the preparation of such colloidal gold were optimized in this work.

3.4.1.1 Synthesis of Gold Nanoparticles by the Turkevich Method

Gold nanoparticles decorated with hydrophilic stabilizers were prepared for hydrophilic interaction of organic phosphonates with the gold surface. A well-established method for the synthesis of such colloids is the reduction of auric acid by sodium citrate.^{286, 287} Gold nanoparticles were prepared by addition of sodium citrate to a boiling auric acid solution. Sodium citrate does not only reduce the auric acid to elemental gold but also acts as a stabilizing agent for gold nanoparticles and thus no other reagents are required. Particle size of the gold nanoparticles was optimized varying the auric acid/citrate ratio between 1:1 and 1:4.

DLS measurements revealed that the particle size decreased with increasing amount of stabilizing agent (Figure 3-48). The stabilization of smaller particles is in concordance with literature reports and is ascribed to the possibility to cover a higher surface area with higher amounts of stabilizing agent.²⁴⁷ The size of the gold nanoparticles can consequently be designed by adjusting the auric acid/citrate ratio.

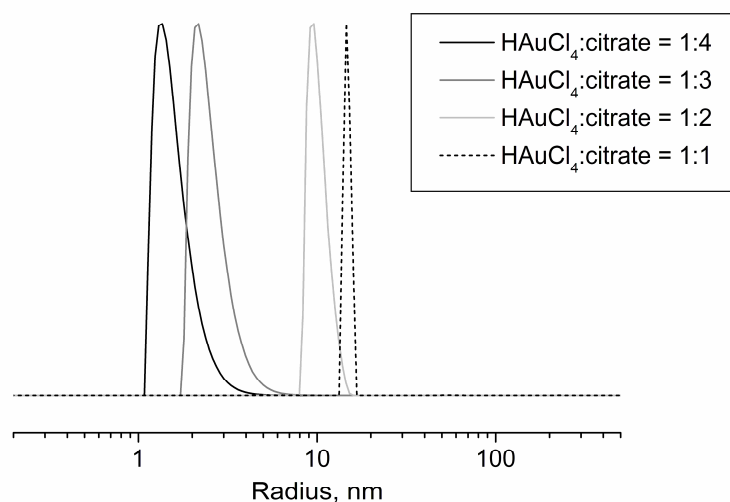


Figure 3-48: DLS plot of citrate stabilized gold nanoparticles prepared with different auric acid/citrate ratios.

3.4.1.2 Reduction of Auric Acid in the Presence of an Organic Thiol

Phosphonates are known to react fast with titanium dioxide surfaces. Thus, it is assumed that effective anisotropic interaction between titania nanoparticles and gold

nanoparticles can be achieved even if the coupling agent is immobilized on the gold nanoparticles. Various reports on the formation of self-assembled monolayers of mercapto alkylphosphonic acids on gold indicate that successful stabilization of gold nanostructures might be possible by this approach.²⁸⁸⁻²⁹⁰ Auric acid was thus reduced by NaBH_4 in the presence of mercapto undecanyl phosphonic acid (MPA) in order to obtain gold nanoparticles stabilized by MPA. Janus nanoparticles can then be obtained by addition of MPA stabilized gold nanoparticles to a Pickering emulsion (Scheme 3-6, **b**). The DLS plots presented in Figure 3-49 revealed that nanoparticles exhibiting considerable stability against agglomeration and growth can be obtained. However, in order to decorate titanium dioxide nanoparticles (between 6 and 80 nm) with considerable amounts of gold nanoparticles, smaller gold particles are required. The addition of higher amounts of stabilizing agent did not result in smaller particles. However, the obtained particle sizes are in concordance with studies by Lu and coworkers on phosphonic-acid functionalized gold nanoparticles.²⁹¹

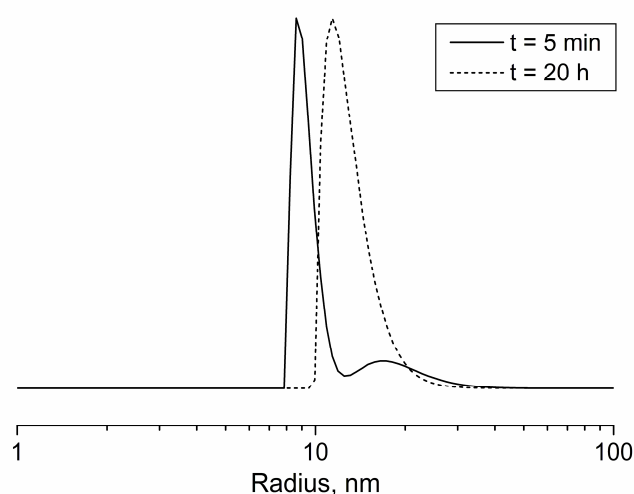


Figure 3-49: DLS plot of gold nanoparticles stabilized by MPA.

Hence, this approach is not suitable for proving the applicability of Pickering emulsions for anisotropic modification of titanium dioxide nanoparticles with organic phosphonates, as smaller gold nanoparticles are required.

3.4.1.3 Synthesis of Gold Nanoparticles by the Brust Method

Gold nanoparticles were prepared according to Brust and Schiffrin²⁴⁸ applying a phase transfer reaction. Auric acid in water was added to a solution of the phase transfer agent tetraoctylammonium bromide (TOAB) in toluene. By stirring the mixture for several minutes auric acid could be transferred to the organic phase. Reduction to gold nanoparticles was performed by addition of NaBH₄. The synthesis method was modified from the literature known Brust method by avoiding the addition of a stabilizing agent. The obtained gold nanoparticles were not stable but grew quite fast owing to the weak interaction of TOAB with gold (Figure 3-50). Nevertheless, the particle size was highly reproducible and such particles can be used for the decoration of Janus TiO₂ particles if they are freshly prepared before application. Moreover, the particle size was optimized by variation of the amount of TOAB. The DLS plots presented in Figure 3-50 revealed a decreasing particle size with increasing TOAB concentration. The possibility to stabilize smaller particles with higher amount of stabilizing agent is assigned to a higher surface area that can be covered.²⁴⁷

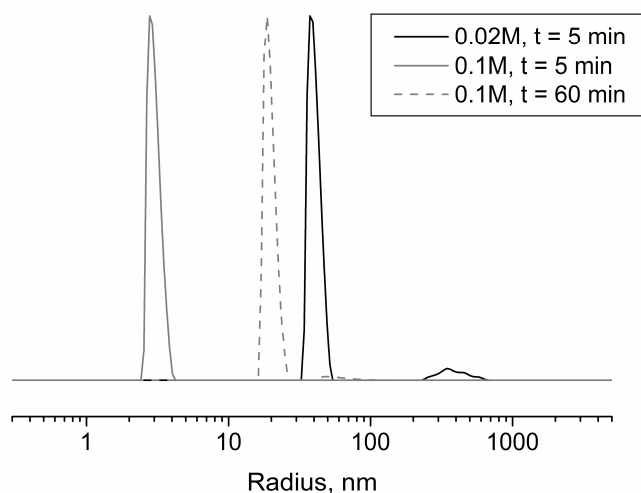


Figure 3-50: DLS plots of gold nanoparticles stabilized with different amount of TOAB measured after different altering times.

3.4.1.4 Stabilization of Gold Nanoparticles obtained by the Brust Method with an Organic Thiol

It is assumed that the instable gold nanoparticles can be stabilized by addition of an organic thiol to the colloid. If MPA is applied the particles can moreover be used for creating anisotropic gold nanoparticle decorated TiO_2 particles by addition of such MPA stabilized gold to a Pickering emulsion (Scheme 3-6, **b**). Thus, MPA was added to the colloid after reduction. TOAB was removed by vigorous washing with toluene. From the DLS plots presented in Figure 3-51 it is seen that the particles were growing upon addition of MPA. Similar particle sizes as for the reduction of auric acid in the presence of MPA were obtained (section 3.4.1.2). This result was not unexpected, as the same final product was aimed by different techniques. Gold nanoparticles exhibiting a diameter of 30 nm are too large for decorating TiO_2 nanoparticles between 6 and 80 nm. Thus, the suggested approach of using gold nanoparticles exhibiting phosphonate groups for anisotropic surface modification of TiO_2 nanoparticles is not possible.

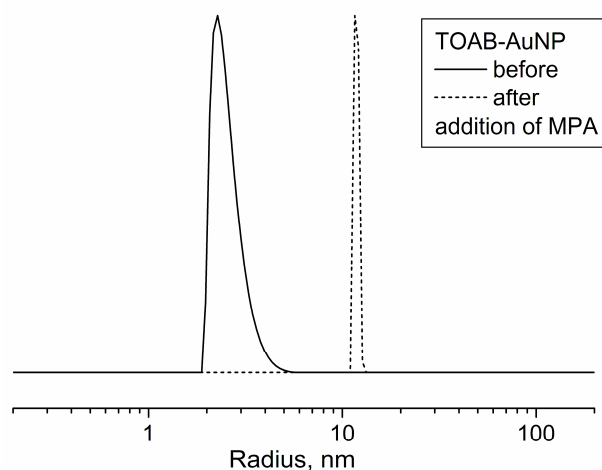


Figure 3-51: DLS plot of gold nanoparticles before and after exchange of TOAB with MPA.

3.4.1.5 Synthesis of Gold Nanoparticles by the Martin Method

Gold nanoparticles exhibiting no stabilizing agent on their surface could be useful for creating interaction with thiols as no competing surface groups are present. Thus, bare gold nanoparticles were prepared according to a procedure by Martin et al.²⁵¹ The concept of the method is the stabilization of nanoparticles by ionic species present on their surface. Thus, auric acid was reduced by NaBH_4 in the presence of hydrochloric

acid and sodium hydroxide. Stable colloidal gold can be obtained applying this procedure even without addition of stabilizing agent. Particle size was optimized varying the ratio of auric acid to NaBH_4 . As seen from the DLS plots presented in Figure 3-52 particle size was increasing with increasing BH_4^- amount, which is in concordance with reports by Martin et al.²⁵¹

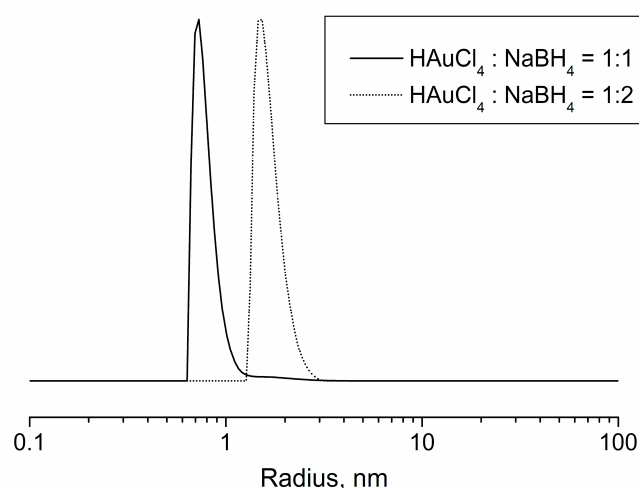


Figure 3-52: DLS plots of gold nanoparticles prepared by the Martin method.

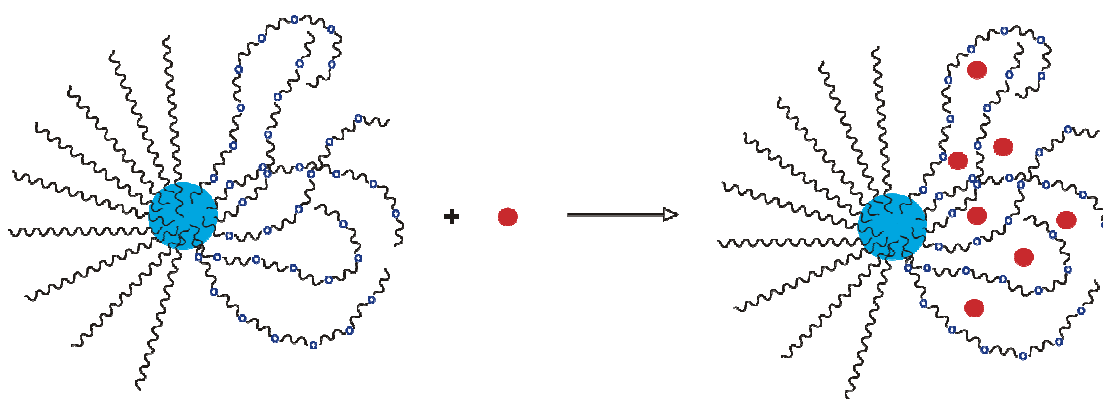
3.4.2 Synthesis of Janus TiO_2 Nanoparticles

As discussed above, various organic phosphonates were used in order to achieve different interactions with gold nanoparticles. Dodecylphosphonate and poly(ethylene glycol) (PEG) exhibiting a phosphonate end group were used for non-covalent interactions with hydrophobic and hydrophilic gold particles while mercapto alkylphosphonates were applied in order to achieve covalent interaction with gold.

3.4.2.1 Poly(ethylene glycol) Janus Nanoparticles

Poly(ethylene glycol) (PEG) is assumed to exhibit considerable interaction with gold nanoparticles stabilized by citrate due to its hydrophilic nature. Thus, poly(ethylene glycol) exhibiting one phosphonate end group (PEG-PA) was prepared from monomethyl poly(ethylene glycol) via vinyl terminated polymer radical addition of diethyl phosphite. The titanium dioxide nanoparticles were modified in Pickering

emulsion with DPA in the oil phase and PEG-PA in the aqueous phase in order to render the other side hydrophobic for selective interaction of the PEG modified side with the hydrophilic gold nanoparticles (Scheme 3-7). Modification with gold nanoparticles was achieved by addition of citrate modified gold nanoparticles to the aqueous phase of the emulsion.



Scheme 3-7: Schematic representation of the preparation of Janus-DPA/PEG@TiO₂ exhibiting interaction with citrate stabilized gold nanoparticles (PEG1-3).

Thermogravimetric analysis of Janus particles before addition of gold nanoparticles was compared with particles modified with PEG-PA and DPA (Figure 3-53). At low temperatures a continuous mass loss was observed similar to PEG-PA@TiO₂, while an onset temperature at 290 °C similar to DPA@TiO₂ indicated the presence of DPA.

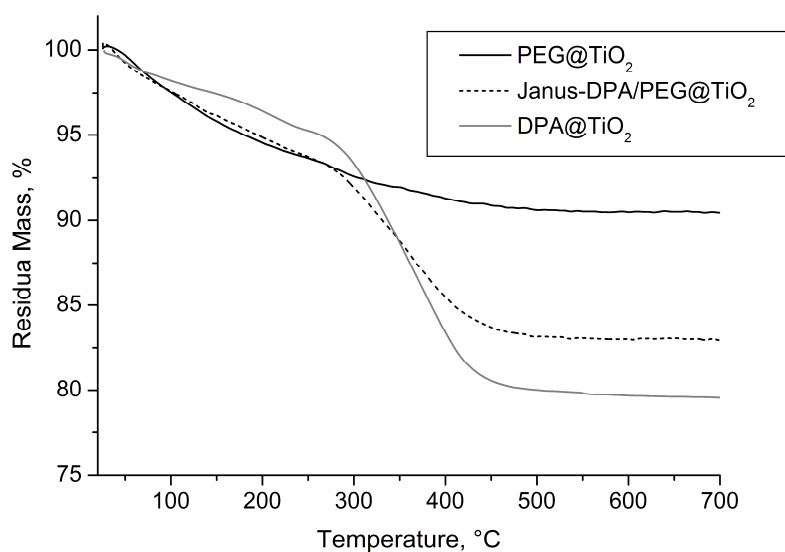


Figure 3-53: TGA plots of particles modified with PEG-PA or DPA in suspension and with PEG-PA and DPA in emulsion.

FT-IR analysis revealed the presence of phosphonate as seen from the broad P-O-Ti vibration between 970 and 1150 cm^{-1} (Figure 3-54). Successful modification with DPA was confirmed by the characteristic CH stretching vibrations at 2850 and 2920 cm^{-1} . The presence of PEG-PA was hard to detect as all characteristic signals are overlapping with other signals. However, the broadening of the P-O-Ti vibration at high wavenumbers compared to DPA@TiO₂ could be assigned to the presence of PEG-PA as observed when comparing the FT-IR spectra of the Janus particles with PEG-PA and PEG-PA@TiO₂.

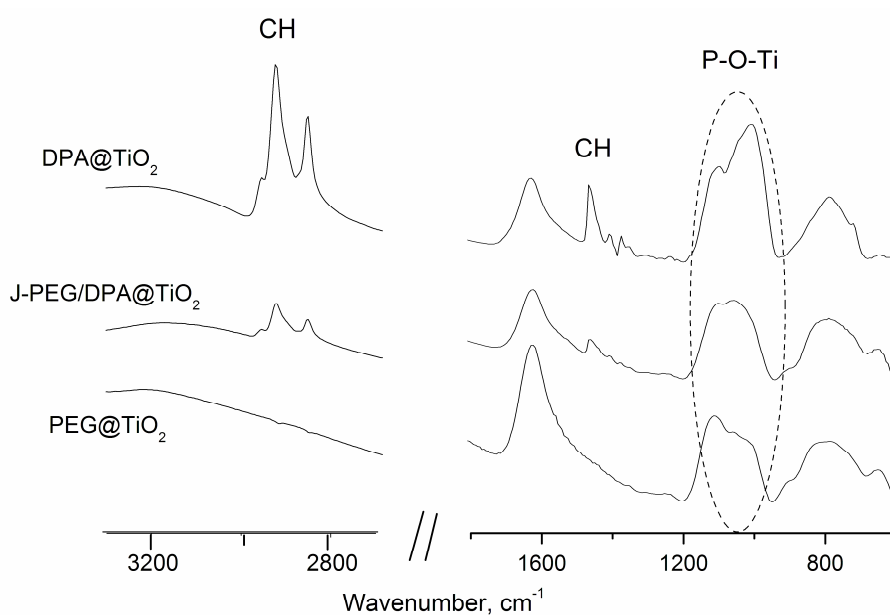


Figure 3-54: FT-IR spectra of DPA@TiO₂, Janus-PEG/DPA@TiO₂ and PEG@TiO₂.

The TEM image presented in Figure 3-55 revealed that the used sol-gel particles were too small to detect anisotropy by TEM. No single particles but only large agglomerates were observed (PEG1). Thus, Evonik AEROXIDE[®] TiO₂ P25 (d = 21 nm) particles were modified applying the same procedures and investigated by TEM (PEG2). The particle size was suitable for analysis by electron microscopy. Several dark spots indicating the presence of gold were observed from the TEM images presented in Figure 3-55, but no particles with anisotropic spreading of contrast could be detected. It is assumed that the interaction of PEG with the gold nanoparticles was too weak to obtain considerable selective decoration. Activation of the P25 surface prior to modification with PEG-PA and DPA by itching with HF or UV illumination¹ was performed in order to obtain higher surface coverage (PEG3). Emulsion droplets were observed as large grey spots in the TEM images because the emulsion was not broken

prior to deposition of the particles on the TEM grids. Gold nanoparticles (black spots) exhibited no interaction with the particles stabilizing the emulsion but were rather randomly distributed on the grid.

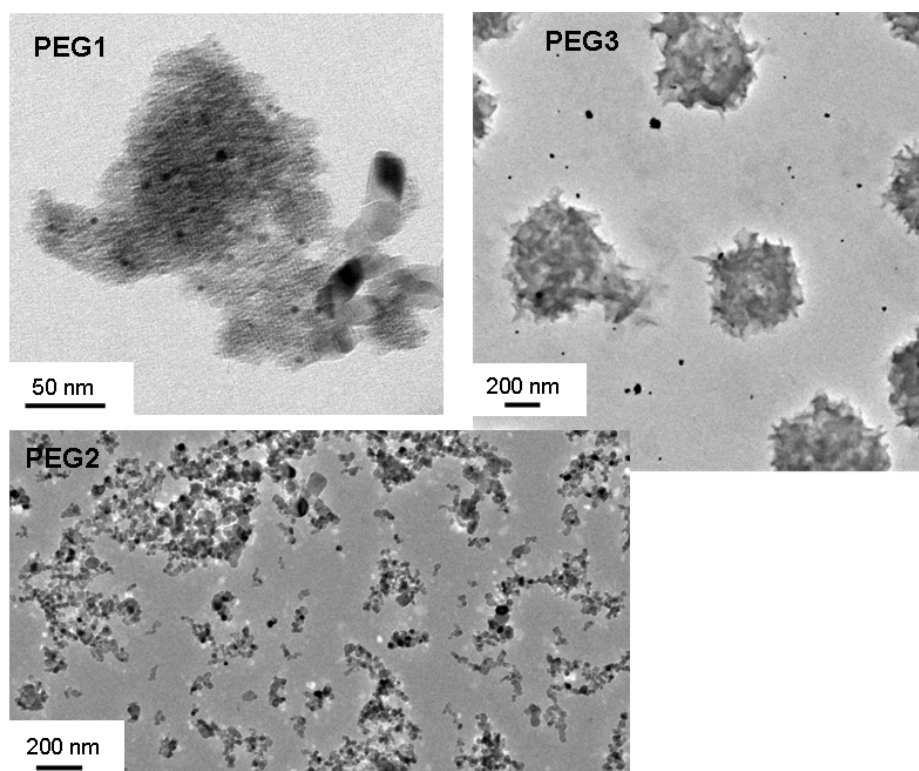


Figure 3-55: TEM images of PEG1, PEG2 and PEG3.

It is concluded that the interaction between PEG and gold was too weak. Hence, further investigations were based on mercapto undecanylphosphonate, which renders a covalent interaction between the gold nanoparticles and the thiol groups possible while the phosphate moiety binds to the TiO_2 surface. The alkyl spacer minimizes steric hindrance and increases the hydrophobicity for a better dispersibility in the oil phase of the emulsion.

3.4.2.2 Thiol-functionalized Janus Nanoparticles

Mercapto undecanylphosphonic acid (MPA) was prepared from 1,11-dibromoundecane via Arbuzov reaction²⁹² with one equivalent triethylphosphite and

subsequent reaction with thiourea according to a procedure developed by Tsai et al. for the synthesis of mercaptodecanyl phosphonic acid.¹⁴⁰ The reaction was tracked by NMR (^1H and ^{31}P) and FT-IR spectroscopy. The ^1H NMR spectrum (Figure 3-56) revealed the presence of a thiol functionality by a signal at 7.4 ppm. ^{31}P NMR revealed only one phosphonate signal at 49.9 ppm proving the purity of the compound.

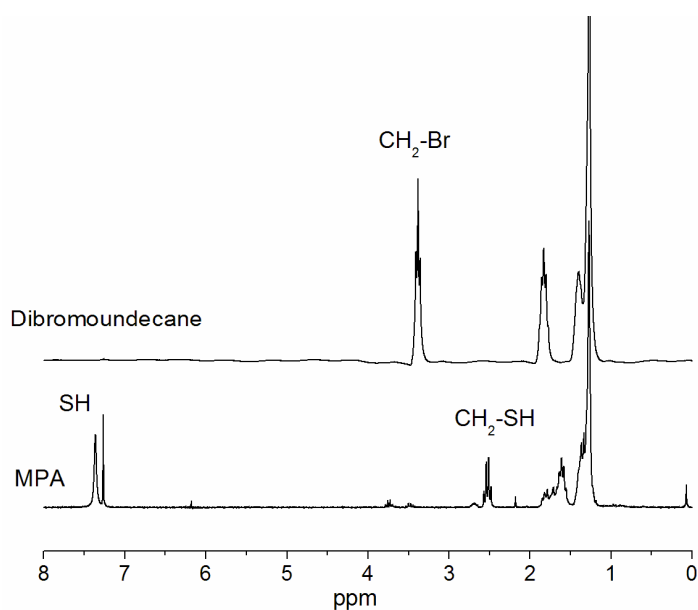


Figure 3-56: ^1H NMR spectrum of Dibromoundecane and MPA.

Various different approaches for anisotropic modification of TiO_2 nanoparticles with MPA and proving the anisotropy were investigated involving all kinds of gold nanoparticles presented above. Anisotropic modification of titanium dioxide nanoparticles was performed rendering the other side either hydrophilic (bare) or hydrophobic (DPA).

Thermogravimetric analysis presented in Figure 3-57 revealed the same onset temperature for both compounds. However, a lower mass loss was observed for particles modified in emulsion, indicating anisotropic modification.

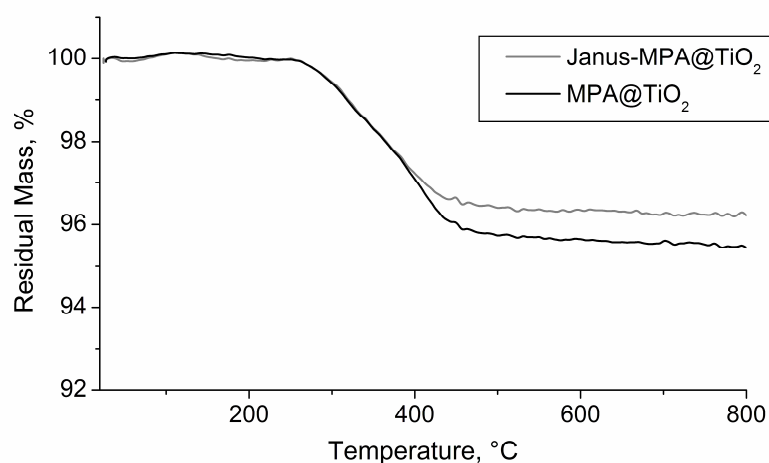


Figure 3-57: TGA plot of MPA@TiO₂ and Janus-MPA@TiO₂.

From the FT-IR spectra presented in Figure 3-58 the presence of P-O-Ti bonds and the disappearance of the P=O signal were observed indicating a similar bonding mode as obtained for DPA@TiO₂.

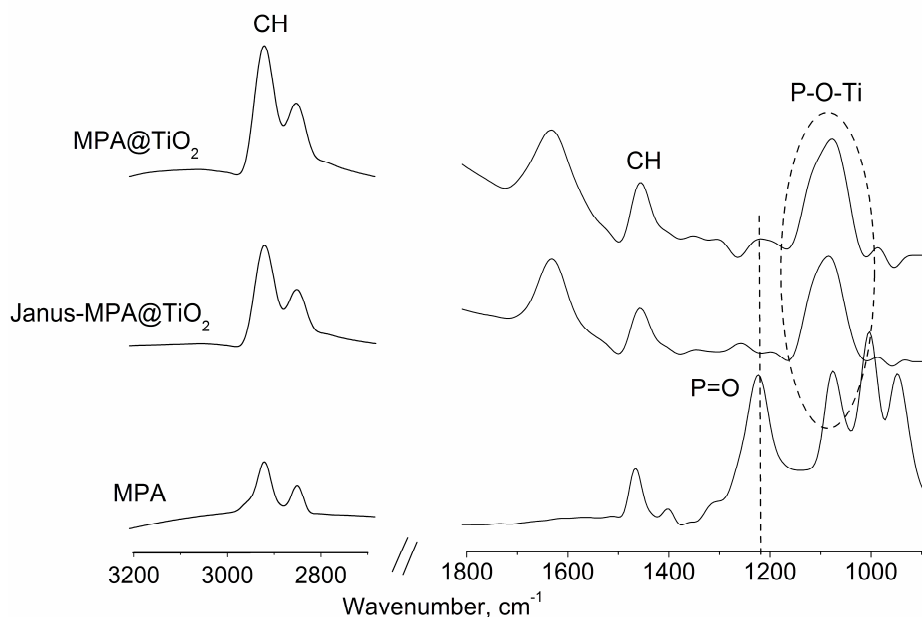
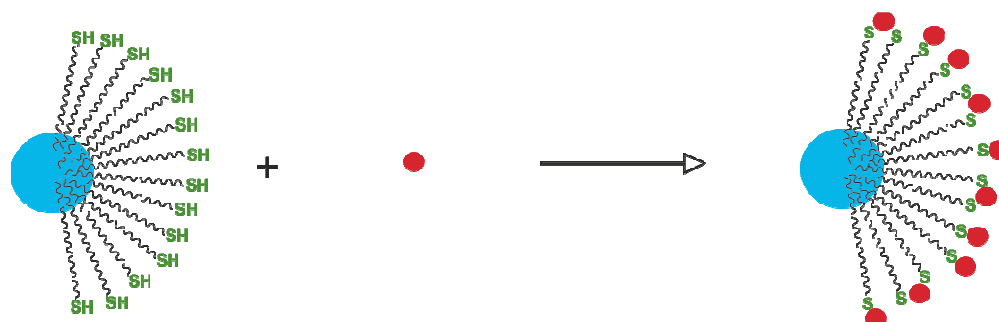


Figure 3-58: FT-IR spectra of MPA, MPA@TiO₂ and Janus-MPA@TiO₂.

Different procedures were applied for creating interaction of the thiol functionality with gold nanoparticles. In a first approach the modified particles were exposed to

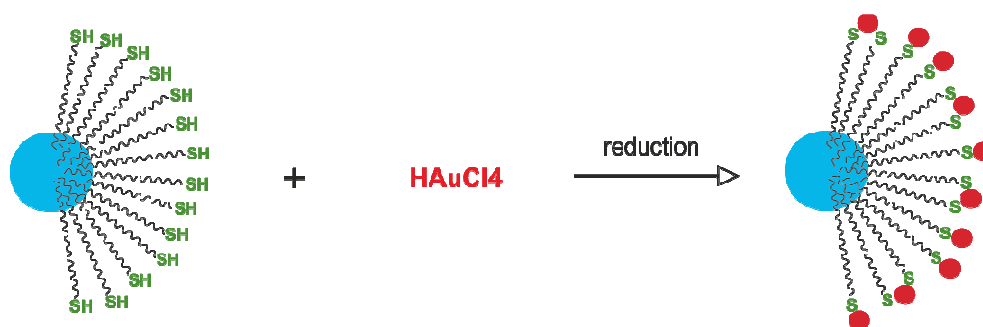
citrate stabilized gold nanoparticles in order to make the differentiated surface visible in electron microscope. An exchange reaction of citrate with thiol was expected which would lead to particles anisotropically decorated with gold nanoparticles (MPA1, Scheme 3-8).



Scheme 3-8: Schematic representation the preparation of MPA1.

Janus-MPA@TiO₂ was dispersed in ethanol applying ultrasonication. After addition of the previously prepared citrate stabilized gold colloid, the suspension was again agitated ultrasonically. Samples for TEM analysis were prepared by immersing a carbon coated copper grid in the suspension followed by drying in air. TEM analysis revealed that the gold particles exhibited about the same size as the titanium dioxide particles (Figure 3-59, MPA1). Thus, no selective decoration of the thiol modified side with gold particles was possible.

It is assumed that the exchange reaction of citrate with thiol is not favourable in such a diffusion limited system. Thus, no selective decoration of the thiol modified area of TiO₂ particles was possible. For this reason, in a second approach auric acid was reduced in the presence of Janus particles (MPA2) as presented in Scheme 3-9. Thiol groups were expected to stabilize gold nanostructures given that sufficient interaction with the gold could be created for avoiding growth of bigger structures.

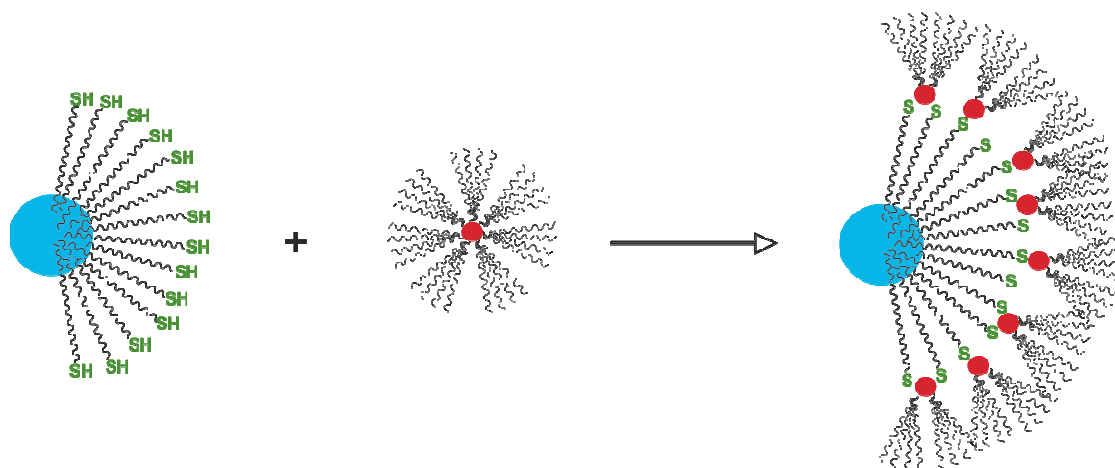


Scheme 3-9: Schematic representation of the preparation of MPA2.

Janus-MPA@TiO₂ particles were suspended in ethanol by ultrasonication. After addition of 1 mM HAuCl₄ the suspension was again agitated ultrasonically and different amounts of NaBH₄ were added subsequently. In the TEM image presented in Figure 3-59 (MPA2) the gold is observed as black spots. It is concluded that gold nanoparticles have successfully been prepared applying in situ reduction of auric acid. However, the metal particles are again too large for selective decoration of one side of the TiO₂ particles.

For the stabilization of smaller gold nanoparticles it is assumed that higher amounts of stabilizing agent are required. Thus, either a second stabilizing agent should be added or the amount of thiol on the surface of TiO₂ particles should be increased. The latter would require higher surface coverage which can be achieved using particles with a more active surface.

In order to improve the stabilization of small gold nanoparticles tetraoctylammonium bromide (TOAB) was used. TOAB stabilized particles were prepared by a slightly modified Brust-Method as described above. Upon addition of such gold particles to Janus nanoparticles, exchange of TOAB with thiol is expected resulting in anisotropic decoration with gold nanoparticles (MPA3) as presented in Scheme 3-10.



Scheme 3-10: Schematic representation of the preparation of MPA3.

Two different approaches were applied for the decoration with TOAB gold nanoparticles: Synthesis of gold nanoparticles in the presence of Janus particles (MPA3a) or subsequent addition of gold colloid to Janus nanoparticles (MPA3b). For the latter approach again two possibilities exist: addition in emulsion (MPA3b1) or suspension (MPA3b2).

For the preparation of gold nanoparticles in the presence of Janus particles, auric acid was added to a suspension of Janus-MPA@TiO₂ in toluene containing TOAB. The reaction mixture was sonicated followed by addition of NaBH₄. For the subsequent decoration methods, TOAB stabilized gold nanoparticles were added to a Pickering emulsion or a suspension of Janus-MPA@TiO₂ respectively and altered for several hours.

A TEM image representative for all three approaches is presented in Figure 3-59 (MPA3a). As seen from the TEM picture, the gold nanoparticles exhibited a diameter of about 5 nm, making them suitable for our purpose. However, it is seen that the coverage of TiO₂ with gold nanoparticles was quite low and thus no selective decoration of one side of the TiO₂ particles could be observed. Furthermore, the gold particles were rather randomly distributed on the surface of the TiO₂ particles than selectively interacting with one side of the particles.

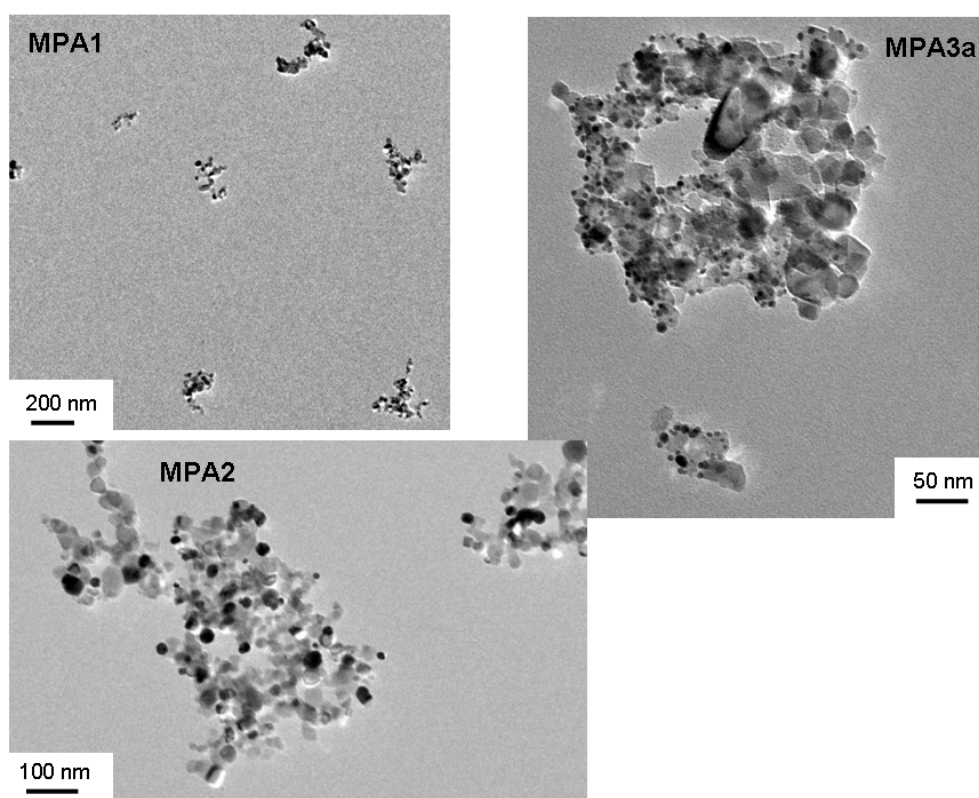


Figure 3-59: TEM images of Janus particles prepared prepared with MPA and P25 (MPA1, MPA2 and MPA3a).

The TEM image revealed that P25 particles exhibited high agglomeration which makes the interpretation of pictures obtained from electron microscopy nearly impossible. Moreover, the bad dispersibility of the used TiO_2 nanoparticles might also have an influence on the structure of the Pickering emulsion. It is assumed that due to the high amount of agglomerates, the emulsion was not stabilized by single particles, but rather by agglomerates of particles. Thus, for subsequent investigations the synthesis of well dispersible titanium dioxide nanoparticles was necessary. From the fact that the gold particles were randomly distributed rather than deposited on the modified side of the particles, it is concluded that stronger interaction between the gold nanoparticles and the modified side of the Janus particles is required. Owing to the immobilization of thiol on titanium dioxide nanoparticles the reaction with gold is highly diffusion limited. Increased interaction was assumed to be achieved by modification of gold nanoparticles with MPA and subsequent modification of TiO_2 nanoparticles with such modified gold particles (Scheme 3-6, **b**). However, as discussed in sections 3.4.1.2 and 3.4.1.4 of this work, no small gold nanostructures could be stabilized with MPA. Thus, the density of thiol groups on the titanium dioxide surface needed to be increased. For this reason, dispersible TiO_2 nanoparticles exhibiting a more active surface were prepared by slight modification of a method by Jiang and Herricks.²⁹³ Titanium glycolate was hydrolysed by dropwise addition to acetone containing <0.5 % water. However, the obtained particles still contained considerable amounts of glycolate and thus calcination was required. TiO_2 nanoparticles with particle sizes between 50 and 100 nm were obtained as seen from the TEM image presented in Figure 3-60.

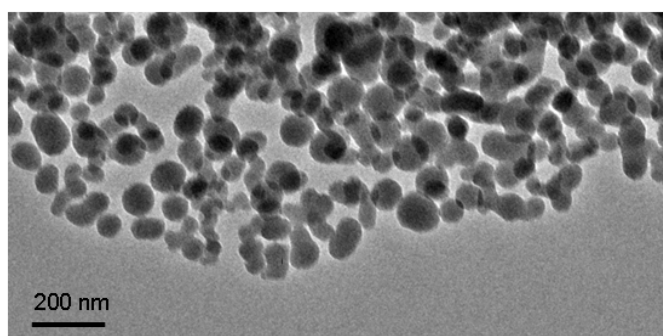


Figure 3-60: TEM image of prepared TiO_2 nanoparticles.

The particle size distribution presented in Figure 3-61 determined from the TEM image revealed a mean diameter of 80 nm.

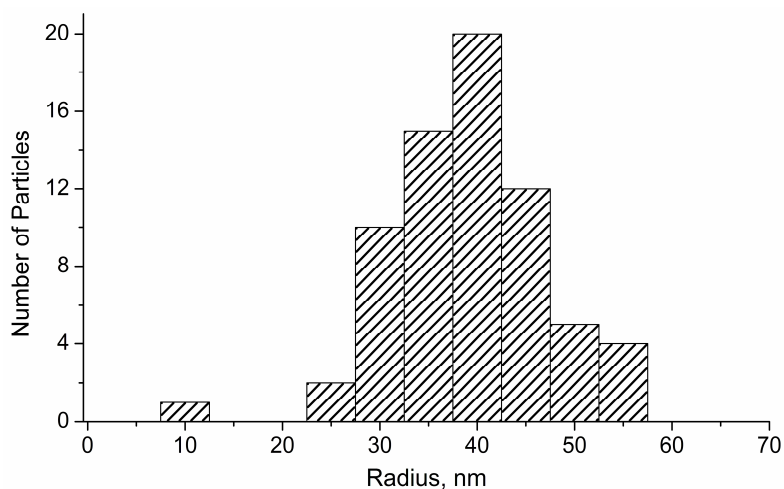


Figure 3-61: Particle size distribution determined from TEM images using ImageJ.

Nitrogen sorption experiments revealed a relatively low surface area (21 m²/g) due to the large particle size and XRD analysis of calcined particles revealed pure anatase phase (JCPDS-21-1272) as seen from Figure 3-62.

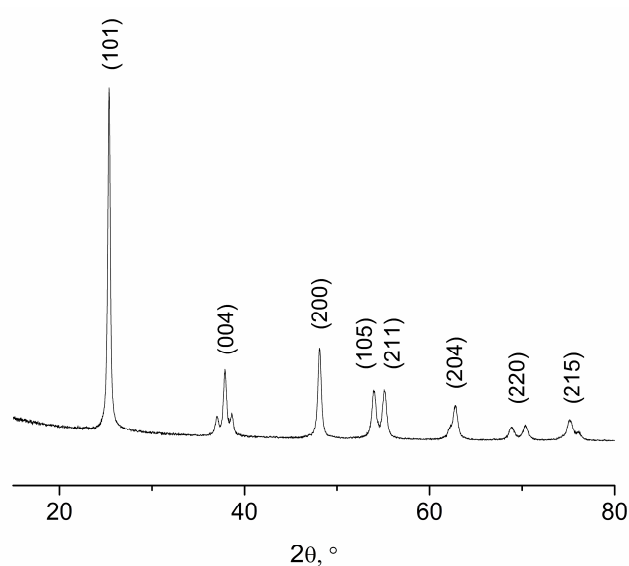


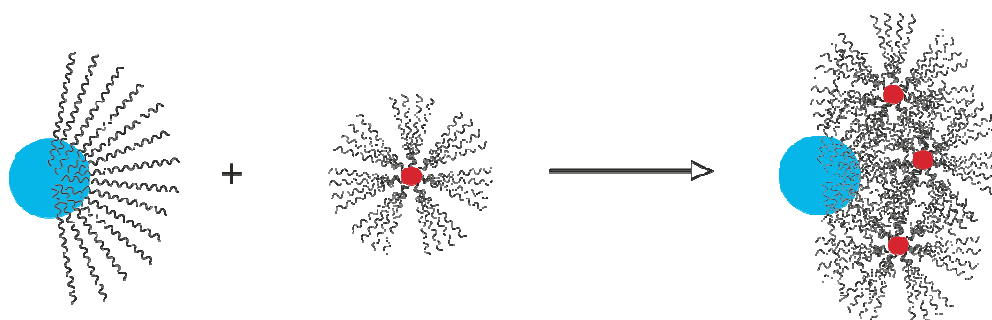
Figure 3-62: XRD pattern of TiO₂ nanoparticles obtained by hydrolysis of Titanium glycolate.

The obtained TiO₂ nanoparticles were modified with MPA in suspension and in emulsion. Thermogravimetric analysis revealed a higher surface coverage compared to P25 particles as seen from Table 3-1 owing to more active groups on the surface. Thus, the as prepared particles were confirmed to be adequate for creating more effective interaction between the modified surface and gold nanoparticles.

Table 3-1: Surface coverage of 60 nm TiO₂ nanoparticles compared to Evonik AEROXIDE® P25

	<i>mass loss (%)</i>	<i>surface area (BET) m²/g</i>	<i>surface coverage (molecules/nm²)</i>
<i>MPA@P25</i>	4.3	50	2.8
<i>MPA@TiO₂-80 nm</i>	2.5	21	3.9

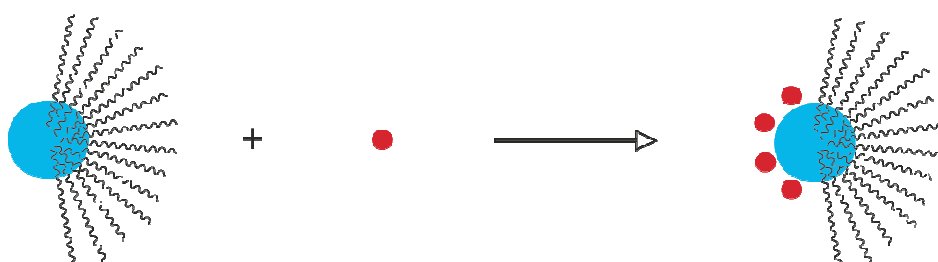
Different approaches involving covalent and non-covalent interaction with gold nanoparticles were investigated using the as-prepared 80 nm TiO₂ particles. Covalent interaction was assumed to be achieved between MPA and gold nanoparticles. Non-covalent interaction was based either on the interaction of alkylphosphonate with TOAB stabilized gold nanoparticles or on hydrophilic interaction between the bare TiO₂ surface and bare gold nanoparticles prepared by the Martin method. Non-covalent hydrophobic interaction was studied applying DPA for anisotropic modification and TOAB stabilized gold nanoparticles in the oil phase of a Pickering emulsion stabilized by TiO₂ nanoparticles (DPA1, Scheme 3-11).



Scheme 3-11: Schematic representation of the preparation of DPA1.

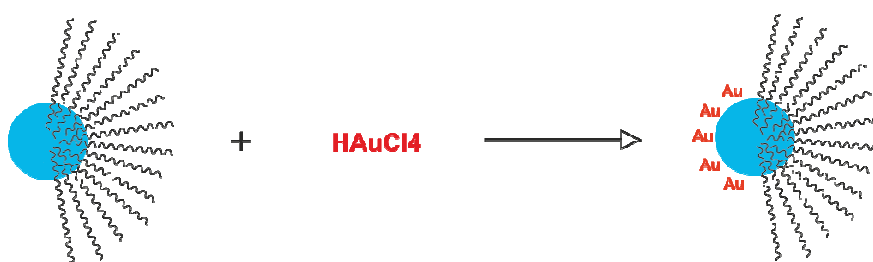
In this approach DPA was mixed with pre-formed gold colloid in toluene and added to an aqueous suspension of titanium dioxide nanoparticles under agitation with an Ultraturrax disperser.

Non-covalent hydrophilic interaction was studied using bare gold nanoparticles (DPA2) or auric acid (DPA3) and TiO₂ nanoparticles anisotropically modified with DPA. Selective hydrophilic interaction of the gold with the bare side of TiO₂ nanoparticles was expected (Scheme 3-12 and Scheme 3-13).



Scheme 3-12: Schematic representation of the preparation of DPA2.

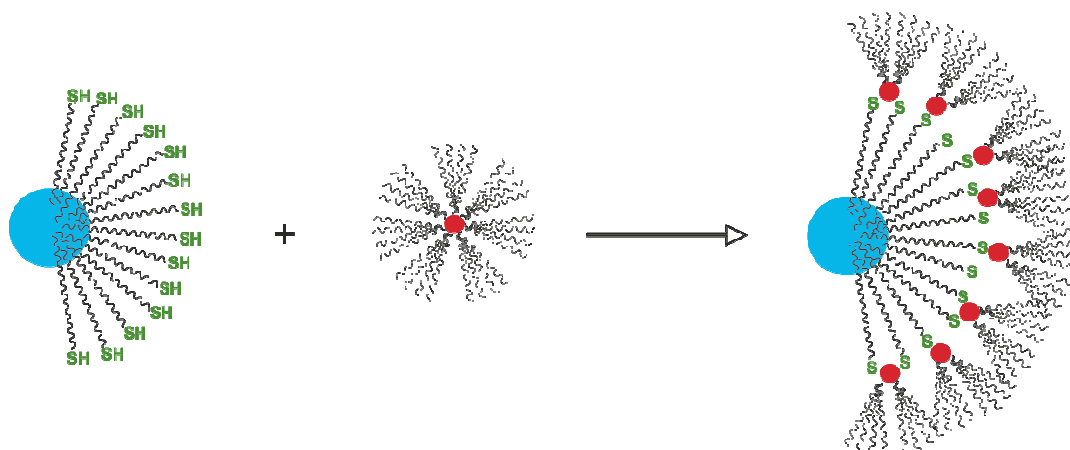
When bare gold nanoparticles were applied a Pickering emulsion stabilized by TiO₂ particles with DPA in the oil phase was formed. Subsequently, gold colloid prepared by the Martin method was added in the water phase of the emulsion.



Scheme 3-13: Schematic representatio of the preparation of DPA3.

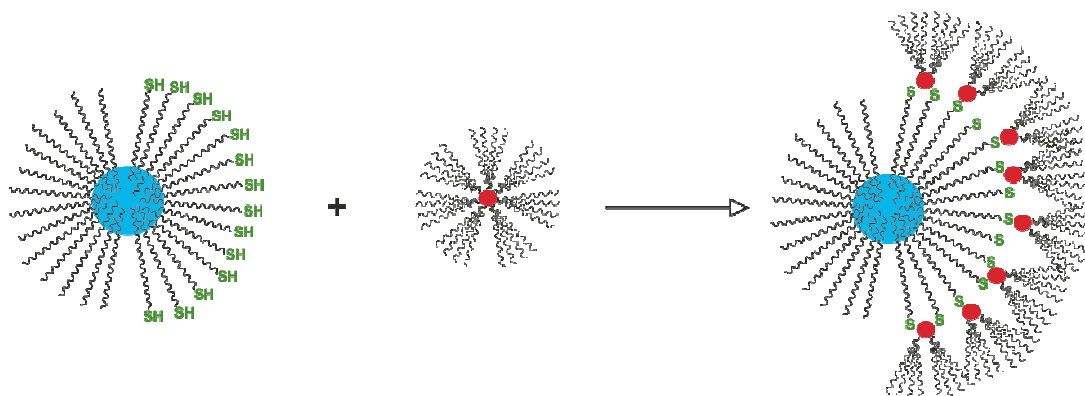
When auric acid was used for the decoration of the bare side of titanium dioxide nanoparticles, a Pickering emulsion with DPA in the oil phase was prepared, followed by addition of auric acid in the water phase.

For covalent interaction 3 different approaches were investigated: First, janus-thiol particles were exposed to TOAB stabilized gold nanoparticles. Upon exchange reaction of weakly binding TOAB with thiol, selective decoration of the modified side was expected (MPA4, Scheme 3-14).



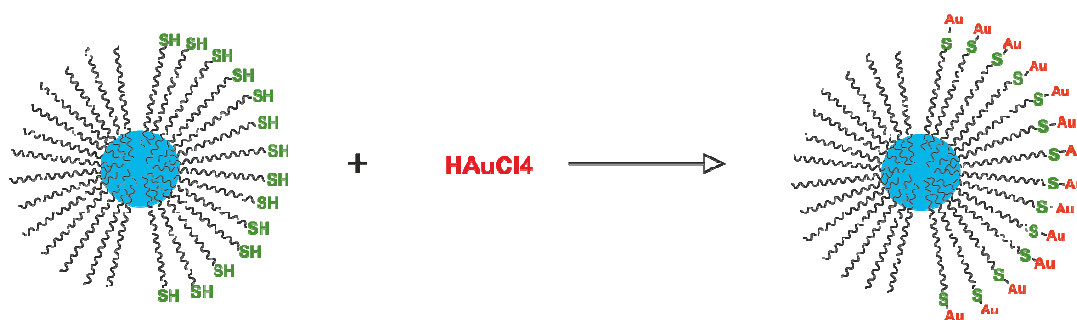
Scheme 3-14: Schematic representation of the preparation of MPA4.

In a second approach, the bare side of TiO_2 particles was protected with DPA (MPA5). Due to more hydrophobic nature of DPA compared to MPA, which exhibits also limited solubility in water, higher selectivity in anisotropic surface modification was expected by this approach (Scheme 3-15).



Scheme 3-15: Schematic representation of the preparation of MPA5.

It is assumed that TOAB particles might also interact with the hydrophobic side of the Janus particles. Thus, in order to obtain selective decoration of the thiol modified side, the same particles were exposed to auric acid in a third approach (MPA6, Scheme 3-16).



Scheme 3-16: Schematic representation of the preparation of MPA6.

TEM images of 60 nm anatase nanoparticles decorated with gold nanoparticles by different approaches are presented in Figure 3-63. However, a selective decoration of one side of Janus particles with gold could not be observed.

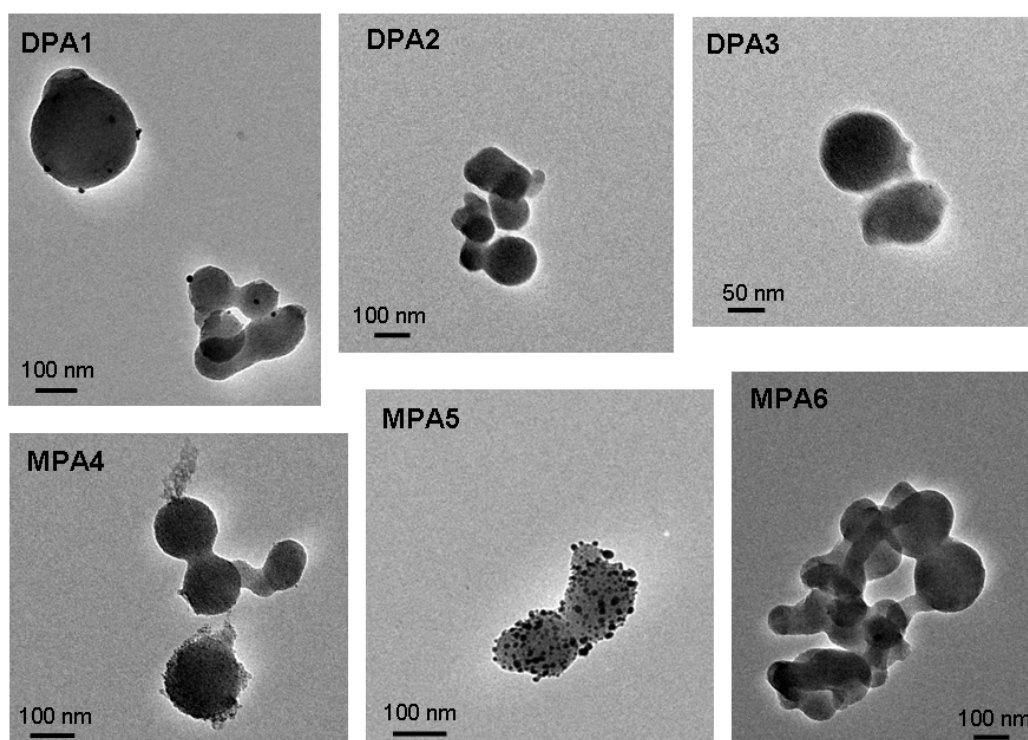


Figure 3-63: TEM images of DPA1-3 and MPA4-6.

As seen from the images obtained by electron microscopy, only low (or no) coverage of titanium dioxide nanoparticles with gold could be achieved. Quite high decoration was obtained when Janus-DPA/MPA@TiO₂ was treated with gold particles prepared by the Brust method as presented in Scheme 3-15 (MPA5). However, this approach did not result in selective decoration of one side of the particles. It is assumed that low surface coverage led to bad interaction between the two kinds of particles. TGA results revealing high surface coverage cannot be trusted owing to the low mass loss of 1-2%. The measurement accuracy of TGA is limited owing to volatile compounds that can be adsorbed on the particles' surface. Additionally, interaction of thiol with the titanium dioxide surface might anticipate its interaction with gold.²⁸² Even if a fast modification kinetic of phosphonates with titanium dioxide surfaces is assumed to prohibit such interaction of thiol with TiO₂, a low surface coverage renders it possible. However, owing to the strong interaction of thiol with gold, such interaction might be cleaved upon addition of gold. Hence it is assumed that low surface coverage is rather to blame for the bad interaction. Moreover, poor dispersibility resulted in bad film formation on the oil/water interface in Pickering emulsions and led to difficult or impossible interpretation of TEM images. Literature reports on the visualization of Janus particles decorated with gold nanoparticles usually involve particle sizes considerably larger than 100 nm.^{170, 223, 294} Such particles can be visualized by SEM, which provides a three dimensional picture of the sample, facilitating the interpretation of images of agglomerates. Moreover, silica particles obtained by the Stöber process are generally used, which are nicely dispersible and observed separated in electron microscopy.^{170, 295} The numerous unsuccessful investigations on the selective anisotropic decoration of Janus particles with gold suggest that a completely new approach for proving the anisotropy might be more successful. Nevertheless it is stated that the drastically increased stability of Pickering emulsions with DPA in the oil phase and the immobility of the particles at the oil/water interface can be considered as an evidence for the anisotropic nature of these particles. Thus, the applicability of Pickering emulsions for the anisotropic modification of TiO₂ nanoparticles with organic phosphonates is strongly suggested.

4 Summary

In this work the modification of photocatalytic titanium dioxide nanoparticles in suspension and in Pickering emulsion has been investigated. The degradation of different organic coupling agents under photocatalytic conditions was studied aiming the applicability for a stable connection to organic substrates.

4.1 Photocatalytic TiO₂ Nanoparticles

First investigations in this work covered an optimization of a literature known procedure for the synthesis of photocatalytic titanium dioxide nanoparticles. The effect of precursor concentration on the size and morphology of the particles was investigated. A linear increase in particle size was observed when the precursor concentration was increased. While at low precursor concentration pure anatase phase was obtained, the brookite content was increased up to 60% at high precursor concentrations. The obtained particles exhibited significant photocatalytic activity and good film formation properties.

4.2 Stability of Organophosphonates under Photocatalytic Conditions

In order to provide a stable connection of the photocatalytic film to the substrate, coupling agents were required, that can bind to the photocatalytic particles and interact with the substrate at the same time. Moreover, the stability of the connection under photocatalytic conditions was essential, as the release of nanoparticles should be avoided. Phosphonates are known to form stable covalent connections to TiO₂ surfaces. Additionally, the direct hole degradation has been suggested to be inhibited in the presence of phosphonates as discussed in the introduction.¹⁴⁷ If a dense film could be

formed – anticipating the contact of water or hydroxyl radicals with the substrate – direct hole degradation was assumed to be the only mechanism that can degrade the substrate. For this reason phosphonates were assumed to provide a versatile coupling agent for the aimed systems. The degradation of different organic phosphonates and phosphates under photocatalytic conditions was investigated in order to gain further insight in the degradation mechanism. Thus, photocatalytic titanium dioxide nanoparticles modified with different organic phosphonates and phosphates were illuminated under various different conditions. The studies revealed a complete removal of all organic compounds from the photocatalysts' surface while the P-O-Ti bonds were found to be stable even upon prolonged illumination (Figure 4-1).

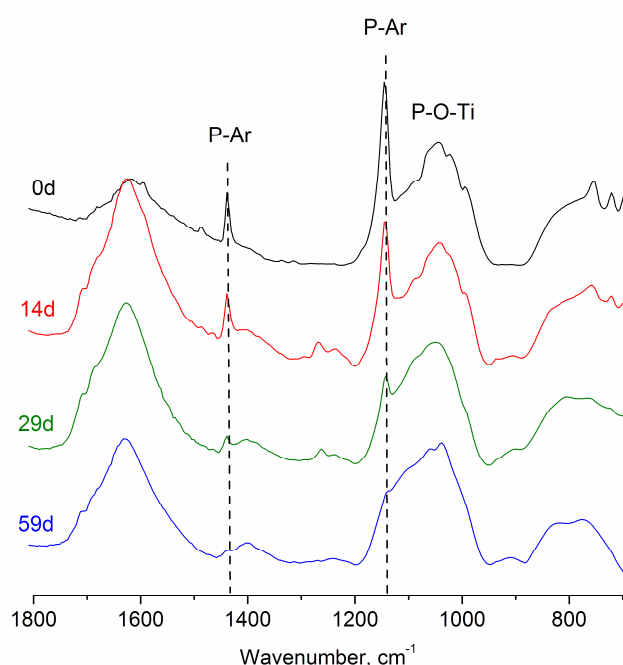
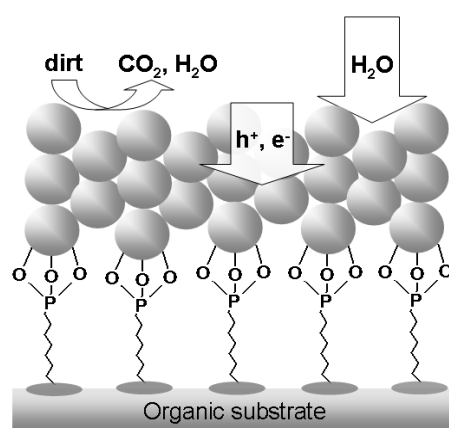


Figure 4-1: FT-IR spectra of PPA@TiO₂ after different times of illumination

Hence, after complete removal of the organic moieties phosphate species remain on the particles' surface. These phosphate species were found to enhance the photocatalytic activity of the particles, which is in concordance with literature reports.^{147, 148} Moreover, investigations on the degradation rate of phosphonic acids under different conditions lead to the conclusion that the degradation proceeds via hydroxyl radicals and via electron transfer from the organic compounds to surface-trapped holes concurrently. ¹³C CPMAS NMR studies after different illumination times revealed degradation

intermediates on the particles' surface, which indicates a sequential degradation rather than breakage of the P-C bond. This assumption was approved by faster decrease of vibrational signals assigned to organic moieties compared to the P-C bond. The degradation rate of organic phosphates was shown to be faster compared to phosphonates which is assigned to a facilitated hydroxyl radical formation owing to the accessory lone pair of the additional oxygen, which can act as a hydrogen bond acceptor. Moreover, the degradation rate of alkylphosphonate was found to be higher compared to arylphosphonate which is assigned to better stabilization of radicals in aromatic moieties.

Hence it was found that the phosphonate bridge cannot act as a protecting barrier for the organic substrate. Direct oxidation by surface trapped holes was found to be possible even in the absence of water. These results suggest that this system cannot protect the substrate when monolayer coatings are applied. However, as found by Lorret¹⁶⁰ for an optimal photocatalytic activity the film thickness of such coatings should be in the range of 100 nm. Thus, multilayer coatings are required. Such coatings should be prepared in such a way that the first layers exhibit functional groups for the interaction with the substrate. Subsequent layers should be composed of bare TiO₂ nanoparticles. Due to the short lifetime and diffusion length of photogenerated electrons and holes,³² it is assumed that the substrate and the first layers of functionalized particles can thus be protected from degradation. Nevertheless, the particles in the first layers need a bare surface for interaction with subsequent layers of bare TiO₂ nanoparticles.



Scheme 4-1: Multilayer film composed of 1 layer of anisotropically modified TiO₂ nanoparticles and subsequent layers of bare nanoparticles.

4.3 Anisotropic Modification with Organophosphonates

A differentiated surface of TiO₂ nanoparticles is required in order provide interaction with the organic substrate on the one hand and render the other side accessible for interaction with subsequent TiO₂ layers on the other hand. For this reason, anisotropic surface modification represented another main issue of this work. A differentiated environment was created applying Pickering emulsions, where the particles are located at the oil/water interface.¹⁹¹ Anisotropic surface modification was achieved by addition of hydrophobic coupling molecules to the oil phase of the emulsion. A drastically increased stability of the emulsion indicated an amphiphilic nature of the particles. Moreover, particles modified in Pickering emulsion were found to exhibit similar bonding modes of phosphonates to the titanium dioxide surface as particles modified in suspension.

Furthermore, an optical proof for the anisotropic nature of such particles was aimed. Literature reports on electron microscopic visualization of organic moieties mostly involve selective labeling with gold nanoparticles.^{170, 223-225} For this reason, TiO₂ nanoparticles were modified anisotropically with organic phosphonates that allow interaction with gold. Non covalent interaction was aimed applying poly(ethylene glycol), while organophosphonates with thiol functionalities were used for covalent interaction. Various approaches including different Janus particles as well as gold nanoparticles exhibiting different surface functionalities were investigated. However, no selective decoration of one side of TiO₂ particles with gold could be detected by electron microscopy. The failure of this method is ascribed to weak interaction between the Janus particles and gold and to the bad agglomeration behaviour of the particles.

However, the drastically increased stability of Pickering emulsions upon addition of hydrophobic coupling molecules is a strong hint for the anisotropic nature of the particles. Furthermore, owing to the degradation of the organic moieties leaving phosphate on the surface – which has been proven to enhance the photocatalytic activity – applying particles fully covered with organophosphonates might be worth investigating.

5 Experimental

5.1 Materials

All chemicals used for synthesis of molecular compounds and modification reactions were obtained by commercial suppliers (Aldrich, Fluka, ABCR) and used as received. Allyl bromide (97%, Aldrich) was freshly distilled before use.

The solvents used for reactions where the absence of water was required were dried applying standard procedures and stored under argon over a molecular sieve (3 or 4 Å). Operations where the absence of humidity or oxygen was required were carried out under argon atmosphere using Schlenk techniques.

5.2 Analytical Techniques

Nuclear Magnetic Resonance (NMR)

NMR spectra in solution were recorded on a Bruker Avance 300 (^1H : 250.13 MHz, ^{13}C : 62.89 MHz, ^{31}P : 101.25 MHz) equipped with a 5 mm broadband probe head and a z-gradient unit.

Solid state NMR spectra were recorded on a Bruker AVANCE DPX300 equipped with a 4 mm broadband MAS probe head (^1H : 299.87 MHz, ^{13}C : 75.40 MHz, ^{31}P : 121.39 MHz). Spectra were acquired using magic angle spinning (MAS) and high power proton decoupling at a rotor spinning rate of 4-9 kHz.

Infrared Spectroscopy (IR)

Infrared spectroscopic measurements were performed on a Bruker Tensor 27 instrument under ambient atmosphere working in ATR MicroFocusing MVP-QL with a diamond crystal or in transmission mode using KBr (IR-grade, Aldrich) disks as a sample matrix. Spectra were recorded with 32 scans at a resolution of 4 cm^{-1} . The software used for analysis was OPUSTM version 4.0.

Thermogravimetric Analysis (TGA)

Thermogravimetric analyses were performed on a Netzsch Iris TG 209 C with a 414 TASC controller in a platinum crucible with a heating rate of 10 K/min under synthetic air.

Raman Spectroscopy

Raman spectra were recorded on a Bruker RFS 100/S Raman spectrometer. Samples were excited with a Nd-YAG laser of 1064 nm wavelength.

Nitrogen Sorption

Nitrogen sorption experiments were carried out on a Micromeritics ASAP 2020 or an ASAP 2010 instrument. The samples were degassed for 5 hours at 40°C prior to measurement. For the interpretation of the data the Brunauer, Emmett and Teller (BET) model was applied.

Transmission Electron Microscopy

Samples for transmission electron microscopy (TEM) measurements were prepared by ultrasonically dispersing the particles in ethanol prior to deposition on a carbon coated TEM Cu grid. TEM measurements were performed on a TECNAI F20 FEGTEM (USTEM, Vienna University of Technology).

Elemental Analysis

Elemental analyses were carried out on a 2400 CHN Elemental Analyzer by Perkin Elmer at the Microanalytical Laboratory, Institute of Physical Chemistry, University of Vienna.

Powder Diffractometry (XRD)

XRD experiments of powders were carried out on a Philips X'Pert diffractometer (Cu K α line: $\lambda = 1.54060, 1.54439 \text{ \AA}$) equipped with an XCelerator multi-channel detector, Bragg Brentano geometr and a silicon single crystal sample holder. The diffraction pattern was recorded between 5 and 90° (2 θ) with 1 s/step and a step size of 0.02°.

Dynamic Light Scattering (DLS)

DLS measurements were performed with an ALV/CGS-3 Compact Goniometer controlled by an ALV/LSE-5003 Multiple Tau Digital Correlator at a scattering angle of 90° and a temperature of 25 °C.

Ultraviolet-Visible Spectroscopy

UV-Vis measurements were performed on a PerkinElmer Lambda 35 with a scan speed of 480 nm/min and a slit width of 1 nm.

Photocatalytic Activity Measurements

The photocatalytic activity was investigated by monitoring the degradation of methylene blue in an aqueous solution containing the dispersed particles according to a procedure by Lorret et al.²⁹⁶ The suspensions were illuminated under continuous stirring in a water-cooled chamber equipped with two 9W UVA black light lamps as described above. 5 mg of the corresponding particles were dispersed in 18 mL of distilled water using an ultrasonic bath for 30 minutes. To the suspension, 2 mL of 200 μM methylene blue solution in water was added and the pH was adjusted to 4 with nitric acid. The resulting suspensions were stirred in the dark for 1 hour and then illuminated with UV-light. The degradation was monitored by sampling at different time intervals. The samples were centrifuged and the UV-Vis-absorption spectra were collected between 800 and 400 nm. The absorption maximum of the methylene blue dye at 664 nm was taken as a measure for the concentration of the dye (C). The initial absorbance at 664

nm of the suspensions stirred in the dark was taken as a measure for the initial dye concentration (C_0).

Other Techniques

The pH was measured using a Mettler Toledo SevenMulti™ meter with saturated KCl glass electrode. The conductivity was determined using a Mettler Toledo SevenMulti™ conductivity meter with Pt/Pt black electrodes.

5.3 Experiments

5.3.1 Synthesis of TiO₂ Nanoparticles

5.3.1.1 Synthesis of TiO₂ Nanoparticles with 4-10 nm Diameter

TiO₂ nanoparticles with small diameters were prepared by slight modification a procedure by Ivanovici.²⁵² 7.5 mL (37.5 mmol) of Ti(OⁱPr)₄ were dissolved in 25 mL of dry ethanol and added dropwise under vigorous stirring to 250 mL of distilled water (4°C) adjusted to pH 1.5 with nitric acid. After 3 days of stirring at room temperature, the solvent was evaporated (40°C) under reduced pressure. 2.8 g (93%) of the particles were obtained as a white powder.

XRD: Anatase (40-100%): a (Å) = 3.79959, c (Å) = 9.4778; crystallite size: 2.7-3.6 nm; brookite (0-60%): a (Å) = 9.247, b = 5.463, c = 5.189; crystallite size: 1.9 nm. FT-IR: 3244, 1638, 1413, 1310, 795. TGA (mass loss, %): 30 – 400°C: 15.3%, 400 – 700°C: 0.5%. BET: 270 m²/g.

DLS results obtained upon variation of the precursor concentration are presented in Table 5-1.

Table 5-1: DLS results obtained for TiO₂ nanoparticles prepared applying different precursor concentrations.

Ti(O ⁱ Pr) ₄ / mL	Ti(O ⁱ Pr) ₄ / mol/L	DLS / radius, nm
1.25	0.17	2.1 ± 0.19
3.75	0.51	2.3 ± 0.20
5.9	0.8	2.8 ± 0.20
7.5	1.02	3.1 ± 0.20
11.8	1.6	3.4 ± 0.20
17.6	2.4	3.8 ± 0.21
23.5	3.2	4.9 ± 0.21

5.3.1.2 Synthesis of TiO₂ Nanoparticles with 60 nm Diameter

TiO₂ nanoparticles with diameters larger than 60 nm were prepared by slight modification of a procedure by Jiang and Herricks.²⁹³ 1 mL (3 mmol) of Ti(OBu)₄ were mixed with 5 mL (90 mmol) of ethylene glycol in a Schlenk flask equipped with an argon inlet and a magnetic stirrer under an argon atmosphere. The reaction mixture was stirred for 20 hours at room temperature. 2 mL of the resulting oil containing Ti(OCH₂CH₂O)₂ were added dropwise to 50 mL of dry acetone (< 0.05% water) provided in an ice cooled round bottom flask equipped with an argon inlet and a magnetic stirrer under an argon atmosphere. The resulting mixture was stirred for 30 minutes and subsequently altered for 1 hour. The particles were separated by centrifugation, washed with water and ethanol and calcined at 500°C for 10 hours. 70 mg (87%) of the particles were obtained as a white powder.

XRD: Anatase 96%: a (Å) = 3.78287, c (Å) = 9.49938; crystallite size: 38.8 nm; rutile 4%: a (Å) = 4.6720, c (Å) = 2.7720. TGA (mass loss, %): 30 – 400°C: 2.3%, 400 – 700°C: 0.5%. BET: 21 m²/g. TEM (radius, nm): 38.9 ± 7.5.

5.3.2 Synthesis of Dodecylphosphonic Acid (DPA)

5.3.2.1 Synthesis of Diethyl Dodecylphosphonate (DPA-Et)

Diethyl dodecylphosphonate was prepared by the Michealis Arbuzov reaction of 1-bromododecane according to Kosolapoff et al.¹²³ 15.6 mL (64 mmol) of 1-bromododecane were mixed with 12.4 mL (74 mmol) of triethyl phosphite in a round bottom flask equipped with a reflux condenser and a magnetic stirrer. The reaction mixture was heated to reflux for 10 hours and the excess triethyl phosphite was subsequently removed by distillation. 13.6 g (66%) of diethyl dodecylphosphonate were obtained as a clear liquid.

¹H NMR (CDCl₃, δ, ppm): 4.08 (m, 4H, -O-CH₂), 1.77-1.50 (m, 4H, -CH₂-CH₂-P), 1.33-1.24 (m, 24H, -CH₂-, -O-CH₂-CH₃), 0.87 (t, J = 6.4 Hz, 3H, -CH₂-CH₃). ¹³C NMR (CDCl₃, δ, ppm): 61.3 (-O-CH₂-CH₃), 31.8 (-CH₂-CH₂-CH₂-P), 30.5 (-CH₂-P), 29.5-24.5 (-CH₂-), 22.6 (-CH₂-CH₃), 22.3 (-CH₂-CH₂-P), 16.3 (-O-CH₂-CH₃), 14.0 (-CH₂-CH₃). ³¹P NMR (CDCl₃, δ, ppm): 32.8.

5.3.2.2 Synthesis of Dodecylphosphonic Acid (DPA)

13.1 g (42 mmol) of diethyl dodecylphosphonate were mixed with 70 mL of concentrated HCl in a round bottom flask equipped with a reflux condenser and a magnetic stirrer. The reaction mixture was refluxed for 20 hours and the volatile byproducts were removed in vacuo. The remaining brown oil was washed with acetonitrile and recrystallized from from n-hexane to afford 9.5 g (90%) of dodecylphosphonic acid as white crystals.

¹H NMR (CDCl₃, δ, ppm): 4.49 (m, 2H, -OH), 1.85-1.50 (m, 4H, -CH₂-CH₂-P), 1.43-1.19 (m, 18H, -CH₂-), 0.88 (t, 3H, -CH₂-CH₃). ¹³C NMR (CDCl₃, δ, ppm): 31.9 (-CH₂-CH₂-P), 30.4 (-CH₂-P), 29.6-24.0 (-CH₂-), 22.7 (-CH₂-CH₃), 21.9 (-CH₂-CH₂-P), 14.1 (-CH₂-CH₃). ³¹P NMR (CDCl₃, δ, ppm): 38.0.

5.3.3 Synthesis of Poly(ethylene glykol)phosphonic Acid (PEG-PA)

5.3.3.1 Synthesis of Poly(ethylene glykol) Monovinyl Ether

6.19 g (8.3 mmol) of poly(ethylene glycol) monomethyl ether (Aldrich, $M_n=750$ g/mol) were dissolved in 20 mL of dry THF and 2 g of fine crunched KOH (35 mmol) were added and stirred at room temperature in a round bottom flask equipped with a magnetic stirrer, a reflux condenser and a dropping funnel for 30 min. 1.9 g (16 mmol) of allyl bromide were dissolved in 10 mL of dry THF and added dropwisely to the reaction mixture via a dropping funnel. After complete addition of allyl bromide the reaction mixture was heated to reflux for 12 hours. The thus obtained yellow oil was filtrated, washed three times with 2 N NaOH and dried over Na_2SO_4 . The solvent was evaporated and after drying in vacuum 3.3 g (50%) of the product were obtained as clear oil.

^1H NMR (CDCl_3 , δ , ppm): 5.44 (m, 1H, $\text{CH}_2=\text{CH}-$), 5.18 (m, 2H, $\text{CH}_2=\text{CH}-$), 4.10 (m, 2H, $\text{CH}_2=\text{CH}-\text{CH}_2-\text{O}$), 3.65 (s, 56H, $\text{O}-\text{CH}_2-\text{CH}_2-\text{O}$), 3.36 (s, 3H, $\text{O}-\text{CH}_3$). FT-IR (ATR, ν , cm^{-1}): 2868, 1681, 1454, 1350, 1199, 1099, 1009, 949, 848.

5.3.3.2 Synthesis of Diethyl Poly(ethylene glycol)phosphonate

Poly(ethylene glycol) phosphonate was prepared by a radical addition of diethyl phosphite to vinyl poly(ethylene glycol).¹²⁸ 3.1 g (3.9 mmol) of vinyl terminated PEG were dissolved in 2 mL (15 mmol) of diethyl phosphite in a round bottom flask under an argon atmosphere and 0.07 g (0.41 mmol) of AIBN were added to the solution. In a three-necked round bottom flask equipped with a reflux condenser, a dropping funnel and a magnetic stirrer, 5 mL (39 mmol) of diethyl phosphite were heated to 120°C under an argon atmosphere. The mixture of PEG and AIBN in diethyl phosphite was added dropwise and after 2 hours of stirring at 120°C the reaction mixture was distilled to remove the excess diethyl phosphite. 2.4 g (73%) of the product were obtained as a clear liquid.

^1H NMR (CDCl_3 , δ , ppm): 4.11 (m, 4H $\text{O}-\text{CH}_2-\text{CH}_3$), 3.65 (s, 54H, $\text{O}-\text{CH}_2-\text{CH}_2-\text{O}$), 3.38 (s, 3H, $\text{O}-\text{CH}_3$), 1.87 (m, 2H, $\text{CH}_2-\text{CH}_2-\text{P}$), 1.32 (m, 6H, $\text{O}-\text{CH}_2-\text{CH}_3$). ^{31}P NMR (CDCl_3 , δ , ppm): 45.5. FT-IR (ATR, ν , cm^{-1}): 2877, 1455, 1351, 1059, 1006, 929, 810.

5.3.3.3 Synthesis of Poly(ethylene glycol)phosphonic Acid (PEG-PA)

2.3 g (2.6 mmol) of diethyl poly(ethylene glycol) phosphonate were mixed with 20 mL of concentrated HCl in a round bottom flask equipped with a reflux condenser and a magnetic stirrer. The reaction mixture was refluxed for 20 hours and the volatile byproducts were removed in vacuo. The resulting clear liquid was dissolved in dichloromethane and extracted with water to yield 1 g (43%) of the product as a clear liquid.

^1H NMR (CDCl_3 , δ , ppm): 3.65 (s, 54H, O- CH_2 - CH_2 -O), 3.38 (s, 3H, O- CH_3), 1.87 (m, 2H, CH_2 - CH_2 -P). ^{31}P NMR (CDCl_3 , δ , ppm): 19.6. FT-IR (ATR, ν , cm^{-1}): 2875, 1455, 1352, 1058, 1006, 929, 810.

5.3.4 Synthesis of 11-Mercapto Undecanylphosphonic Acid

5.3.4.1 Synthesis of Diethyl 11-Bromo Undecanylphosphonate

11-Mercapto-undecylphosphonic acid was prepared according to a procedure by Tsai et al.¹⁴⁰ 10 g (32 mmol) of 1,11-dibromoundecane were mixed with 4.5 mL (27 mmol) of triethylphosphite in a round bottom flask equipped with a reflux condenser, a bubble trap and an argon inlet. The reaction mixture was stirred at 130°C for 15 hours. After cooling the reaction mixture to room temperature, 5 mL of distilled water were added and stirred for 2 hours. The mixture was extracted with CH_2Cl_2 , the united organic phases were washed with water and brine, dried over MgSO_4 and the solvent was removed under reduced pressure to yield 10.2 g (84%) of a colourless oil.

^1H NMR (CDCl_3 , δ , ppm): 4.0 (m, 4H, O- CH_2 - CH_3), 3.3 (t, $J = 6.6$ Hz, 2H, CH_2 -Br), 1.9-1.2 (m, 26H, chain + O- CH_2 - CH_3). ^{31}P NMR (CDCl_3 , δ , ppm): 44.5.

5.3.4.2 Synthesis of 11-Bromo Undecanylphosphonic Acid

5 g (13 mmol) of diethyl 11-bromo-undecanylphosphonate were dissolved in 10 mL of dry CH_2Cl_2 under an argon atmosphere in a round bottom flask equipped with a reflux condenser, a bubble trap and an argon inlet. 5 mL (37 mmol) bromotrimethylsilane were added via syringe under an argon flow and the mixture was stirred for 15 hours at room temperature and refluxed for additional 2 hours. The excess

reagent and solvent were removed under reduced pressure and the orange liquid was hydrolyzed with water for 2 hours. The white precipitate was removed by filtration and the filtrate was extracted with CH_2Cl_2 . The united organic phases were washed with water and dried over MgSO_4 . The solvent was removed under reduced pressure and the resulting white powder was recrystallized from $\text{CH}_2\text{Cl}_2/\text{n-hexane}$. 1.8 g (45%) of the product was obtained as colorless crystals.

^1H NMR (CDCl_3 , δ , ppm): 3.4 (t, $J = 6.8$ Hz, 2H, $\text{CH}_2\text{-Br}$), 1.9-1.3 (m, 20H, chain).
 ^{31}P NMR (CDCl_3 , δ , ppm): 50.4.

5.3.4.3 Synthesis of 11-Mercapto Undecanylphosphonic Acid (MPA)

0.5 g (1.6 mmol) of 11-bromo-undecanylphosphonic acid were dissolved in 10 mL ethanol and mixed with a solution of 0.54 g (7.1 mmol) thiourea in 10 mL of distilled water in a round bottom flask equipped with a reflux condenser. After 15 hours of reflux, the ethanol was removed under reduced pressure followed by addition of 6 mL 30% NH_4OH . The reaction mixture was stirred at 75°C for 2 hours and after cooling to room temperature the pH was adjusted to 1.3 with 6 N HCl. The acidic aqueous solution was extracted with diethyl ether, the organic phase was washed with 1 N HCl and dried over MgSO_4 . After removing the solvent under reduced pressure, 0.32 g (75%) of the product was obtained as a white solid.

^1H NMR (CDCl_3 , δ , ppm): 7.4 (s, 1H, SH), 2.5 (q, $J = 7.3$ Hz, 2H, $\text{CH}_2\text{-SH}$), 1.8-1.2 (m, 21H, chain). ^{13}C NMR (CDCl_3 , δ , ppm): 34.0 ($-\text{CH}_2\text{-SH}$), 30.5 ($-\text{CH}_2\text{-CH}_2\text{-SH}$), 30.2 ($-\text{CH}_2\text{-P}$), 29.5-23.9 ($-\text{CH}_2\text{-}$), 21.9 ($-\text{CH}_2\text{-CH}_2\text{-P}$). ^{31}P NMR (CDCl_3 , δ , ppm): 49.9.

5.3.5 Modification of TiO_2 Nanoparticles in Suspension

Different amounts of the respective coupling agent were dissolved in 500 mL of a 3:1 mixture of methanol and water. 100 mL of a 1 wt% suspension of TiO_2 nanoparticles (sol-gel prepared particles with 6 or 80 nm diameter or P25) in water were added and the suspension was stirred at room temperature for 3 days. The particles were separated by centrifugation, washed several times with ethanol and dried at 100°C under reduced pressure.

DPA@TiO₂: ³¹P MAS NMR (δ, ppm): 30.6. ¹³C CPMAS NMR (δ, ppm): 20.2, 13.1, 4.3. FT-IR (KBr, ν, cm⁻¹): 2922, 2851, 1627, 1466, 1406, 1378, 1190-910, 789.

Table 5-2: Mass loss and surface coverage obtained from thermogravimetric analysis for different TiO₂ nanoparticles modified with dodecyl phosphonic acid.

Particle	Surface Area (BET), m ² /g	Coupling Agent, *10 ⁻³ M	Mass Loss, %	Surface Coverage, molecules/nm ²
6 nm	270	2.5	21.7	3.1
6 nm	270	1.25	14.2	2.1
P25	50	2.5	4.4	3.4
P25-HF	50	2.5	6.7	5.2
P25-UV	50	2.5	4.1	3.2
80 nm	21	2.5	2.5	4.7

PPA@TiO₂: ³¹P MAS NMR (δ, ppm): 14.8. ¹³C MAS NMR (δ, ppm): 123.3, 119.3. FT-IR (KBr, ν, cm⁻¹): 3057, 2970, 1627, 1486, 1439, 1383, 1145, 1300-920, 849.

Table 5-3: Mass loss and surface coverage obtained from thermogravimetric analysis for TiO₂ nanoparticles modified with different amounts of phenyl phosphonic acid.

Particle	Surface Area (BET), m ² /g	Coupling Agent, *10 ⁻³ M	Mass Loss, %	Surface Coverage, molecules/nm ²
6 nm	270	2.5	9.3	3.4
6 nm	270	3.5	10.1	3.8
6 nm	270	6.3	11.7	4.5

PPoA@TiO₂: ³¹P MAS NMR (δ, ppm): 1.2. ¹³C MAS NMR (δ, ppm): 125.1, 117.9. FT-IR (KBr, ν, cm⁻¹): 3069, 2972, 1625, 1593, 1491, 1226, 1100-924, 777. TGA (mass loss, %): 30 – 260°C: 4.3%, 260 – 600°C: 11.4%.

PEG-PA@TiO₂: ³¹P MAS NMR (δ , ppm): 15.2. FT-IR (KBr, ν , cm⁻¹): 1627, 1170-980, 774. TGA: 30 – 600°C: 9.7%.

MPA@TiO₂: ³¹P MAS NMR (δ , ppm): 42.1 . FT-IR (KBr, ν , cm⁻¹): 2921, 2851, 1625, 1465, 1385, 1138, 1050, 991, 823.

Table 5-4: Mass loss and surface coverage obtained from thermogravimetric analysis for different TiO₂ nanoparticles modified with 11-mercaptoundecyl phosphonic acid.

Particle	Surface Area (BET), m ² /g	Coupling Agent, *10 ⁻³ M	Mass Loss, %	Surface Coverage, molecules/nm ²
6 nm	270	2.5	19.1	2.3
P25	50	2.5	4.3	2.8
80 nm	21	2.5	2.5	3.9

5.3.6 Preparation of Pickering Emulsions

In a glass vessel with 5 cm height and 1 cm diameter, 4 mL of a suspension of TiO₂ nanoparticles in distilled water (0.5, 1 or 2 wt%) was prepared. The corresponding amount of NaCl (0 to 1 M) was added and the suspension was adjusted to the requested pH with 1M NaOH or 1M HCl. Upon agitation with an IKA[®] T25 Ultra Turrax[®] at 12000 rpm, 1 mL of oil phase (cyclohexane with or without DPA, toluene or hexane) was added dropwise. The emulsion was agitated for another 10 minutes at 12 rpm. Immediately after stopping the agitation, conductivity of the emulsions was measured. The water-emulsion and the oil-emulsion interfaces were tracked and the changes were recorded after 1, 2, 3, 4, 5, 7.5, 10, 15 and 20 minutes.

5.3.7 Modification of TiO₂ in Pickering Emulsion

5.3.7.1 Modification of one Hemisphere

A suspension of 1 wt% sol-gel 6 nm or 80 nm nanoparticles, AEROXIDE[®] TiO₂ P25 in 4 mL of distilled water was prepared and adjusted to pH 3 with 1 M NaOH or 1 M HCl. Upon agitation with an IKA[®] T25 Ultra Turrax[®] at 20000 rpm, 1 mL of oil phase (cyclohexane or toluene) containing $2.5 \cdot 10^{-3}$ mol/L of the hydrophobic coupling agent (DPA or MPA) was added dropwise. The emulsion was agitated for another 20 minutes at 20000 rpm and subsequently aged for 1 hour. The particles were separated by centrifugation, washed several times with ethanol and dried under reduced pressure.

Janus-DPA@TiO₂: ³¹P MAS NMR (δ , ppm): 30.3. FT-IR (KBr, ν , cm⁻¹): 2921, 2851, 1623, 1464, 1185-910, 791. TGA (mass loss, %): 30 – 260°C: 6.3%, 260 – 600°C: 7.6%.

Table 5-5: Mass loss and surface coverage obtained from thermogravimetric analysis for different TiO₂ nanoparticles anisotropically modified with dodecyl phosphonic acid.

Particle	Surface Area (BET), m ² /g	Mass Loss, %	Surface Coverage, molecules/nm ²
6 nm	270	7.6	1.1
P25	50	3.7	2.9
80 nm	21	1.9	3.5

Janus-MPA@TiO₂: ³¹P MAS NMR (δ , ppm): 41.9. FT-IR (KBr, ν , cm⁻¹): 2971, 1626, 1448, 1384, 1135, 1049, 912, 807.

Table 5-6: Mass loss and surface coverage obtained from thermogravimetric analysis for different TiO₂ nanoparticles anisotropically modified with 11-mercaptoundecyl phosphonic acid.

Particle	Surface Area (BET), m ² /g	Mass Loss, %	Surface Coverage, molecules/nm ²
P25	50	4.9	3.2

80 nm		21		1.8		2.8
-------	--	----	--	-----	--	-----

5.3.7.2 Modification of two Hemispheres with Different Coupling Agents

Hydrophobic and Hydrophilic Coupling Agent:

A suspension of 1 wt% sol-gel 80 nm nanoparticles in 4 mL of distilled water was prepared and adjusted to pH 3 with 1 M HCl. Upon agitation with an IKA[®] T25 Ultra Turrax[®] at 20000 rpm, 1 mL of toluene containing 2.5×10^{-3} mol/L of DPA was added dropwise. The emulsion was agitated for another 10 minutes followed by addition of 2.5×10^{-3} mol/L of PEG-PA to the aqueous phase. After agitating for 20 minutes the particles were separated by centrifugation, washed several times with water and ethanol and dried under reduced pressure.

FT-IR (ATR, ν , cm^{-1}): 2922, 2852, 1629, 1467, 1150-1020, 803. TGA (mass loss, %): 30 – 160°C: 2.8%; 160 – 280°C: 4.8%, 280 – 600°C: 16.0%.

Two Hydrophobic Coupling Agents:

7 mg of Janus-DPA@TiO₂ (80 nm particles) were dispersed in 5 mL of ethanol applying an ultrasonic bath. 3 mg (0.01 mmol) of MPA were added to the suspension and the mixture was sonicated for 30 minutes. The particles were separated by centrifugation, washed several times with ethanol and dried under reduced pressure.

FT-IR (ATR, ν , cm^{-1}): 2924, 2853, 1632, 1465, 1150-1020, 805. TGA(mass loss, %): 30 – 200°C: 0.3%; 200 – 600°C: 3.5%.

5.3.8 Synthesis of Gold Nanoparticles

5.3.8.1 Synthesis of Gold Nanoparticles according to Turkevich²⁴⁶

1 mL of a 2 mM sodium citrate solution was added to different amounts of a boiling 1mM HAuCl₄ solution (the molar ratio of HAuCl₄ : sodium citrate was varied between

1:4 an 1:1). The reaction mixture was kept at 100°C until the color changed from yellow to deep red, violet or blue.

Table 5-7: Particle size obtained from DLS for different H_{AuCl₄}/citrate ratios

H _{AuCl₄} / Na Citrate	1:1	1:2	1:3	1:4
DLS radius, nm	15.3 ± 0.05	9.6 ± 0.13	2.5 ± 0.22	1.5 ± 0.23

5.3.8.2 Synthesis of Gold Nanoparticles according to Brust²⁴⁸

0.2 mL of 0.05 M H_{AuCl₄} (0.01 mmol) were added to a solution of different amounts of tetraoctylammoniumbromide (TOAB) in 1.5 mL of toluene and stirred for several minutes until the water phase was colorless. 1 mL of 0.02 M NaBH₄ (0.02 mmol) solution were added and the reaction mixture was stirred until the colour of the organic phase changed from yellow to deep red.

Table 5-8: Particle size obtained from DLS for different TOAB concentrations and altering times.

TOAB, mol/L		0.02	0.07	0.1
DLS radius, nm	t = 5 min	40 ± 0.08	3.3 ± 0.13	2.9 ± 0.1
	t = 30 min	-	-	19.8 ± 0.08

5.3.8.3 Synthesis of Gold Nanoparticles according to Martin²⁵¹

To 5 mL of an equimolar solution containing of H_{AuCl₄} and HCl (0.025 M) in water different amounts of an aqueous 0.05 M NaBH₄/NaOH solution were added upon vigorous stirring. The colour changed from yellow to deep red.

Table 5-9: Particle size obtained from DLS for different HAuCl₄/NaBH₄ ratios and altering times.

HAuCl ₄ / NaBH ₄		2:1	1:1	1:2
DLS radius, nm	t = 5 min	0.6 ± 0.14	0.6 ± 0.21	5.0 ± 0.07
	t = 60 min	1.2 ± 0.14	0.8 ± 0.08	2.0 ± 0.14

5.3.8.4 Reduction of Auric Acid in the Presence of MPA

To 5 mL of a solution of 2 mg of MPA (7×10^{-3} mmol) in ethanol 2.5 mL of a 1 mM HAuCl₄ solution in water (2.5×10^{-3} mmol) were added. The mixture was stirred for 10 minutes prior to addition of 2 mL of an aqueous 5 mM NaBH₄ solution (1×10^{-2} mmol). The colour of the reaction mixture changed from yellow to light red immediately upon addition of NaBH₄.

DLS (radius, nm): 12.0 ± 0.025 .

5.3.8.5 Exchange Reaction on TOAB Stabilized Gold Nanoparticles

5 mg of MPA were added to 2 mL of TOAB stabilized colloidal gold in toluene prepared according to the Brust Method.²⁴⁸ The suspension was stirred for one hour in the dark. After that time the particles were isolated by centrifugation and residual TOAB was removed by washing and redispersing two times in toluene.

DLS (radius, nm): t = 5 min: 10.0 ± 0.27 , t = 20 min: 14.1 ± 0.18 .

5.3.9 Experiments for Proving the Anisotropy

5.3.9.1 Decoration of Janus-DPA/PEG@TiO₂ with Gold Nanoparticles (AuNP) (PEG1-3)

Janus-DPA/PEG@TiO₂ was decorated with gold nanoparticles in situ in the emulsion. An emulsion containing DPA in the oil phase and PEG-PA in the water phase

was prepared according to the procedure described in section 5.3.7.2. To the aqueous phase containing PEG-PA, 1 mL of citrate stabilized gold colloid (prepared according to the procedure in section 5.3.8.1 with auric acid/citrate = 1:3) was added. After agitation for another 15 minutes the emulsion was altered for 2 hours. The particles were separated by centrifugation and washed several times with water and ethanol. Samples for TEM analysis were prepared by dispersing 1 mg of the product in 5 mL of ethanol applying an ultrasonic bath. A carbon-coated copper grid was dip-coated in the resulting suspension and dried in air.

5.3.9.2 Decoration of Janus-MPA@TiO₂ with Citrate Stabilized AuNP (MPA1)

7 mg of Janus-MPA@TiO₂ were dispersed in 5 mL of ethanol applying an ultrasonic bath for 30 minutes. 2 mL of citrate stabilized gold colloid (prepared according to the procedure described in section 5.3.8.1 with auric acid/citrate = 1:3) was added and the mixture was sonicated for another 2 hours. The resulting light red suspension was diluted with 5 mL of ethanol and sonicated for another 10 minutes prior to preparation of samples for TEM by immersing a carbon-coated copper grid in the suspension.

5.3.9.3 Reduction of Auric Acid in the Presence of Janus-MPA@TiO₂ (MPA2)

7 mg of Janus-MPA@TiO₂ were dispersed in 5 mL of ethanol applying an ultrasonic bath for 30 minutes. After addition of 5 mL of 1 mM HAuCl₄ the suspension was agitated in an ultrasonic bath for 2 hours and subsequently different amounts of NaBH₄ were added. Samples for TEM analysis were prepared by dispersing 1 mg of the product in 5 mL of ethanol or toluene applying an ultrasonic bath. A carbon-coated copper grid was dip-coated in the resulting suspension and dried in air.

5.3.9.4 Decoration of Janus-MPA@TiO₂ with TOAB Stabilized AuNP (MPA3+4)

Synthesis of AuNP in the Presence of Janus-MPA@TiO₂ (MPA3a):

0.2 mL 0.05 M HAuCl₄ were added to 1.5 mL of a suspension in toluene containing 0.11 g TOAB and 1.5 mg Janus-MPA@TiO₂. The reaction mixture was agitated using

the ultrasonic bath for 30 minutes followed by addition of 1 mL of 0.02 M NaBH₄. The suspension was again agitated in the ultrasonic bath for 30 minutes and altered for 2 hours. The particles were separated by centrifugation and washed several times with toluene and ethanol. Samples for TEM analysis were prepared by dispersing 1 mg of the product in 5 mL of ethanol or toluene applying an ultrasonic bath. A carbon-coated copper grid was dip-coated in the resulting suspension and dried in air.

Addition of AuNP to Janus-MPA@TiO₂ in Emulsion (MPA3b1+MPA4):

Janus-MPA@TiO₂ was decorated with gold nanoparticles in situ in the emulsion. An emulsion containing MPA in toluene was prepared according to the procedure described in section 5.3.7.1. After 10 minutes of agitation, 1 mL of TOAB stabilized gold colloid (prepared according to section 5.3.8.2, with 0.1 M TOAB) in toluene was added and the emulsion was agitated for another 15 minutes. The emulsion was altered for 2 hours and the particles were separated by centrifugation and washed several times with toluene and ethanol. Samples for TEM analysis were prepared by dispersing 1 mg of the product in 5 mL of ethanol or toluene applying an ultrasonic bath. A carbon-coated copper grid was dip-coated in the resulting suspension and dried in air.

Addition of AuNP to Janus-MPA@TiO₂ in Suspension (MPA3b2):

To a suspension of 1.5 mg of Janus-MPA@TiO₂ in 1.5 mL of toluene, a suspension of TOAB-stabilized AuNP in toluene was added (0.2 mL containing 3 mg AuNP) and agitated in the ultrasonic bath for 30 minutes. After altering for 2 hours, the particles were separated by centrifugation and washed several times with toluene and ethanol. Samples for TEM analysis were prepared by dispersing 1 mg of the product in 5 mL of ethanol or toluene applying an ultrasonic bath. A carbon-coated copper grid was dip-coated in the resulting suspension and dried in air.

5.3.9.5 Decoration of Janus-DPA@TiO₂ with TOAB stabilized AuNP (DPA1)

Janus-DPA@TiO₂ was decorated with gold nanoparticles in situ in the emulsion. 0.4 mL of toluene containing 3 mg (0.01 mmol) of DPA were mixed with 0.3 mL of TOAB stabilized gold colloid prepared according to the procedure described in section 5.3.8.2 (with 0.1 M TOAB). An emulsion containing DPA and gold colloid in toluene was prepared according to the procedure described in section 5.3.7.1. The emulsion was

agitated for 20 minutes and altered for 2 hours. The particles were separated by centrifugation and washed several times with toluene and ethanol. Samples for TEM analysis were prepared by dispersing 1 mg of the product in 5 mL of ethanol or toluene applying an ultrasonic bath. A carbon-coated copper grid was dip-coated in the resulting suspension and dried in air.

5.3.9.6 Decoration of Janus-DPA@TiO₂ with bare AuNP (DPA2)

Janus-DPA@TiO₂ was decorated with bare gold nanoparticles in situ in the emulsion. An emulsion containing DPA in toluene was prepared according to the procedure described in section 5.3.7.1. After 10 minutes of agitation, 1 mL of bare gold nanoparticles (prepared according to section 5.3.8.3, with auric acid/NaBH₄ = 1:2) in water was added and the emulsion was agitated for another 15 minutes. The emulsion was altered for 2 hours and the particles were separated by centrifugation and washed several times with water and ethanol. Samples for TEM analysis were prepared by dispersing 1 mg of the product in 5 mL of ethanol or toluene applying an ultrasonic bath. A carbon-coated copper grid was dip-coated in the resulting suspension and dried in air.

5.3.9.7 Staining of Janus-DPA@TiO₂ with Auric Acid (DPA3)

Janus-DPA@TiO₂ was stained with auric acid in situ in the emulsion. An emulsion containing DPA in toluene was prepared according to the procedure described in section 5.3.7.1. After 10 minutes of agitation, 0.5 mL of 0.05 M HAuCl₄ solution in water was added and the emulsion was agitated for another 15 minutes. The emulsion was altered for 2 hours and the particles were separated by centrifugation and washed several times with water and ethanol. Samples for TEM analysis were prepared by dispersing 1 mg of the product in 5 mL of ethanol or toluene applying an ultrasonic bath. A carbon-coated copper grid was dip-coated in the resulting suspension and dried in air.

5.3.9.8 Decoration of Janus-DPA/MPA@TiO₂ with TOAB stabilized AuNP (MPA5)

3 mg of Janus-DPA/MPA@TiO₂ were dispersed in 2 mL of toluene applying an ultrasonic bath for 30 minutes. 2 mL of TOAB stabilized gold colloid (prepared according to the procedure described in section 5.3.8.2 with 0.1 M TOAB) was added and the mixture was sonicated for another 2 hours. The particles were separated by centrifugation and washed several times with toluene and ethanol. Samples for TEM analysis were prepared by dispersing 1 mg of the product in 5 mL of ethanol or toluene applying an ultrasonic bath. A carbon-coated copper grid was dip-coated in the resulting suspension and dried in air.

5.3.9.9 Staining of Janus-DPA/MPA@TiO₂ with Auric Acid (MPA6)

13 mg of HAuCl₄ were dissolved in 5 mL of ethanol prior to addition of 3 mg of Janus-DPA/MPA@TiO₂ (prepared according to the procedure described in section 5.3.7.2). The mixture was sonicated for 30 minutes and then altered for 2 hours. The particles were separated by centrifugation and washed several times with water and ethanol. Samples for TEM analysis were prepared by dispersing 1 mg of the product in 5 mL of ethanol applying an ultrasonic bath. A carbon-coated copper grid was dip-coated in the resulting suspension and dried in air.

5.3.10 Illumination Experiments

Illumination experiments were conducted in a water-cooled chamber equipped with two 9 W UVA black light lamps (Sylvania UVA-BLB Lynx S). The UV-light intensities were quantified using a Vilber Lourmat VLX-3W 365 nm (± 10 nm) detector. The emission spectrum of the used UVA lamp was integrated over 300-400 nm. The irradiance value I (mW/cm²) was calculated using the following equation:

$$I_{300-400nm} = \frac{I_{detector,355-375nm} * A_{spectrum,300-400nm}}{A_{spectrum,355-375nm}}$$

The measured irradiance values (355-375 nm) range from 0.9 mW.cm⁻² (between the two lamps) to 1.3 mW/cm² (directly under one of the lamps). The calculated irradiance over the wavelength range from 300 to 400 nm thus ranges from 1.5 to 2.2 mW.cm⁻². The illumination studies were conducted by placing the samples directly under one of the lamps in order to obtain reproducible results.

The dried powders were dispersed at different concentrations in water, ethanol/water mixtures or n-heptane and illuminated under continuous stirring. Samples were taken after certain time intervals, centrifuged, washed with ethanol and dried in vacuum. The samples were analyzed by ¹³C CPMAS NMR, ³¹P MAS NMR, FT-IR, TGA and elemental analysis. For FT-IR measurements, 2 mg ±0.3 of the samples were homogenized and pressed with 150 mg ±2 of KBr. The kinetics of the photocatalytic degradation were investigated by monitoring the intensity change

- of the P-C vibrational signal at 1140 cm⁻¹ or the CH stretching signal at 3056 cm⁻¹ for PPA@TiO₂
- of the P-O-C vibration at 1220 cm⁻¹ for PPOA@TiO₂
- of the asymmetric aliphatic CH stretching vibration at 2921 cm⁻¹ for DPA@TiO₂

6 References

1. Wang, R.; Hashimoto, K.; Fujishima, A.; Chikuni, M.; Kojima, E.; Kitamura, A.; Shimohigoshi, M.; Watanabe, T. *Nature* **1997**, 388, (6641), 431-432.
2. Watanabe, T.; Nakajima, A.; Wang, R.; Minabe, M.; Koizumi, S.; Fujishima, A.; Hashimoto, K. *Thin Solid Films* **1999**, 351, (1,2), 260-263.
3. Watanabe, T.; Yoshida, N.; Shibayama, Y. **2009**-JP62424 2010005019, 20090708.
4. Bonafous, L.; Cassar, L.; Cassat, P.; Colombet, P.; Guillot, L. 2003-292134 1405835, 20030829., **2004**.
5. De Castro Neto, J. C.; Antonio, N. M. 2007-100778 1818691, 20070118., **2007**.
6. Li, L. 2004-851128 20050261120, 20040524., **2005**.
7. Valpey, R. S., III; Jones, M. A. 2003-US33505 2004037944, 20031023., **2004**.
8. Mills, A.; Hill, G.; Crow, M.; Hodgen, S. *J. Appl. Electrochem.* **2005**, 35, (7-8), 641-653.
9. Paz, Y. *Appl. Catal., B* **2010**, 99, (3-4), 448-460.
10. Ravelli, D.; Dondi, D.; Fagnoni, M.; Albini, A. *Chem. Soc. Rev.* **2009**, 38, (7), 1999-2011.
11. Friedmann, D.; Mendive, C.; Bahnemann, D. *Appl. Catal., B* **2010**, 99, (3-4), 398-406.
12. Yoon, T. P.; Ischay, M. A.; Du, J. *Nat. Chem.* **2010**, 2, (7), 527-532.
13. Herrmann, J. M. *Catal. Today* **1999**, 53, (1), 115-129.
14. Wilderman, M. *Z. physik. Chem.* **1908**, 59;60, 553-80,703-55;70-86.
15. Fujishima, A.; Honda, K. *Nature* **1972**, 238, (5358), 37-8.
16. Osterloh, F. E. *Chem. Mater.* **2008**, 20, (1), 35-54.
17. Youngblood, W. J.; Lee, S.-H. A.; Maeda, K.; Mallouk, T. E. *Acc. Chem. Res.* **2009**, 42, (12), 1966-1973.

18. Frank, S. N.; Bard, A. J. *J. Phys. Chem.* **1977**, 81, (15), 1484-8.
19. Pruden, A. L.; Ollis, D. F. *J. Catal.* **1983**, 82, (2), 404-17.
20. Hsiao, C. Y.; Lee, C. L.; Ollis, D. F. *J. Catal.* **1983**, 82, (2), 418-23.
21. Malato, S.; Fernandez-Ibanez, P.; Maldonado, M. I.; Blanco, J.; Gernjak, W. *Catal. Today* **2009**, 147, (1), 1-59.
22. Choi, H.; Al-Abed, S. R.; Dionysiou, D. D. *Nanotechnol. Appl. Clean Water* **2009**, 39-46.
24. O'Regan, B.; Graetzel, M. *Nature* **1991**, 353, (6346), 737-40.
25. Burnside, S. D.; Shklover, V.; Barbe, C. A.; Brooks, K.; Comte, P.; Arendse-Duriaux, F.; Jirousek, M.; Graetzel, M. *Mater. Res. Soc. Symp. Proc.* **1998**, 519, 59-64.
26. Bessho, T.; Zakeeruddin, S. M.; Yeh, C.-Y.; Diau, E. W.-G.; Graetzel, M. *Angew. Chem., Int. Ed.* **2010**, 49, (37), 6646-6649.
27. Bahnemann, D.; Cunningham, J.; Fox, M. A.; Pelizzetti, E.; Pichat, P.; Serpone, N. *Aquat. Surf. Photochem.* **1994**, 261-316.
28. Herrmann, J. M.; Guillard, C.; Arguello, M.; Aguera, A.; Tejedor, A.; Piedra, L.; Fernandez-Alba, A. *Catal. Today* **1999**, 54, (2-3), 353-367.
29. Fox, M. A.; Sackett, D. D.; Younathan, J. N. *Tetrahedron* **1987**, 43, (7), 1643-60.
30. Kraeutler, B.; Bard, A. J. *J. Am. Chem. Soc.* **1978**, 100, (19), 5985-92.
31. Serpone, N.; Lawless, D.; Khairutdinov, R.; Pelizzetti, E. *J. Phys. Chem.* **1995**, 99, (45), 16655-61.
32. Hoffmann, M. R.; Martin, S. T.; Choi, W.; Bahnemann, D. W. *Chem. Rev.* **1995**, 95, (1), 69-96.
33. Fujishima, A.; Rao, T. N.; Tryk, D. A. *J. Photochem. Photobiol., C* **2000**, 1, (1), 1-21.
34. Nakato, Y.; Tsumura, A.; Tsubomura, H. *J. Phys. Chem.* **1983**, 87, (13), 2402-5.
35. Ishibashi, K. i.; Fujishima, A.; Watanabe, T.; Hashimoto, K. *J. Photochem. Photobiol. A* **2000**, 134, (12), 139-142.
36. Minero, C.; Mariella, G.; Maurino, V.; Pelizzetti, E. *Langmuir* **2000**, 16, (6), 2632-2641.

References

37. Carraway, E. R.; Hoffman, A. J.; Hoffmann, M. R. *Environ. Sci. Technol.* **1994**, 28, (5), 786-93.
38. Martin, S. T.; Herrmann, H.; Choi, W.; Hoffmann, M. R. *J. Chem. Soc., Faraday Trans.* **1994**, 90, (21), 3315-22.
39. Martin, S. T.; Herrmann, H.; Hoffmann, M. R. *J. Chem. Soc., Faraday Trans.* **1994**, 90, (21), 3323-30.
40. Jacoby, W. A.; Blake, D. M.; Fennell, J. A.; Boulter, J. E.; Vargo, L. M.; George, M. C.; Dolberg, S. K. *J. Air Waste Manage. Assoc.* **1996**, 46, (9), 891-898.
41. Sleiman, M.; Conchon, P.; Ferronato, C.; Chovelon, J.-M. *Appl. Catal., B* **2007**, 71, (3-4), 279-290.
42. Carp, O.; Huisman, C. L.; Reller, A. *Prog. Solid State Chem.* **2004**, 32, (1-2), 33-177.
43. Hernandez-Alonso, M. D.; Fresno, F.; Suarez, S.; Coronado, J. M. *Energy Environ. Sci.* **2009**, 2, (12), 1231-1257.
44. Colmenares, J. C.; Luque, R.; Campelo, J. M.; Colmenares, F.; Karpinski, Z.; Romero, A. A. *Materials* **2009**, 2, (4), 2228-2258.
45. Steinbach, F. *Fortschr. Chem. Forsch.* **1972**, 25, 117-54.
46. Bahnemann, D. W.; Bockelmann, D.; Goslich, R.; Hilgendorff, M.; Weichgrebe, D. *Trace Met. Environ.* **1993**, 3, 301-19.
47. Yang, L.; Liu, Z. *Energy Convers. Manage.* **2007**, 48, (3), 882-889.
48. Zhang, W.; Li, Y.; Wang, C.; Wang, P. *Desalination* **2011**, 266, (1-3), 40-45.
49. Tariq, M. A.; Faisal, M.; Muneer, M.; Bahnemann, D. *J. Mol. Catal. A: Chem.* **2007**, 265, (1-2), 231-236.
50. Palmisano, G.; Addamo, M.; Augugliaro, V.; Caronna, T.; Di Paola, A.; Lopez, E. G.; Loddo, V.; Marci, G.; Palmisano, L.; Schiavello, M. *Catal. Today* **2007**, 122, (1-2), 118-127.
51. Bhatkhande, D. S.; Kamble, S. P.; Sawant, S. B.; Pangarkar, V. G. *Chem. Eng. J.* **2004**, 102, (3), 283-290.
52. Arana, J.; Martinez Nieto, J. L.; Herrera Melian, J. A.; Dona Rodriguez, J. M.; Gonzalez Diaz, O.; Perez Pena, J.; Bergasa, O.; Alvarez, C.; Mendez, J. *Chemosphere* **2004**, 55, (6), 893-904.

53. Diebold, U. *Surf. Sci. Rep.* **2003**, 48, (5-8), 53-229.
54. Gao, Y.; Liu, H. *Mater. Chem. Phys.* **2005**, 92, (2-3), 604-608.
55. Maira, A. J.; Yeung, K. L.; Soria, J.; Coronado, J. M.; Belver, C.; Lee, C. Y.; Augugliaro, V. *Appl. Catal., B* **2001**, 29, (4), 327-336.
56. Saquib, M.; Muneer, M. *Dyes Pigm.* **2003**, 56, (1), 37-49.
57. Gogate, P. R.; Pandit, A. B. *Adv. Environ. Res.* **2004**, 8, (3-4), 501-551.
58. Wang, W.-Y.; Ku, Y. *Colloids Surf., A* **2007**, 302, (1-3), 261-268.
59. Mrowetz, M.; Selli, E. *J. Photochem. Photobiol., A* **2006**, 180, (1-2), 15-22.
60. Sun, J.; Wang, X.; Sun, J.; Sun, R.; Sun, S.; Qiao, L. *J. Mol. Catal. A: Chem.* **2006**, 260, (1-2), 241-246.
61. Soares, E. T.; Lansarin, M. A.; Moro, C. C. *Braz. J. Chem. Eng.* **2007**, 24, (1), 29-36.
62. Nogueira, R. F. P.; Jardim, W. F. *J. Chem. Educ.* **1993**, 70, (10), 861-2.
63. Doushita, K.; Kawahara, T. *J. Sol-Gel Sci. Technol.* **2001**, 22, (1/2), 91-98.
64. Ding, Z.; Lu, G. Q.; Greenfield, P. F. *J. Phys. Chem. B* **2000**, 104, (19), 4815-4820.
65. Hurum Deanna, C.; Gray Kimberly, A.; Rajh, T.; Thurnauer Marion, C. *J Phys Chem B* **2005**, 109, (2), 977-80.
66. Mills, A.; Lepre, A.; Elliott, N.; Bhopal, S.; Parkin, I. P.; O'Neill, S. A. *J. Photochem. Photobiol., A* **2003**, 160, (3), 213-224.
67. Cassie, A. B. D.; Baxter, S. *Trans. Faraday Soc.* **1944**, 40, 546-51.
68. Barthlott, W.; Neinhuis, C. *Planta* **1997**, 202, (1), 1-8.
69. Crick, C. R.; Parkin, I. P. *Chem.-Eur. J.* **2010**, 16, (12), 3568-3588.
70. Linsebigler, A. L.; Lu, G.; Yates, J. T., Jr. *Chem. Rev.* **1995**, 95, (3), 735-58.
71. Thompson, T. L.; Yates, J. T., Jr. *Chem. Rev.* **2006**, 106, (10), 4428-4453.
72. Chen, X.; Mao, S. S. *Chem. Rev.* **2007**, 107, (7), 2891-2959.
73. Mo, S.-D.; Ching, W. Y. *Phys. Rev. B: Condens. Matter* **1995**, 51, (19), 13023-32.
74. Allsopp, W. J.; Van Doren, R. E. *Amer. Paint J.* **1972**, 57, (12), 27, 30, 66-9.
75. Stewart, E. W. *Plast. Compd.* **1985**, 8, (1), 58, 60.

References

76. Philips, L. G.; Barbano, D. M. *Journal of Dairy Sciences* **1997**, 80, (11), 2726-2731.
77. Schulz, J.; Hohenberg, H.; Pflucker, F.; Gartner, E.; Will, T.; Pfeiffer, S.; Wepf, R.; Wendel, V.; Gers-Barlag, H.; Wittern, K. P. *Adv. Drug Delivery Rev.* **2002**, 54, (Suppl. 1), S157-S163.
78. Rao, P. S.; Hayon, E. *Biochem. Biophys. Res. Commun.* **1973**, 51, (2), 468-73.
79. Henglein, A. *Ultramicroscopy* **1984**, 14, (3), 195-200.
80. Kudo, A.; Miseki, Y. *Chem. Soc. Rev.* **2009**, 38, (1), 253-278.
81. Tanaka, K.; Capule, M. F. V.; Hisanaga, T. *Chem. Phys. Lett.* **1991**, 187, (1-2), 73-6.
82. Bickley, R. I.; Gonzalez-Carreno, T.; Lees, J. S.; Palmisano, L.; Tilley, R. J. D. *J. Solid State Chem.* **1991**, 92, (1), 178-90.
83. Ohno, T.; Sarukawa, K.; Tokieda, K.; Matsumura, M. *J. Catal.* **2001**, 203, (1), 82-86.
84. Ozawa, T.; Iwasaki, M.; Tada, H.; Akita, T.; Tanaka, K.; Ito, S. *J. Colloid Interface Sci.* **2005**, 281, (2), 510-513.
85. Serpone, N.; Emeline, A. V. *Res. Chem. Intermed.* **2005**, 31, (4-6), 391-432.
86. Beranek, R.; Tsuchiya, H.; Sugishima, T.; Macak, J. M.; Taveira, L.; Fujimoto, S.; Kisch, H.; Schmuki, P. *Appl. Phys. Lett.* **2005**, 87, (24), 243114/1-243114/3.
87. Guo, C.-W.; Cao, Y.; Dai, W.-L.; Fan, K.-N.; Deng, J.-F. *Chem. Lett.* **2002**, (6), 588-589.
88. Gaertner, G. F.; Lydtin, H. *Nanostruct. Mater.* **1994**, 4, (5), 559-68.
89. Beck, D. D.; Siegel, R. W. *J. Mater. Res.* **1992**, 7, (10), 2840-5.
90. Buhro, W. E.; Colvin, V. L. *Nat. Mater.* **2003**, 2, (3), 138-139.
91. Burda, C.; Chen, X.; Narayanan, R.; El-Sayed, M. A. *Chem. Rev. (Washington, DC, U. S.)* **2005**, 105, (4), 1025-1102.
92. Mie, G. *Phys. Z.* **1908**, 8, 769.
93. Genzel, L.; Martin, T. P.; Kreibig, U. *Z. Phys. B* **1975**, 21, (4), 339-46.
94. Roldughin, V. I. *Russ. Chem. Rev.* **2000**, 69, (10), 821-843.
95. Roduner, E. *Chem. Soc. Rev.* **2006**, 35, (7), 583-592.

96. Fox, M. A.; Dulay, M. T. *Chem. Rev.* **1993**, 93, (1), 341-57.
97. Shin, H.; Jung, H. S.; Hong, K. S.; Lee, J.-K. *J. Solid State Chem.* **2005**, 178, (1), 15-21.
98. Okada, K.; Yamamoto, N.; Kameshima, Y.; Yasumori, A.; MacKenzie, K. J. D.; Condrate, R.A. *J. Am. Ceram. Soc.* **2001**, 84, (7), 1591-1596.
99. Hanaor, D. A. H.; Sorrell, C. C. *J. Mater. Sci.* **2011**, 46, (4), 855-874.
100. Chang, H.; Kim, S. J.; Jang, H. D.; Choi, J. W. *Colloids Surf., A* **2008**, 313+314, 282-287.
101. Boer, J.; Burckhardt, W. *Key Eng. Mater.* **1997**, 132-136, (Pt. 1, Euro Ceramics V), 152-156.
102. Hirano, M.; Nakahara, C.; Ota, K.; Tanaike, O.; Inagaki, M. *J. Solid State Chem.* **2003**, 170, (1), 39-47.
103. Ito, S.; Yoshida, S.; Watanabe, T. *Chem. Lett.* **2000**, (1), 70-71.
104. Wang, C.-C.; Ying, J. Y. *Chem. Mater.* **1999**, 11, (11), 3113-3120.
105. Mills, A.; Elliott, N.; Parkin, I. P.; O'Neill, S. A.; Clark, R. J. *J. Photochem. Photobiol., A* **2002**, 151, (13), 171-179.
106. Mardare, D.; Tasca, M.; Delibas, M.; Rusu, G. I. *Appl. Surf. Sci.* **2000**, 156, (1-4), 200-206.
107. Dutta Sharma, S.; Singh, D.; Saini, K. K.; Kant, C.; Sharma, V.; Jain, S. C.; Sharma, C. P. *Appl. Catal., A* **2006**, 314, (1), 40-46.
108. Choi, W.; Termin, A.; Hoffmann, M. R. *J. Phys. Chem.* **1994**, 98, (51), 13669-79.
109. Schubert, U.; Hüsing, N., *Synthesis of Inorganic Materials.* **2004**.
110. Livage, J.; Henry, M.; Sanchez, C. *Prog. Solid State Chem.* **1988**, 18, (4), 259-341.
111. Brinker, C.; Scherer, G., *Sol-Gel Science: The Physics and Chemistry of Sol-Gel Processing.* **1990**
112. Schubert, U. *J. Sol-Gel Sci. Technol.* **2003**, 26, (1/2/3), 47-55.
113. Livage, J.; Sanchez, C. *J. Non-Cryst. Solids* **1992**, 145, (1-3), 11-19.
114. Jian, Z.; Pu, Y.; Fang, J.; Ye, Z. *Photochem. Photobiol.* 86, (5), 1016-1021.
115. Wight, A. P.; Davis, M. E. *Chem. Rev.* **2002**, 102, (10), 3589-3613.

References

116. Sanchez, C.; Lebeau, B.; Ribot, F.; In, M. *J. Sol-Gel Sci. Technol.* **2000**, 19, (1/2/3), 31-38.
117. Sharp, K. G. *Adv. Mater.* **1998**, 10, (15), 1243-1248.
118. Wen, J.; Wilkes, G. L. *Chem. Mater.* **1996**, 8, (8), 1667-1681.
119. Mutin, P. H.; Delenne, C.; Medoukali, D.; Corriu, R.; Vioux, A. *Mater. Res. Soc. Symp. Proc.* **1998**, 345-350.
120. Vioux, A.; Mutin, P. H.; Le Bideau, J.; Leclercq, D. *Mater. Res. Soc. Symp. Proc.* **2001**, 628.
121. Vioux, A.; le Bideau, J.; Mutin, P. H.; Leclercq, D. *Top. Curr. Chem.* **2004**, 232, 145-174.
122. Clearfield, A. *Prog. Inorg. Chem.* **1998**, 47, 371-510.
123. Mutin, P. H.; Guerrero, G.; Vioux, A. *J. Mater. Chem.* **2005**, 15, (35-36), 3761-3768.
124. Kosolapoff, G. M. *J. Am. Chem. Soc.* **1945**, 67, 1180-2.
125. McKenna, C. E.; Higa, M. T.; Cheung, N. H.; McKenna, M. C. *Tetrahedron Lett.* **1977**, (2), 155-8.
126. Arbusov, A. E.; Dunin, A. A. *Ber. Dtsch. Chem. Ges. B* **1927**, 60B, 291-5.
127. Sasse, K., In *Methoden der Organischen Chemie*, Houben-Weyl, Ed. Thieme, Stuttgart: **1964**.
128. Fokin, A. V.; Kolomiets, A. F.; Iznoskova, M. G. *Izv. Akad. Nauk SSSR, Ser. Khim.* **1974**, (12), 2837-40.
129. Pudovik, A. N.; Konovalova, I. V. *Synthesis* **1979**, (2), 81-96.
130. Enders, D.; Saint-Dizier, A.; Lannou, M.-I.; Lenzen, A. *Eur. J. Org. Chem.* **2005**, (1), 29-49.
131. Semenzin, D.; Etemad-Moghadam, G.; Albouy, D.; Diallo, O.; Koenig, M. *J. Org. Chem.* **1997**, 62, (8), 2414-2422.
132. Francova, D.; Kickelbick, G. *Monatsh. Chem.* **2009**, 140, (4), 413-422.
133. Senhaji, O.; Robin, J. J.; Achchoubi, M.; Boutevin, B. *Macromol. Chem. Phys.* **2004**, 205, (8), 1039-1050.
134. Imokawa, G.; Tsutsumi, H.; Kurosaki, T. *J. Am. Oil Chem. Soc.* **1978**, 55, (11), 839-43.

-
135. Guerrero, G.; Mutin, P. H.; Vioux, A. *Chem. Mater.* **2001**, 13, (11), 4367-4373.
136. Zhang, X.-J.; Ma, T.-Y.; Yuan, Z.-Y. *J. Mater. Chem.* **2008**, 18, (17), 2003-2010.
137. Alberti, G.; Costantino, U.; Dionigi, C.; Murcia-Mascaros, S.; Vivani, R. *Supramol. Chem.* **1995**, 6, (1-2), 29-40.
138. Alberti, G.; Casciola, M. *Solid State Ionics* **1997**, 97, (1-4), 177-186.
139. Gao, W.; Reven, L. *Langmuir* **1995**, 11, (6), 1860-3.
140. Van Alsten, J. G. *Langmuir* **1999**, 15, (22), 7605-7614.
141. Tsai, M.-Y.; Sun, Y.-T.; Lin, J.-C. *J. Colloid Interface Sci.* **2007**, 308, (2), 474-484.
142. Lee, H.; Kepley, L. J.; Hong, H. G.; Akhter, S.; Mallouk, T. E. *J. Phys. Chem.* **1988**, 92, (9), 2597-601.
143. Pawsey, S.; McCormick, M.; De Paul, S.; Graf, R.; Lee, Y. S.; Reven, L.; Spiess, H. W. *J. Am. Chem. Soc.* **2003**, 125, (14), 4174-4184.
144. Randon, J.; Blanc, P.; Paterson, R. *J. Membr. Sci.* **1995**, 98, (1+2), 119-29.
145. Pawsey, S.; Yach, K.; Reven, L. *Langmuir* **2002**, 18, (13), 5205-5212.
146. Brodard-Severac, F.; Guerrero, G.; Maquet, J.; Florian, P.; Gervais, C.; Mutin, P. H. *Chem. Mater.* **2008**, 20, (16), 5191-5196.
147. Koeroesi, L.; Papp, S.; Bertoti, I.; Dekany, I. *Chem. Mater.* **2007**, 19, (19), 4811-4819.
148. Zhao, D.; Chen, C.; Wang, Y.; Ji, H.; Ma, W.; Zang, L.; Zhao, J. *J. Phys. Chem. C* **2008**, 112, (15), 5993-6001.
149. Raja, P.; Nadtochenko, V.; Klehm, U.; Kiwi, J. *Appl. Catal., B* **2008**, 81, (3-4), 258-266.
150. Yu, J. C.; Zhang, L.; Zheng, Z.; Zhao, J. *Chem. Mater.* **2003**, 15, (11), 2280-2286.
151. Besov, A. S.; Vorontsov, A. V.; Parmon, V. N. *Appl. Catal., B* **2009**, 89, (3-4), 602-612.
152. Kozlova, E. A.; Vorontsov, A. V. *Appl. Catal., B* **2006**, 63, (1-2), 114-123.
153. Trubitsyn, D. A.; Vorontsov, A. V. *J. Phys. Chem. B* **2005**, 109, (46), 21884-21892.

References

154. Vorontsov, A. V.; Davydov, L.; Reddy, E. P.; Lion, C.; Savinov, E. N.; Smirniotis, P. G. *New J. Chem.* **2002**, 26, (6), 732-744.
155. Obee, T. N.; Satyapal, S. *J. Photochem. Photobiol., A* **1998**, 118, (1), 45-51.
156. Harada, K.; Hisanaga, T.; Tanaka, K. *Water Res.* **1990**, 24, (11), 1415-17.
157. Sakkas, V. A.; Dimou, A.; Pitarakis, K.; Mantis, G.; Albanis, T. *Environ. Chem. Lett.* **2005**, 3, (2), 57-61.
158. Rabindranathan, S.; Devipriya, S.; Yesodharan, S. *J. Hazard. Mater.* **2003**, 102, (2-3), 217-229.
159. Kiselev, A.; Mattson, A.; Andersson, M.; Palmqvist, A. E. C.; Oesterlund, L. *J. Photochem. Photobiol., A* **2006**, 184, (1-2), 125-134.
160. Moss, J. A.; Szczepankiewicz, S. H.; Park, E.; Hoffmann, M. R. *J. Phys. Chem. B* **2005**, 109, (42), 19779-19785.
161. deGennes, P. G. *Reviews of Modern Physics* **1992**, 64, (3), 645 - 648.
162. Nisisako, T.; Torii, T.; Takahashi, T.; Takizawa, Y. *Adv. Mater.* **2006**, 18, (9), 1152-1156.
163. Binks, B. P.; Fletcher, P. D. I. *Langmuir* **2001**, 17, (16), 4708-4710.
164. Behrend, C. J.; Anker, J. N.; McNaughton, B. H.; Brasuel, M.; Philbert, M. A.; Kopelman, R. *J. Phys. Chem. B* **2004**, 108, (29), 10408-10414.
165. Behrend, C. J.; Anker, J. N.; Kopelman, R. *Appl. Phys. Lett.* **2004**, 84, (1), 154-156.
166. Iacovella, C. R.; Horsch, M. A.; Zhang, Z.; Glotzer, S. C. *Langmuir* **2005**, 21, (21), 9488-9494.
167. Hong, L.; Cacciuto, A.; Luijten, E.; Granick, S. *Nano Lett.* **2006**, 6, (11), 2510-4.
168. Nelson, D. R. *Nano Lett.* **2002**, 2, (10), 1125-1129.
169. Zhang, Z.; Keys Aaron, S.; Chen, T.; Glotzer Sharon, C. *Langmuir* **2005**, 21, (25), 11547-51.
170. Perro, A.; Meunier, F.; Schmitt, V.; Ravaine, S. *Colloids Surf., A* **2009**, 332, (1), 57-62.
171. Zhang, J.; Wang, X.; Wu, D.; Liu, L.; Zhao, H. *Chem. Mater.* **2009**, 21, (17), 4012-4018.
172. Serra, C. A.; Chang, Z. *Chem. Eng. Technol.* **2008**, 31, (8), 1099-1115.

-
173. Dendukuri, D.; Hatton, T. A.; Doyle, P. S. *Langmuir* **2007**, *23*, (8), 4669-4674.
174. Nie, Z.; Li, W.; Seo, M.; Xu, S.; Kumacheva, E. *J. Am. Chem. Soc.* **2006**, *128*, (29), 9408-9412.
175. Shepherd Robert, F.; Conrad Jacinta, C.; Rhodes Summer, K.; Link Darren, R.; Marquez, M.; Weitz, David, A.; Lewis Jennifer, A. *Langmuir* **2006**, *22*, (21), 8618-22.
176. Roh, K.-H.; Martin, D. C.; Lahann, J. *Nat. Mater.* **2005**, *4*, (10), 759-763.
177. Bhaskar, S.; Pollock, K. M.; Yoshida, M.; Lahann, J. *Small* **2010**, *6*, (3), 404-411.
178. Lin, T.; Wang, H.; Wang, X. *Adv. Mater.* **2005**, *17*, (22), 2699-2703.
179. Bhaskar, S.; Hitt, J.; Chang, S.-W. L.; Lahann, J. *Angew. Chem., Int. Ed.* **2009**, *48*, (25), 4589-4593.
180. Hwang, S.; Roh, K.-H.; Lim, D. W.; Wang, G.; Uher, C.; Lahann, J. *Phys. Chem. Chem. Phys.* *12*, (38), 11894-11899.
181. Nisisako, T.; Torii, T. *Adv. Mater.* **2007**, *19*, (11), 1489-1493.
182. Wurm, F.; Kilbinger Andreas, F. M. *Angew Chem Int Ed Engl* **2009**, *48*, (45), 8412-21.
183. Teo, B. M.; Suh, S. K.; Hatton, T. A.; Ashokkumar, M.; Grieser, F. *Langmuir* **2011**, *27*, (1), 30-33.
184. Jiang, S.; Chen, Q.; Tripathy, M.; Luijten, E.; Schweizer, K. S.; Granick, S. *Adv. Mater.* **2010**, *22*, (10), 1060-1071.
185. Paunov, V. N.; Cayre, O. J. *Adv. Mater.* **2004**, *16*, (9-10), 788-791.
186. Cayre, O.; Paunov, V. N.; Velev, O. D. *J. Mater. Chem.* **2003**, *13*, (10), 2445-2450.
187. Fujimoto, K.; Nakahama, K.; Shidara, M.; Kawaguchi, H. *Langmuir* **1999**, *15*, (13), 4630-4635.
188. Casagrande, C.; Fabre, P.; Raphael, E.; Veyssie, M. *Europhys. Lett.* **1989**, *9*, (3), 251-5.
189. Takei, H.; Shimizu, N. *Langmuir* **1997**, *13*, (7), 1865-1868.
190. Hong, L.; Jiang, S.; Granick, S. *Langmuir* **2006**, *22*, (23), 9495-9499.
191. Pickering, S. U. *J. Chem. Soc., Trans.* **1907**, *91*, 2001-2021.

References

192. Perro, A.; Reculosa, S.; Ravaine, S.; Bourgeat-Lami, E.; Duguet, E. *J. Mater. Chem.* **2005**, 15, (35-36), 3745-3760.
193. Finkle, P.; Draper, H. D.; Hildebrand, J. H. *J. Am. Chem. Soc.* **1923**, 45, 2780-8.
194. Schulman, J. H.; Leja, J. *Trans. Faraday Soc.* **1954**, 50, 598-605.
195. Briggs, T. R. *J. Ind. Eng. Chem.* **1921**, 13, 1008-10.
196. Lucassen-Reynders, E. H.; van den Tempel, M. *J. Phys. Chem.* **1963**, 67, 731-4.
197. Binks, B. P.; Lumsdon, S. O. *Phys. Chem. Chem. Phys.* **1999**, 1, (12), 3007-3016.
198. Frelichowska, J.; Bolzinger, M.-A.; Chevalier, Y. *Colloids Surf., A* **2009**, 343, (1-3), 70-74.
199. Saleh, N.; Sarbu, T.; Sirk, K.; Lowry, G. V.; Matyjaszewski, K.; Tilton, R. D. *Langmuir* **2005**, 21, (22), 9873-9878.
200. Morishita, C.; Kawaguchi, M. *Colloids Surf., A* **2009**, 335, (1-3), 138-143.
201. Torres, L. G.; Iturbe, R.; Snowden, M. J.; Chowdhry, B. Z.; Leharne, S. A. *Colloids Surf., A* **2007**, 302, (1-3), 439-448.
202. Binks, B. P.; Lumsdon, S. O. *Langmuir* **2000**, 16, (8), 3748-3756.
203. Stiller, S. Pickering emulsions on basis of inorganic UV filters. **2003**.
204. Li, D.; He, Y.; Wang, S. *J. Phys. Chem. C* **2009**, 113, (30), 12927-12929.
205. Lan, Q.; Liu, C.; Yang, F.; Liu, S.; Xu, J.; Sun, D. *J Colloid Interface Sci* **2007**, 310, (1), 260-9.
206. Ashby, N. P.; Binks, B. P. *Phys. Chem. Chem. Phys.* **2000**, 2, (24), 5640-5646.
207. Guillot, S.; Bergaya, F.; de Azevedo, C.; Warmont, F.; Tranchant, J.-F. *J Colloid Interface Sci* **2009**, 333, (2), 563-9.
208. Nonomura, Y.; Kobayashi, N. *J Colloid Interface Sci* **2009**, 330, (2), 463-6.
209. Dai, L. L.; Sharma, R.; Wu, C.-Y. *Langmuir* **2005**, 21, (7), 2641-2643.
210. Golemanov, K.; Tcholakova, S.; Kralchevsky, P. A.; Ananthapadmanabhan, K. P.; Lips, A. *Langmuir* **2006**, 22, (11), 4968-4977.
211. Binks, B. P.; Lumsdon, S. O. *Langmuir* **2001**, 17, (15), 4540-4547.
212. Yuan, Q.; Yang, L.; Wang, M.; Wang, H.; Ge, X.; Ge, X. *Langmuir* **2009**, 25, (5), 2729-2735.

-
213. Bayer, I. S.; Steele, A.; Martorana, P. J.; Loth, E.; Miller, L. *Appl. Phys. Lett.* **2009**, 94, (16), 163902/1-163902/3.
214. Blaker, J. J.; Lee, K.-Y.; Li, X.; Menner, A.; Bismarck, A. *Green Chem.* **2009**, 11, (9), 1321-1326.
215. Branch, E. L. *Am. Food J.* **1924**, 19, 460-1.
216. Menner, A.; Ikem, V.; Salgueiro, M.; Shaffer, M. S. P.; Bismarck, A. *Chem. Commun.* **2007**, (41), 4274-4276.
217. Song, X.; Zhao, Y.; Wang, H.; Du, Q. *Langmuir* **2009**, 25, (8), 4443-4449.
218. Bachinger, A.; Ivanovici, S.; Kickelbick, G. *J. Nanosci. Nanotechnol.* **2011**, submitted.
219. Chen, T.; Colver, P. J.; Bon, S. A. F. *Adv. Mater. (Weinheim, Ger.)* **2007**, 19, (17), 2286-2289.
220. Pugh, R. J. *Langmuir* **2007**, 23, (15), 7972-7980.
221. Gers-Barlag, H.; Mueller, A. 1999-116872 987004, 19990906., **2000**.
222. Goepfel, A.; Koopmann, S.; Schulz, J.; Grotelueschen, B. 2002-23510 1310235, 20021022., **2003**.
223. Liu, B.; Wei, W.; Qu, X.; Yang, Z. *Angew. Chem., Int. Ed.* **2008**, 47, (21), 3973-3975.
224. Wang, B.; Li, B.; Dong, B.; Zhao, B.; Li, C. Y. *Macromolecules* 43, (22), 9234-9238.
225. Suzuki, D.; Tsuji, S.; Kawaguchi, H. *J. Am. Chem. Soc.* **2007**, 129, (26), 8088-8089.
226. Xu, L.-P.; Pradhan, S.; Chen, S. *Langmuir* **2007**, 23, (16), 8544-8548.
227. Haruta, M.; Kobayashi, T.; Sano, H.; Yamada, N. *Chem. Lett.* **1987**, (2), 405-8.
228. Aguilar-Guerrero, V.; Gates, B. C. *Catal. Lett.* **2009**, 130, (1-2), 108-120.
229. Prati, L.; Rossi, M. *J. Catal.* **1998**, 176, (2), 552-560.
230. Abad, A.; Concepcion, P.; Corma, A.; Garcia, H. *Angew. Chem., Int. Ed.* **2005**, 44, (26), 4066-4069.
231. Deng, W.; Frenkel, A. I.; Si, R.; Flytzani-Stephanopoulos, M. *J. Phys. Chem. C* **2008**, 112, (33), 12834-12840.

References

232. Rodriguez, J. A.; Liu, P.; Hrbek, J.; Evans, J.; Perez, M. *Angew. Chem., Int. Ed.* **2007**, 46, (8), 1329-1332.
233. Ono, L. K.; Sudfeld, D.; Roldan Cuenya, B. *Surf. Sci.* **2006**, 600, (23), 5041-5050.
234. Haruta, M. *Chem. Rec.* **2003**, 3, (2), 75-87.
235. Qian, X.; Peng, X.-H.; Ansari, D. O.; Yin-Goen, Q.; Chen, G. Z.; Shin, D. M.; Yang, L.; Young, A. N.; Wang, M. D.; Nie, S. *Nat. Biotechnol.* **2008**, 26, (1), 83-90.
236. Prajapati, P. M.; Shah, Y.; Sen, D. J. *J. Chem. Pharm. Res.* **2010**, 2, (1), 30-37.
237. Fay, F.; Scott, C. J.; McCarron, P. A. *Curr. Nanosci.* **2010**, 6, (6), 560-570.
238. Chen, J.; Yang, M.; Zhang, Q.; Cho, E. C.; Cobley, C. M.; Kim, C.; Glaus, C.; Wang, L. V.; Welch, M. J.; Xia, Y. *Adv. Funct. Mater.* **2010**, 20, (21), 3684-3694.
239. Wei, Q.; Wei, A. *Supramol. Chem. Org.-Inorg. Hybrid Mater.* **2010**, 319-349.
240. Edgar, J. A.; Cortie, M. B. *Gold* **2010**, 369-397.
241. Jain, P. K.; El-Sayed, M. A. *Chem. Phys. Lett.* **2010**, 487, (4-6), 153-164.
242. Singh, R.; Premkumar, T.; Shin, J.-Y.; Geckeler, K. E. *Chem.-Eur. J.* **2010**, 16, (6), 1728-1743.
243. Cobley, C. M.; Chen, J.; Cho, E. C.; Wang, L. V.; Xia, Y. *Chem. Soc. Rev.* **2011**, 40, (1), 44-56.
244. Faraday, M. *Philosophical Transactions the Royal Society, London* **1857**, 147, 145.
245. Thompson, D. *Gold Bull.* **2007**, 40, (4), 267-269.
246. Turkevich, J.; Stevenson, P. C.; Hillier, J. *J. Phys. Chem.* **1953**, 57, 670-3.
247. Frens, G. *Nature, Phys. Sci.* **1973**, 241, (105), 20-2.
248. Brust, M.; Walker, M.; Bethell, D.; Schiffrin, D. J.; Whyman, R. *J. Chem. Soc., Chem. Commun.* **1994**, (7), 801-2.
249. Hasan, M.; Bethell, D.; Brust, M. *J Am Chem Soc* **2002**, 124, (7), 1132-3.
250. Perrault, S. D.; Chan, W. C. W. *J. Am. Chem. Soc.* **2009**, 131, (47), 17042-17043.
251. Martin, M. N.; Basham, J. I.; Chando, P.; Eah, S.-K. *Langmuir* **2010**, 26, (10), 7410-7417.

-
252. Ivanovici, S. Synthetic Methods to Control the Structure of Titania - Polymer Hybrid Materials and Nanocomposites. Vienna University of Technology, Vienna, **2008**.
253. Ohno, T.; Tokieda, K.; Higashida, S.; Matsumura, M. *Appl. Catal., A* **2003**, 244, (2), 383-391.
254. Huang, B.-S.; Wey, M.-Y. *Int. Conf. Chem. Chem. Eng.* **2010**, 147-149.
255. Mahshid, S.; Askari, M.; Ghamsari, M. S. *J. Mater. Process. Technol* **2007**, 189, (1-3), 296-300.
256. Beusen, J.; Van Bael, M. K.; Van den Rul, H.; D'Haen, J.; Mullens, J. *J. Eur. Ceram. Soc.* **2007**, 27, (16), 4529-4535.
257. Liao, D.; Liao, B. *Int. J. Chem. React. Eng.* **2007**, 5, No pp given.
258. Kongsuebchart, W.; Praserttham, P.; Panpranot, J.; Sirisuk, A.; Supphasrirongjaroen, P.; Satayaprasert, C. *J. Cryst. Growth* **2006**, 297, (1), 234-238.
259. Hirano, M.; Ota, K.; Oya, S. *Ceram. Trans.* **2010**, 99-104.
260. Zhou, W. Y.; Cao, Q. Y.; Yu, X. Y.; Jia, J. L.; Xu, Y. H. *Adv. Appl. Ceram.* **2010**, 109, (7), 389-393.
261. Li, L.; Liu, C.-y. *Eur. J. Inorg. Chem.* **2009**, (25), 3727-3733.
262. Xie, J.; Lu, X.; Liu, J.; Shu, H. *Pure Appl. Chem.* **2009**, 81, (12), 2407-2415.
263. Arnal, P.; Corriu, R. J. P.; Leclercq, D.; Mutin, P. H.; Vioux, A. *J. Mater. Chem.* **1996**, 6, (12), 1925-1932.
264. Isley, S. L.; Penn, R. L. *J. Phys. Chem. B* **2006**, 110, (31), 15134-15139.
265. Yu, Z.; Chuang, S. S. C. *J. Catal.* **2007**, 246, (1), 118-126.
266. Houas, A.; Lachheb, H.; Ksibi, M.; Elaloui, E.; Guillard, C.; Herrmann, J. M. *Appl. Catal., B* **2001**, 31, (2), 145-157.
267. Jiu, J.; Isoda, S.; Adachi, M.; Wang, H. *J. Mater. Sci.: Mater. Electron.* **2007**, 18, (6), 593-597.
268. Addamo, M.; Augugliaro, V.; Di Paola, A.; Garcia-Lopez, E.; Loddo, V.; Marci, G.; Palmisano, L. *Thin Solid Films* **2008**, 516, (12), 3802-3807.
269. Simonsen, M. E.; Jensen, H.; Li, Z.; SoEgaard, E. G. *J. Photochem. Photobiol., A* **2008**, 200, (2-3), 192-200.

References

270. Guillard, C.; Beaugiraud, B.; Dutriez, C.; Herrmann, J.-M.; Jaffrezic, H.; Jaffrezic-Renault, N.; Lacroix, M. *Appl. Catal., B* **2002**, 39, (4), 331-342.
271. Paz, Y.; Heller, A. *J. Mater. Res.* **1997**, 12, (10), 2759-2766.
272. Hyett, G.; Green, M.; Parkin, I. P. *J. Am. Chem. Soc.* **2006**, 128, (37), 12147-12155.
273. Fujishima, A.; Rao, T. N. *Pure Appl. Chem.* **1998**, 70, (11), 2177-2187.
274. Minabe, T.; Tryk, D. A.; Sawunyama, P.; Kikuchi, Y.; Hashimoto, K.; Fujishima, A. *J. Photochem. Photobiol., A* **2000**, 137, (1), 53-62.
275. Theurich, J.; Lindner, M.; Bahnemann, D. W. *Langmuir* **1996**, 12, (26), 6368-6376.
276. Hashimoto, K.; Irie, H.; Fujishima, A. *Jpn. J. Appl. Phys., Part 1* **2005**, 44, (12), 8269-8285.
277. Pilkenton, S.; Xu, W.; Raftery, D. *Anal. Sci.* **2001**, 17, (1), 125-130.
278. Allert, M.; Rizk, S. S.; Looger, L. L.; Hellinga, H. W. *Proc. Natl. Acad. Sci. U. S. A* **2004**, 101, (21), 7907-7912.
279. Hyatt, D. C.; Youn, B.; Zhao, Y.; Santhamma, B.; Coates, R. M.; Croteau, R. B.; Kang, C. *Proc. Natl. Acad. Sci. U. S. A.* **2007**, 104, (13), 5360-5365.
280. Mutin, P. H.; Lafond, V.; Popa, A. F.; Granier, M.; Markey, L.; Dereux, A. *Chem. Mater.* **2004**, 16, (26), 5670-5675.
281. Snyder, R. G.; Strauss, H. L.; Elliger, C. A. *J. Phys. Chem.* **1982**, 86, (26), 5145-50.
282. Thurnauer, M. C.; Rajh, T.; Tiede, D. M. *Acta Chem. Scand.* **1997**, 51, (5), 610-618.
283. Verwey, E. J. W.; Overbeek, J. T. G. *Trans. Faraday Soc.* **1946**, 42B, 117-23.
284. Levine, S.; Dube, G. P. *Philos. Mag.* **1940**, 29, 105-28.
285. Lomoschitz, C. J. Synthesis of Phosphorus Coupling Agents and Their Use in the Modification of ZrO₂ and Barium Glass Surfaces. *Thesis*. Vienna University of Technology, Vienna, **2010**.
286. Turkevich, J.; Stevenson, P. C.; Hillier, J. *Discuss. Faraday Soc.* **1951**, No. 11, 55-75.

-
287. Kimling, J.; Maier, M.; Okenve, B.; Kotaidis, V.; Ballot, H.; Plech, A. *J. Phys. Chem. B* **2006**, 110, (32), 15700-15707.
288. Haslag, C. S.; Bowden, E. F.; Njue, C. K. *Abstracts of Papers, 225th ACS National Meeting, New Orleans, LA, United States, March 23-27, 2003* **2003**, ANYL-113.
289. Hong, H. G.; Mallouk, T. E. *Langmuir* **1991**, 7, (10), 2362-9.
290. Tsai, M.-Y.; Lin, J.-C. *J. Biomed. Mater. Res.* **2001**, 55, (4), 554-565.
291. Zhang, F.; Zhou, Y.; Chen, Y.; Shi, Z.; Tang, Y.; Lu, T. *J. Colloid Interface Sci.* **2010**, 351, (2), 421-426.
292. Arbuzov, B. A. *Pure Appl. Chem.* **1964**, 9, (2), 307-35.
293. Jiang, X.; Herricks, T.; Xia, Y. *Adv. Mater.* **2003**, 15, (14), 1205-1209.
294. Jang, S.-G.; Kim, S.-H.; Lee, S.-Y.; Jeong, W.-C.; Yang, S.-M. *J. Colloid Interface Sci.* **2010**, 350, (2), 387-395.
295. Stoeber, W.; Fink, A.; Bohn, E. *J. Colloid Interface Sci.* **1968**, 26, (1), 62-9.
296. Lorret, O.; Francova, D.; Waldner, G.; Stelzer, N. *Appl. Catal., B* **2009**, 91, (1-2), 39-46
297. Lorret, O. *personal communication* **2009**

Curriculum Vitae

Dipl.Ing. Angelika Bachinger

Braunhirschengasse 5/8

1150 Wien, Austria

Tel: +43-650-6673733

Email: angelika.bachinger@gmail.com

Born: July, 26th 1982 in Ried/I., Austria

Citizenship: Austrian

Unmarried, no children

EDUCATION:

- 07/2008 – present: PhD in Materials Chemistry,
Vienna University of Technology, Austria
Topic: *“Organophosphonates on Titanium Dioxide Photocatalysts: Isotropic and Anisotropic Modification and Photocatalytic Properties”*
- 03/2007 – 04/2008: Diploma Thesis in Materials Chemistry,
Vienna University of Technology, Austria
Topic: *“Click reactions of sphaerosilicates and polyhedral oligomeric silsesquioxanes. A novel strategy towards hybrid materials”*
- 10/2001 – 04/2008: Study of Technical Chemistry, focusing on Polymer Chemistry and Materials Chemistry, Vienna University of Technology, Austria

EMPLOYMENT HISTORY:

- 04/2009 – 04/2011 Research and Teaching Associate at the Vienna University of Technology, Institute for Materials Chemistry (Vienna, Austria)
- 07/2008 – 04/2009 Research Associate at the Vienna University of Technology, Institute for Materials Chemistry (Vienna, Austria)

Various summerjobs at Leitz (Riedau, Austria), Plasser und Theurer (Linz, Austria), Austria Tabak Ökolab (Vienna, Austria) and Borealis (Schwechat, Austria) in the years 1998 to 2006.

HONORS AND GRANTS:

IUPAC Poster prize at the 13th Austrian Chemistry Days, 2009, Poster: A. Bachinger, S. Ivanovici, G. Kickelbick. "Anisotropic Surface Modification of Photocatalytically Active Titania Nanoparticles"

PUBLICATIONS:

A. Bachinger, G. Kickelbick:

"*Pickering Emulsions stabilized by Anatase Nanoparticles*". Chemical Monthly (2010), 141:685-690.

A. Bachinger, S. Ivanovici, G. Kickelbick:

"*On the Formation of Janus TiO₂ Nanoparticles using a Pickering Emulsion Approach*", Journal of Nanoscience and Nanotechnology, submitted.

M. Raza, A. Bachinger, G. Kickelbick:

"*Interaction and Photocatalytic Properties of Different Organic Capping Agents with TiO₂*", in preparation.

A. Bachinger, G. Kickelbick:

"*Photocatalytic Stability of Organic Phosphonates and Phosphates on TiO₂ Nanoparticles*", in preparation.

A. Bachinger, G. Kickelbick:

"*Synthesis of Spherosilicates with Ethynylgroups and their Functionalization by Huisgen 1,3-dipolar Cycloaddition Reaction*", in preparation.

PRESENTATIONS:

A. Bachinger, S. Ivanovici, G. Kickelbick:

"*A Click Chemistry Approach to the Incorporation of Modified Spherosilicates to Organic and Inorganic Polymers*";

Poster: 12. Österreichische Chemietage, Klagenfurt; 10.09.2007 - 13.09.2007; in: "12. Österreichische Chemietage - Abstracts", (2007), ISBN: 978-3-900554-61-3; S. 75.

A. Bachinger, G. Kickelbick:

"*Preparation of Alkyne and Azide modified Spherosilicates*";

Poster: Junior Scientist Conference 2008, Vienna; 16.11.2008 - 18.11.2008; in: "Proceedings of the Junior Scientist Conference 2008", (2008), ISBN: 978-3-200-01612-5; S. 157 - 158.

A. Bachinger, S. Ivanovici, G. Kickelbick:

"*Anisotropic Surface Modification Of Photocatalytically Active Titania Nanoparticles*";

Poster: 13. Österreichische Chemietage, Wien; 24.08.2009 - 27.08.2009; in: "13. Österreichische Chemietage", (2009), ISBN: 978-3-900554-66-8; 1 S.

A. Bachinger, S. Ivanovici, G. Kickelbick:

"*Photocatalytically Active TiO₂ Janus Nanoparticles*";

Vortrag: Minisymposium: From Molecules to Materials, Saarbrücken, Deutschland; 10.09.2009 - 11.09.2009; in: *“From Molecules to Materials”*, (2009).

A. Bachinger, G. Kickelbick:

“Click Reactions on Spherosilicates”;

Poster: 5th European Silicon Days 2009, Wien; 20.09.2009 - 22.09.2009; in: *“5th European Silicon Days - Programme, Abstracts and List of Participants”*, (2009), S. 91.

A. Bachinger, G. Kickelbick:

“Pickering Emulsions Stabilized by Anatase Nanoparticles”;

Poster: Junior Scientist Conference 2010, Vienna; 07.04.2010 - 09.04.2010; in: *“Proceedings”*, (2010), ISBN: 978-3-200-01797-9; S. 225 - 226.

A. Bachinger, G. Kickelbick:

“Photocatalytic Degradation of Organic Compounds with Covalent Connection to Anatase Nanoparticles”;

Poster: EuCheMs Chemistry Congress 2010, Nürnberg, 29.08.2010 – 02.09.2010; in: *“Proceedings”*